ANALYSIS AND DESIGN OF A CONSTANT FORCE GRIPPER

SABİT KUVVETLİ BİR KISKACIN ANALİZİ VE TASARIMI

TURAN SOYÖZEN

Prof. Dr. ENGİN TANIK

Supervisor

Submitted to

Graduate School of Science and Engineering of Hacettepe University

as a Partial Fulfillment to the Requirements

for the Award of the Degree of Doctor of Philosophy

in Mechanical Engineering

2022

ABSTRACT

ANALYSIS AND DESIGN OF A CONSTANT FORCE GRIPPER

Turan SOYÖZEN

Doctor of Philosophy, Department of Mechanical Engineering

Supervisor: Prof. Dr. Engin TANIK

November 2022, 113 pages

Constant force mechanisms have significant advantages over conventional force control methods, especially in terms of cost and design complexity. In this thesis a novel constant force gripper mechanism is introduced. This mechanism has great potential for constant force gripping applications. The mechanism is driven with constant input torque that can easily be supplied from a DC motor, since constant current yields constant torque output for a DC motor. Thus, sensors and controller can be eliminated from the system. Constant force is achieved via several links and springs. Numerous mechanical solutions for torque transmission and creation of equivalent systems by shifting spring positions are presented. By means of dimensionless parameters approach, parametric solutions and scalable applications are obtained to achieve constant force throughout large strokes. Finally, a prototype is built and theoretical approaches are verified with experimental results.

Keywords: constant force mechanisms, robotic grippers, four-bar mechanisms

ÖZET

SABİT KUVVETLİ BİR KISKACIN ANALİZİ VE TASARIMI

Turan SOYÖZEN

Doktora Tezi, Makina Mühendisliği Bölümü

Danışman: Prof. Dr. Engin TANIK

Kasım 2022, 113 sayfa

Sabit kuvvet mekanizmaları, özellikle maliyet ve tasarım karmaşıklığı açılarından geleneksel kuvvet kontrol yöntemlerine göre önemli avantajlar sağlamaktadır. Bu tezde, özgün bir sabit kuvvet mekanizması tanıtılmaktadır. Söz konusu mekanizma, sabit kuvvet gerektiren tutucu uygulamaları için büyük potansiyele sahiptir. Mekanizma, bir DC motora sabit akım verilerek kolayca elde edilebilen bir sabit giriş torku ile çalışmaktadır. Böylece sensörler ve kontrolcü sistemden çıkarılabilir. Sabit kuvvet, yalnızca birkaç link ve yay aracılığıyla elde edilmektedir. Tork aktarımı ve yay konumlarının değiştirilmesi ile eşdeğer sistemlerin oluşturulabilmesi için çeşitli çözümler sunulmuştur. Boyutsuz parametre yaklaşımı sayesinde, istenilen strok boyunca sabit kuvvet sağlayabilen ölçeklenebilir parametrik çözümler sunulmuştur. Son olarak, geliştirilen prototip ile teorik yaklaşımlar deneysel sonuçlarla karşılaştırılmıştır.

Anahtar kelimeler: sabit kuvvet mekanizmaları, robotik tutucular, dört çubuk mekanizmaları

TEŞEKKÜR

Yalnızca bu tez çalışmasında değil, tüm eğitim-öğretim ve profesyonel meslek hayatımda her zaman bilgi, birikim ve tecrübelerinden faydalanmama imkân tanıyarak bana yol gösterici olan, saygıdeğer hocam Sayın **Prof. Dr. Engin TANIK**'a,

Doğrulama sürecinde kıymetli emeğini ve desteğini esirgemeyen, bir mühendis olarak birçok konuda örnek aldığım Sayın **Dr. Raşit KARAKUŞ**'a,

Bu çalışmayı tamamlayabilmek için gerekli manevi desteği yıllar boyunca yüksek bir özveri ve sabırla sağlayarak her an yanımda olan, başta kıymetli eşim **Zeynep SOYÖZEN** olmak üzere tüm **aileme**,

Sonsuz teşekkürlerimi sunarım.

Turan SOYÖZEN

14.11.2022

TABLE OF CONTENTS

LIST OF TABLES

LIST OF FIGURES

1 INTRODUCTION AND LITERATURE SURVEY

Reuleaux defined machine as “a combination of resistant bodies so arranged that by their means the mechanical forces of nature can be compelled to do work accompanied by certain determinate motion” and mechanism as “an assemblage of resistant bodies, connected by movable joints, to form a closed kinematic chain with one link fixed and having the purpose of transforming motion.” [1] Although these definitions seem indistinctive at a glance, in general machines are arrangement of mechanisms and other elements to transform energy to perform a desired function. Machines may need to utilize some special purpose mechanisms to do a specific task, such as applying constant force for an interval.

Machinery used in numerous industries such as robotics, electronics, or medical devices, may require some sort of constant force application. [2] They can be used in different applications for various reasons such as gripping various size objects with same force or providing a constant force to robotic end effector. [3]

Usually, closed loop control is implemented whenever a constant force is required for an application. [4] An active device such as an electrical or pneumatic actuator changes input by obtaining feedback from contact region when a constant force is required as shown in Figure 1. Sensors must be positioned to monitor actual force applied on the object and generate this feedback. In this manner, reliable and precise force control can be achieved.

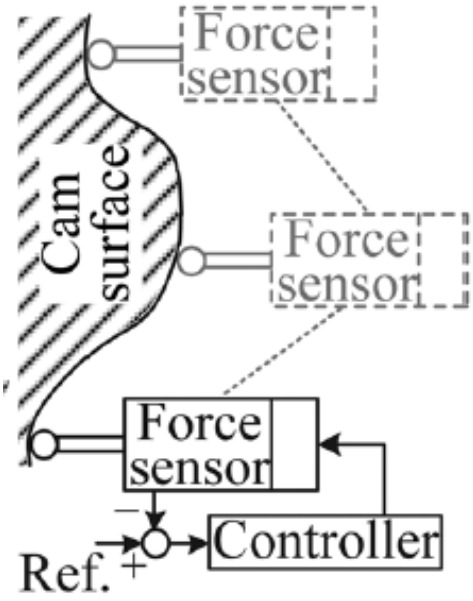

Figure 1. End-effector with an active force controller [5]

However, this method has some drawbacks. First, complex algorithms must be utilized to maintain fast and precise responses. [6], [7] Besides, high quality sensors must be positioned on end effectors which generally have small contact areas. For this reason, sensors should be small enough to be fit in required position. Also, providing electric to these sensors require cables and increases manufacturing complexity and cost. Precision of a system is highly dependent to performance of electronic components, which also yields cost increase. [8]

For these reasons, instead of using conventional sensor-controller method, special type of mechanisms can be utilized to deliver constant force through a stroke.

1.1 Constant Force Mechanisms

A mechanism designed to deliver output force which does not vary for a large range of input motion can be classified as a constant force mechanism. [9] Instead of being manipulated by a controlled actuator, these mechanisms deliver a "near constant" force by their nature over an interval. The term "near constant" is remarkable here, since these mechanisms cannot deliver an exact constant force. They deliver a near constant force which fluctuates in between an upper and lower limit. Nevertheless, in most of the applications exact precision is not required. If these fluctuations are acceptable for a given task, such a linkage can be used as a constant force mechanism.

1.1.1 Rigid-Link Constant Force Mechanisms

To create constant force in an environment where objects (i.e. links) are in motion, one of the most straightforward method is implementing springs into the system to be able to utilize Hooke's Law. Obtaining a linear relationship between distance and force is highly advantageous in terms of constant force creation. Thus, most of the constant force mechanisms includes some springs.

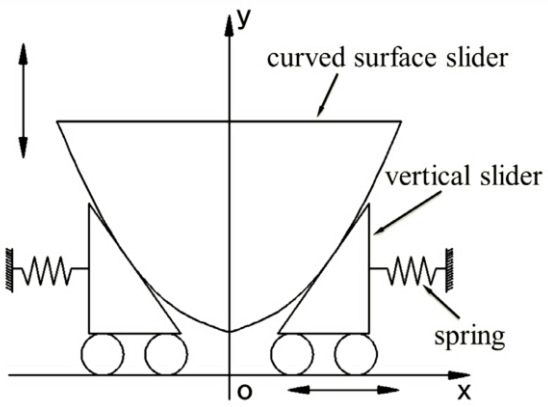

Figure 2. Curved surface constant force mechanism [10]

Curved surface constant force mechanism [10] is one of these. This mechanism basically consists of a curved surface and two inclined surfaces with rollers which are connected with springs as presented at Figure 2. Since the normal forces applied to curved surface are dependent shape of the curved surface, constant force can be obtained by optimizing the relation between surface shape and other parameters.

Quasi-zero-stiffness isolator [11] given in Figure 3 consists of one vertical and two oblique springs. When point *P* crosses below *MN* line, force applied by oblique springs start to decrease, however force generated by vertical spring will be still increasing. Thus, by optimizing spring stiffnesses, a constant force may be generated.

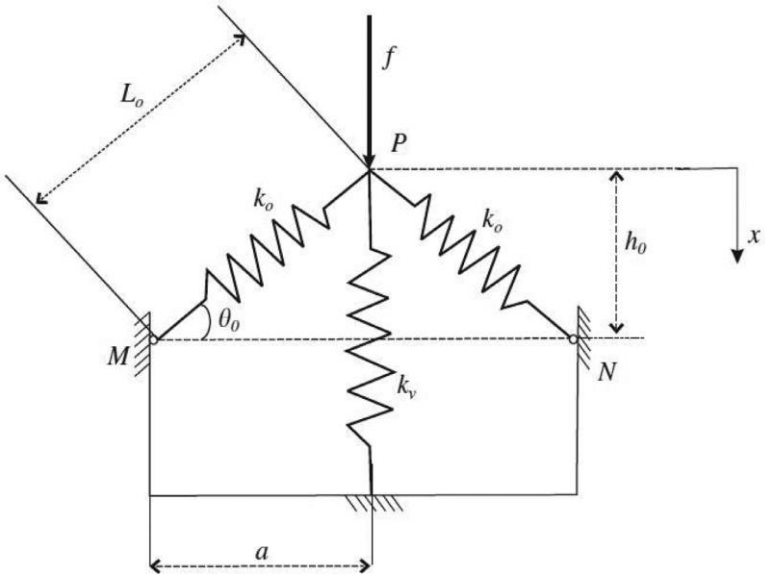

Figure 3. Quasi-zero-stiffness isolator [11]

Another constant force mechanism is presented at [12] which consists two springs connected to seven rigid links.

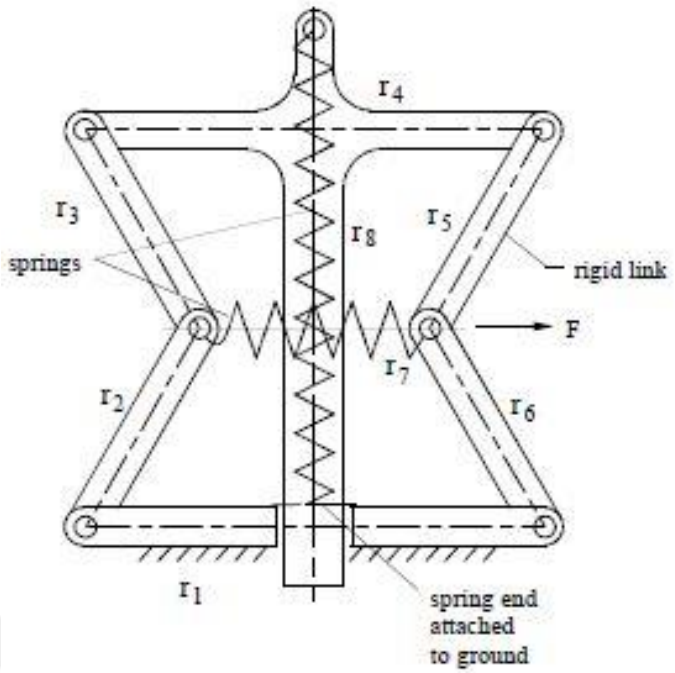

Figure 4. A rigid-link constant force mechanism [12]

Patented hinged lever constant force mechanism [13] is a simple yet effective type of constant force mechanism. It only consists of a rigid link and a linear spring as presented in Figure 5.

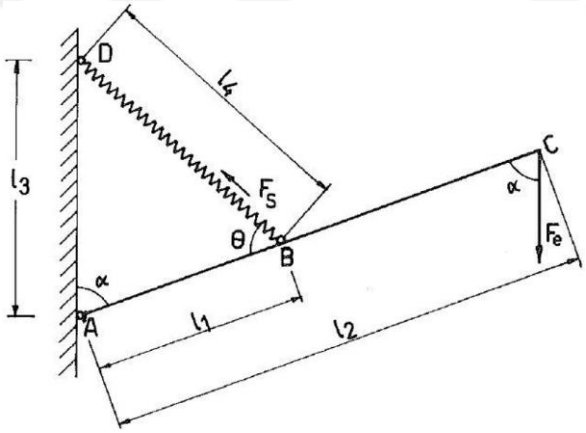

Figure 5. Hinged lever constant force mechanism [13]

Following equations can be written using the nomenclature in Figure 5.

$$F_s l_1 \sin\theta = F_e l_2 \sin\alpha$$

$$F_s = k\delta$$

where k and δ represents the spring stiffness and spring elongation respectively. These can be rearranged as

$$F_e = \frac{k\delta l_1 \sin\theta}{l_2 \sin\alpha}$$

To eliminate trigonometric functions, sine rule can be applied and equation becomes

$$F_e = \frac{k\delta l_1 l_3}{l_2 l_4}$$

where only variable left in equation is spring elongation, δ. Now, consider a spring which has and zero unstretched length, i.e. $\delta = l_4$. Thus

$$F_e = \frac{k l_1 l_3}{l_2}$$

Finally, output force F_e is not dependent to any variable and has a constant value which is related with four structural parameters.

To provide the zero length springs in aforementioned assumption, special manufacturing techniques or additional mechanisms are required. Thus, a spring having a force-displacement curve starting from the origin can be obtained. [8]

Both this type of spring and an early application of hinged lever constant force mechanism/manipulator is first mentioned in a patent granted by a vehicle suspension engineer, George Carwandine at 1934 [14]. With this invention, Carwandine established Anglepoise, a British desk lamp manufacturing company.

Figure 6. Carwandine's design [14] and Anglepoise Model 1208

Since usage of revolute joints is generally essential for rigid-link constant force mechanisms, friction and backlash are common disadvantages. For this reason, there are also various works to utilize compliant mechanisms in order to generate constant force outputs.

1.1.2 Compliant Constant Force Mechanisms

Using flexible members rather than rigid links is an efficient method to prevent friction and backlash. This type of mechanisms is considered as compliant mechanisms, and they can provide advantages in terms of cost, weight and manufacturing ease compared to rigid-link mechanisms. [9] Deformations of compliant links on a compliant mechanism can be optimized in order to deliver constant force.

Most of the compliant constant force mechanisms superimposes positive-stiffness and negative-stiffness systems to create a zero-stiffness system as illustrated in Figure 7. Elastic components can be used for positive-stiffness behavior to create forces which are proportional to deformation, and bistable beams can be used to create negative-stiffness. [8] Figure 8 also illustrates the conceptual design of a zero-stiffness constant force mechanism [15].

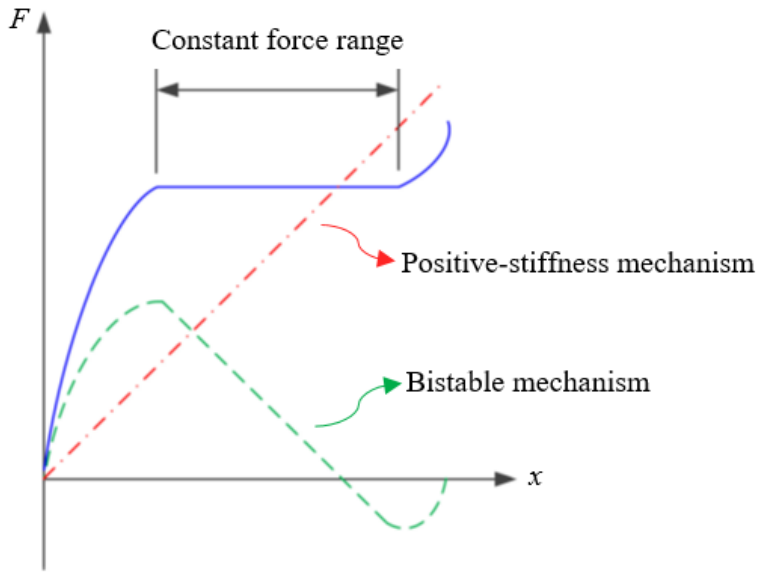

Figure 7. Superimposition of force vs. displacement curves of positive-stiffness and bistable mechanisms in order to obtain constant force [15]

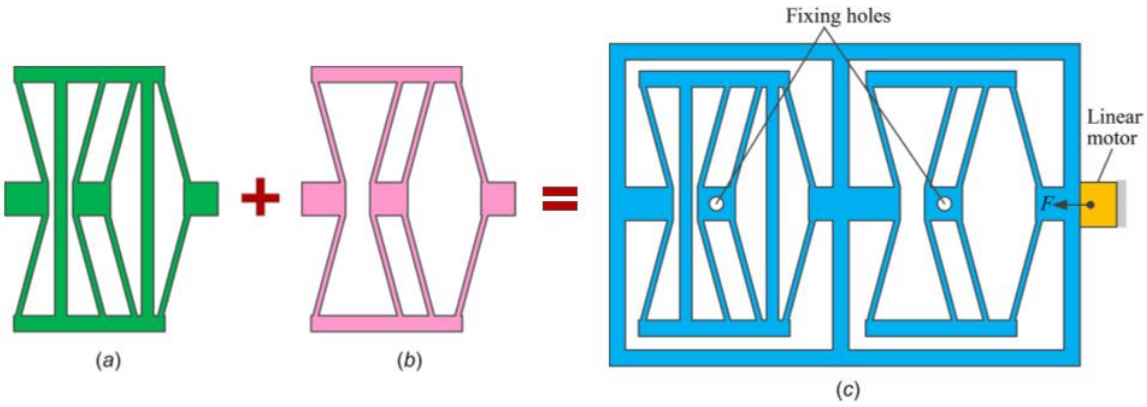

Figure 8. (a) Bistable mechanism (b) Positive-stiffness mechanism (c) Constant force mechanism [15]

As another example, Liu et al. designed a constant force gripper [16], which includes bistable beams as shown in Figure 9 to create constant force output.

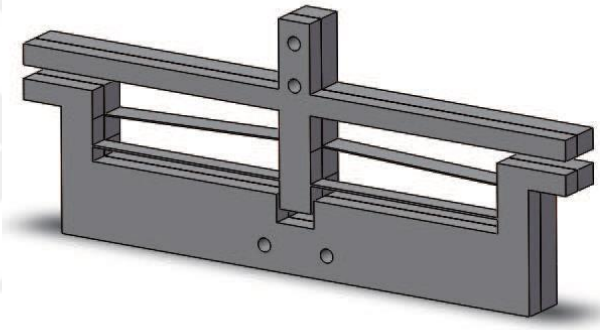

Figure 9. Compliant constant force module [16]

As an alternative to superimposed zero-stiffness systems, special beam shapes which yield zero-stiffness can also be used. For example, Lan and Chen developed a monolithic compliant constant force mechanism as shown in Figure 10, by utilizing a special beam shape, and their experimental product is capable of delivering a nearly constant axial force of 8 to 8.59 N during a height variance of 5 mm [17]. Lan et al. also developed an adjustable compliant constant force mechanism as given in Figure 11, which passively regulates the contact force [5].

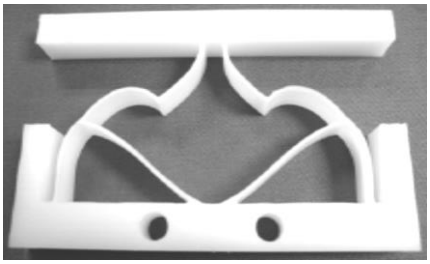

Figure 10. A monolithic compliant constant force mechanism [17]

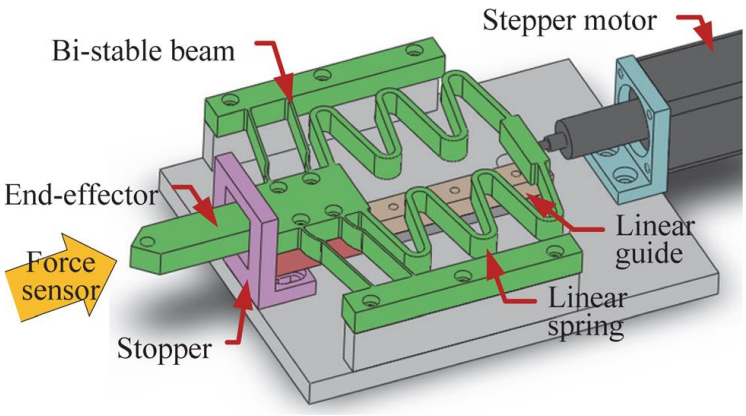

Figure 11. Adjustable compliant constant force mechanism [5]

Briefly, compliant constant force mechanisms have some advantages such as no backlash and wear, reduced number of components, and higher accuracy over rigid-link constant force mechanisms. However, complicated mathematical models or analysis tools are required to implement compliant constant force mechanism designs into commercial or industrial applications. Also, they may require precision manufacturing which increases the cost, and since material parameters are essential in these designs, slight changes in these parameters may affect the characteristics of the mechanism greatly. [8]

1.2 Grippers

Gripping or grasping an object is one of the important tasks for the robot manipulators. Requirements for gripping operation may vary greatly with respect to specific task, such as cycle time, gripping force, need for precision, working environment, and shape, size and weight of the part to be gripped. [18] Besides, gripping operations are required in vastly divergent industries including but not limited to factories, assembly lines, agriculture [19], surgery [20], oil stations [21], power plants, military operations such as mine clearing, and even nuclear reactors [22]. This situation yields to a need for very different types of grippers in terms of configuration or actuation method.

1.2.1 Rigid Grippers

Simplest way of holding an object is restraining its motion in required directions via applying force through other rigid bodies. This type of grippers consists of fingers or “claws”, which provides enough space when approaching to the object to be grasped and can be closed to hold the object. Fingers usually have revolute or prismatic joints for this closing operation. This type of grippers can either provide form closed of force closed gripping operation, as

shown in Figure 12. Also, there are programmable grippers which can achieve both gripping styles, as shown in Figure 13. The shape and quantity of fingers can be configured according to the specific task for which they are designed.

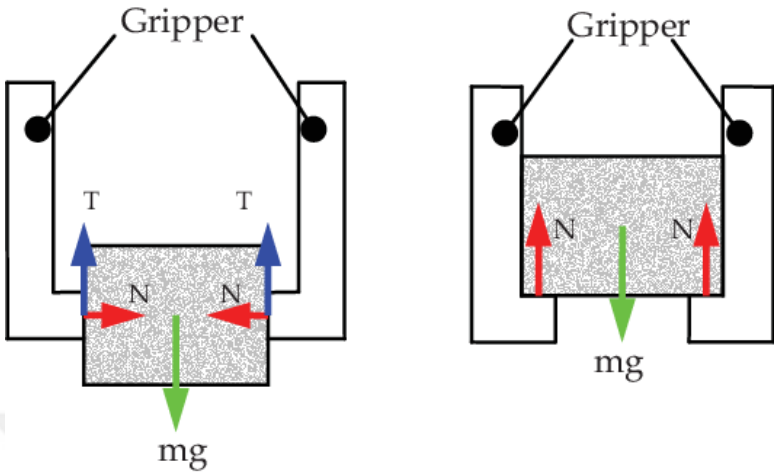

Figure 12. Force closed (left) and form closed (right) gripping [23]

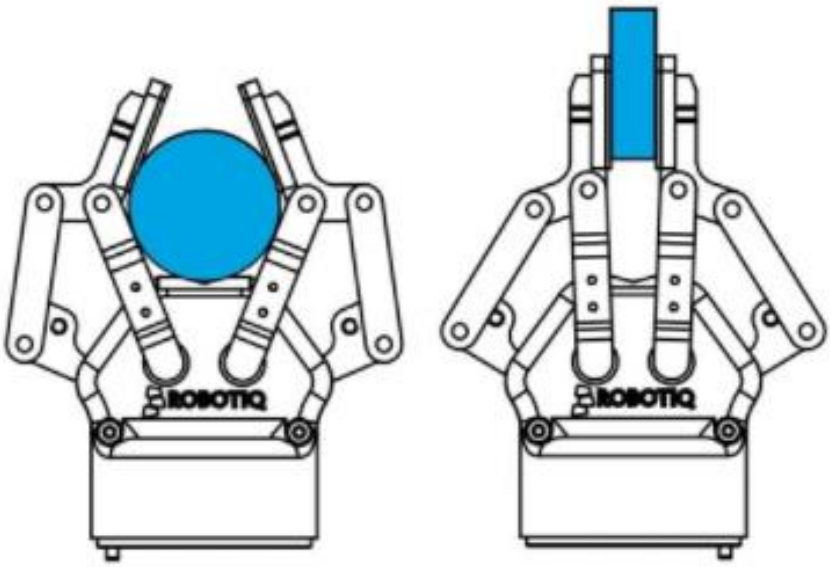

Figure 13. A gripper with different gripping modes [24]

Figure 14. Two finger grippers with prismatic (left) and pin (right) joints [25]

1.2.2 Flexible Grippers

This type of grippers has flexible fingers that can alter its shape according to either reaction forces of the object to be gripped, or internal forces created by its actuators. This can be achieved by various methods, including but not limited to using specially shaped compliant materials as fingers (Figure 15) or vacuuming a water filled silicone cap and wrapping it around the object (Figure 17). These grippers are advantageous especially when the object to be hold is fragile or can be easily deformed, or has an unorthodox shape. [18]

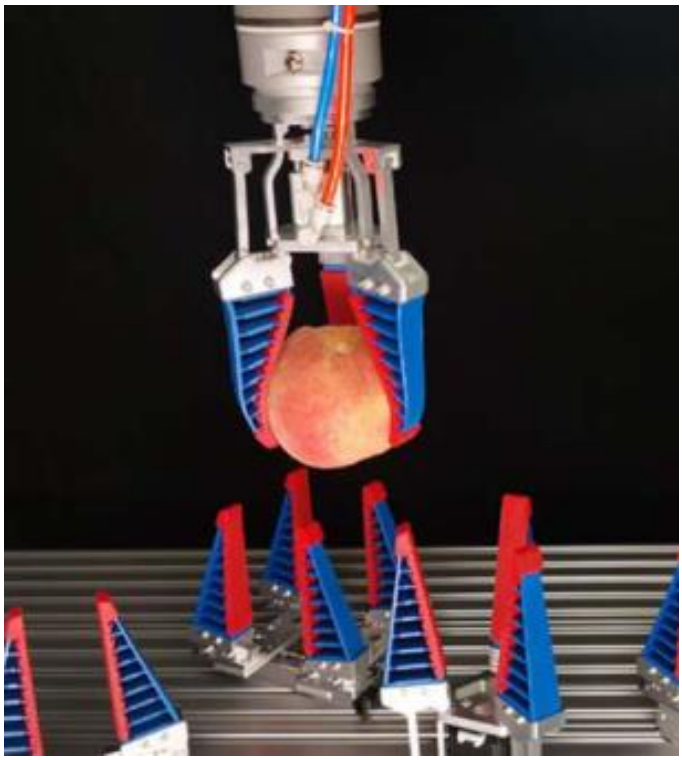

Figure 15. Flexible adaptive gripper [26]

Another type of flexible grippers is bellows gripper. Especially preferred for cylindrical objects, this type of gripper consists of an elastomer bladder which can be inflated to hold the part and deflated to release it. Different configurations to hold the part from inner or outer surface are available as shown in Figure 16.

Figure 16. Inside (left) and outside (right) type bellow grippers

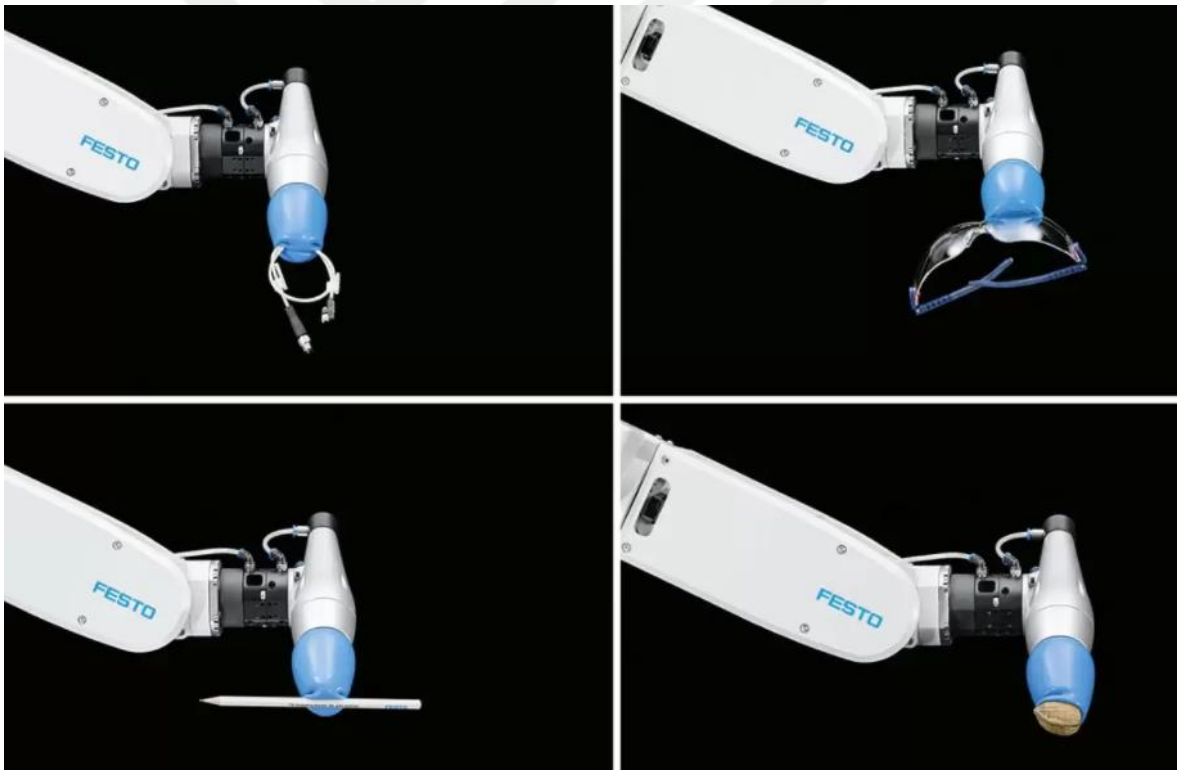

Figure 17. A flexible gripper, modelled on a chameleon's tongue [27]

Since gripping technologies and some "hot topic" research areas such as stretchable electronics and electro-adhesion (Figure 18) meet on a common ground, there are also various studies to design and develop actuators for soft robotics, using polymer rubbers as

grippers (Figure 19). Detailed overviews and surveys [28] [29] available to summarize recent developments in this area.

Figure 18. Gripping with electro-adhesion [30]

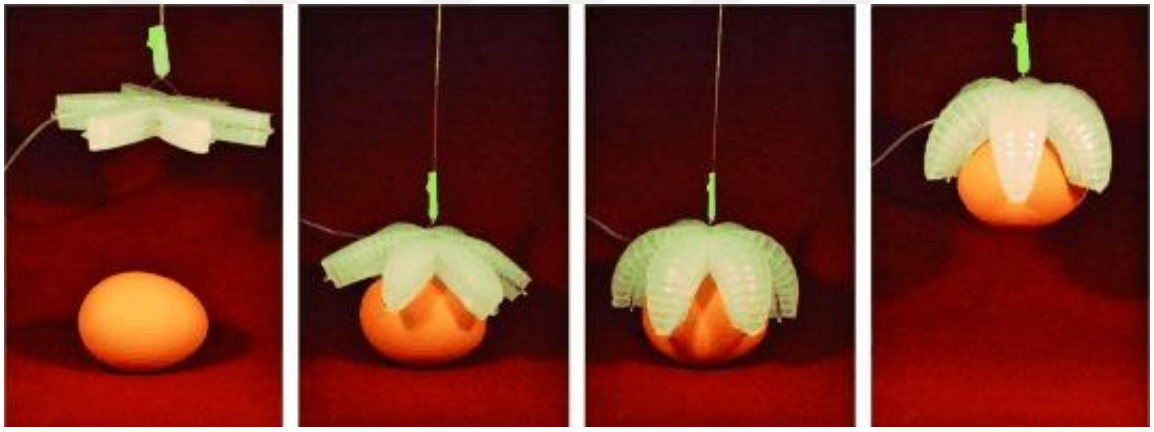

Figure 19. Gripping with pressurizing soft elastomers [31]

1.2.3 Application Specific Grippers

Apart from grippers mentioned in Section 1.2.1 and 1.2.2, there are also specialized grippers for specific tasks. These designs are stimulating in order to comprehend that, industry specific needs, operating conditions, environmental requirements, or any other design parameter may create the need to find solutions beyond existing ones. For example, needle grippers can be used for porous or textile-based materials such as fabrics, fleece, filter materials, insulation foams etc. which are difficult to handle using conventional methods. A needle gripper is shown in Figure 20 as an example.

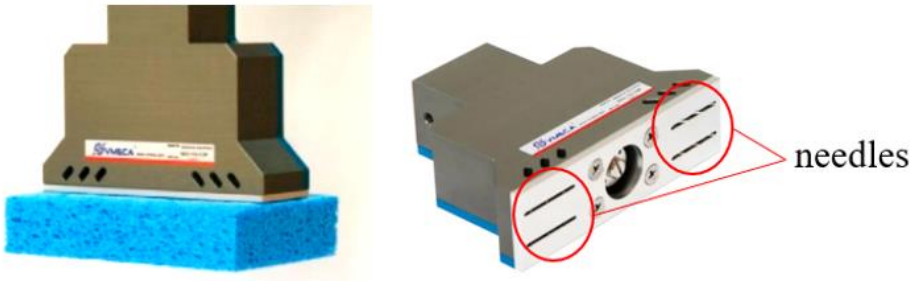

Figure 20. Needle gripper [32]

Another example to application specific gripper is O-ring gripper. This type of gripper is similar to a multi fingered parallel grippers, with radially expandable jaws that can grip the O-ring from the inside surface. After the O-ring is tensioned, it can be inserted into corresponding groove on a cylindrical shaft, as shown in Figure 21. With some additional dies, this type of grippers can also be used in bores for internal assembly.

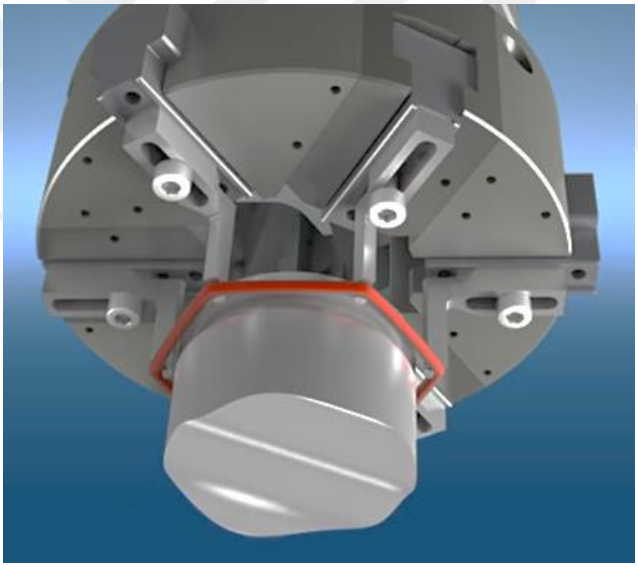

Figure 21. O-ring gripper [25]

1.2.4 Actuation Methods

Most common actuation methods for grippers are cable driving, vacuuming, pressurizing (either pneumatic or hydraulic) and using servo electric motors. As in all engineering design options, each of these actuation methods have some advantages and disadvantages. These are summarized by Samadikhoshkho et al. as presented in Table 1.

Table 1. Comparison of gripper actuation methods [33]

Gripper Type	Advantages	Disadvantages
Cable-driven	- Optimal weight and space	- Control complexity
Vacuum	- Highly flexible - Clean	- Operational issues
Pneumatic	- Small dimension - Low weight - Clean	- Not precise enough - High operating cost
Hydraulic	- High force	- Not clean enough - High maintenance cost
Servo-electric	- Highly flexible - Low maintenance cost - Easily controllable - Clean	- Low force

2 PROPOSED NOVEL CONSTANT FORCE LINK

2.1 Introduction of Proposed Link

In this thesis, we propose a constant force link consisting a pivoted link and spring as presented in Figure 22. The aim is to obtain constant horizontal force vs. stroke for a constant input torque T. This torque may be applied with an electric motor with a specified constant maximum current, or by mechanical means. Thus, sensors, controllers are not mandatory for this mechanical logic element that yields cost decrease. A constant torque T is applied and a tension spring with a stiffness k is positioned as shown. F is a horizontal non-follower gripping force at B and is a function of input angle α, which is initially $\alpha_0 = 90°$. β is the angle in between spring and horizontal axis that also varies with input angle α, and β_0 represents its initial value. s represents length of the spring for a given input angle α and $|AC| = s_0$ represents unstretched length of the spring. Let $|OA| = m$ and $|OB| = l$.

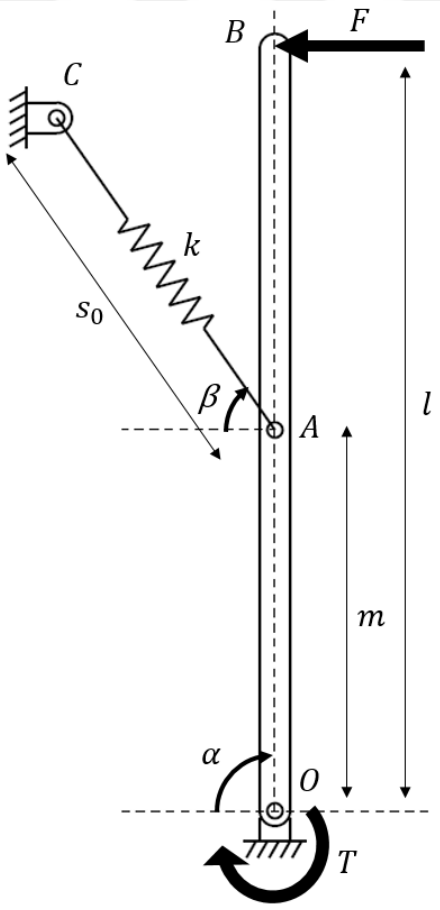

Figure 22. Proposed Link

2.2 Force Analysis

To define the relationship between F and input angle α, moment about O can be taken as follows

$$\sum M_O = 0$$

$$\vec{T} = \overrightarrow{OA} \times \vec{F_s} + \overrightarrow{OB} \times \vec{F}$$

where F_s is the force exerted by spring and values of both F_s and F are positive. Thus

$$T = km(s - s_0)\sin(\alpha - \beta) + Fl\sin\alpha$$

$$F = \frac{T - km(s - s_0)\sin(\alpha - \beta)}{l\sin\alpha} \quad (1)$$

In Equation (1) all parameters except β and s are either defined or a function of input α. Thus, it is required to define β and s as functions of α and other known parameters. From the kinematics of the system

$$-s_0\cos\beta_0 + \mathrm{i}(m + s_0\sin\beta_0) = m\mathrm{e}^{\mathrm{i}(\pi-\alpha)} + s\mathrm{e}^{\mathrm{i}(\pi-\beta)}$$

Thus

$$-s_0\cos\beta_0 = m\cos(\pi - \alpha) + s\cos(\pi - \beta)$$

$$m + s_0\sin\beta_0 = m\sin(\pi - \alpha) + s\sin(\pi - \beta)$$

Which can be rearranged as

$$s\cos\beta = s_0\cos\beta_0 - m\cos\alpha \quad (2)$$

$$s\sin\beta = m + s_0\sin\beta_0 - m\sin\alpha \quad (3)$$

From Equations (2) and (3) β and s can be determined as

$$\beta = \tan^{-1}\left(\frac{m + s_0\sin\beta_0 - m\sin\alpha}{s_0\cos\beta_0 - m\cos\alpha}\right) \quad (4)$$

$$s = \frac{s_0\cos\beta_0 - m\cos\alpha}{\cos\beta} \quad (5)$$

By using Equations (4) and (5), Equation (1) is now a function of α and structural parameters, and can be rewritten as in Equation (6).

$$F = \frac{T + km^2\left(\frac{\cos\alpha}{\cos\beta}\right)\sin(\alpha-\beta)}{l\sin\alpha} \tag{6}$$

Also, let x is the horizontal displacement of B as follows

$$x = |OB'|_x - |OB|_x$$
$$x = -l\cos\alpha \tag{7}$$

where B' is the position of B for an arbitrary value of α. It is visualized in Figure 23.

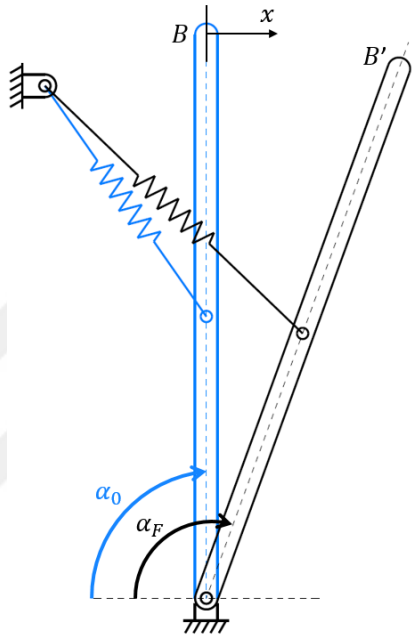

Figure 23. Constant force link at initial and final positions

While α varies from 90° to α_F, F values are also varying in between F_{min} and F_{max}, and let F_{mean} is the mean value as given in Figure 24. Note that, Figure 24 is given to clarify F_{min}, F_{max} and F_{mean} values solely and plot in Figure 24 does not necessarily represent the behavior of the mechanism.

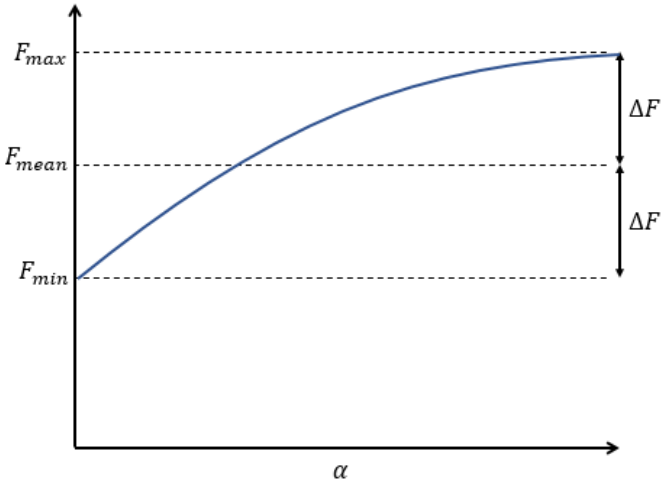

Figure 24. Representation of F_{max}, F_{min} and F_{mean} values

To represent the deviation of F, a parameter, F_{dev} is defined as follows

$$F_{dev} = \frac{\Delta F}{F_{mean}} = \frac{F_{max} - F_{min}}{F_{max} + F_{min}} 100 \tag{8}$$

where

$$\Delta F = \frac{F_{max} - F_{min}}{2}$$

If all the required parameters are defined, x and F for every value of α can be calculated. It is summarized in Table 2.

Table 2. Design parameters, input and outputs

Parameters that require to be defined	**Input variable**	**Output variables**
$Structure\ parameters: m, l, k, s_0, \beta_0$	α	$x(\alpha), F(\alpha)$
$Force\ parameter: T$		

We aim to obtain design charts to evaluate the parameters on the left side of Table 2 for any x and F values intended.

2.3 Role of Spring in the System

In order to prove necessity of the spring in the system, two positions where $\alpha_0 = 90°$ and $\alpha_F = 90° + \rho$ are analyzed with and without spring, where ρ is the angle which satisfies $0° < \rho < 90°$. F_1 and F_2 represent the horizontal forces without spring and F_{1s} and F_{2s}

represent the horizontal forces with spring at $\alpha_0 = 90°$ and $\alpha_F = 90° + \rho$, respectively. These forces are visualized in Figure 25 and 26.

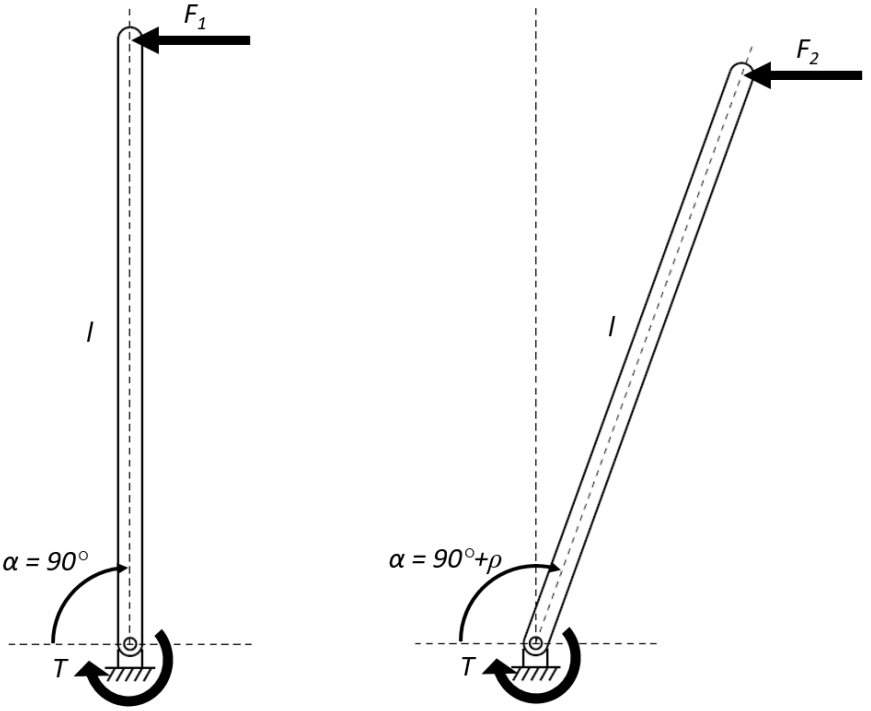

Figure 25. Representation of F_1 and F_2

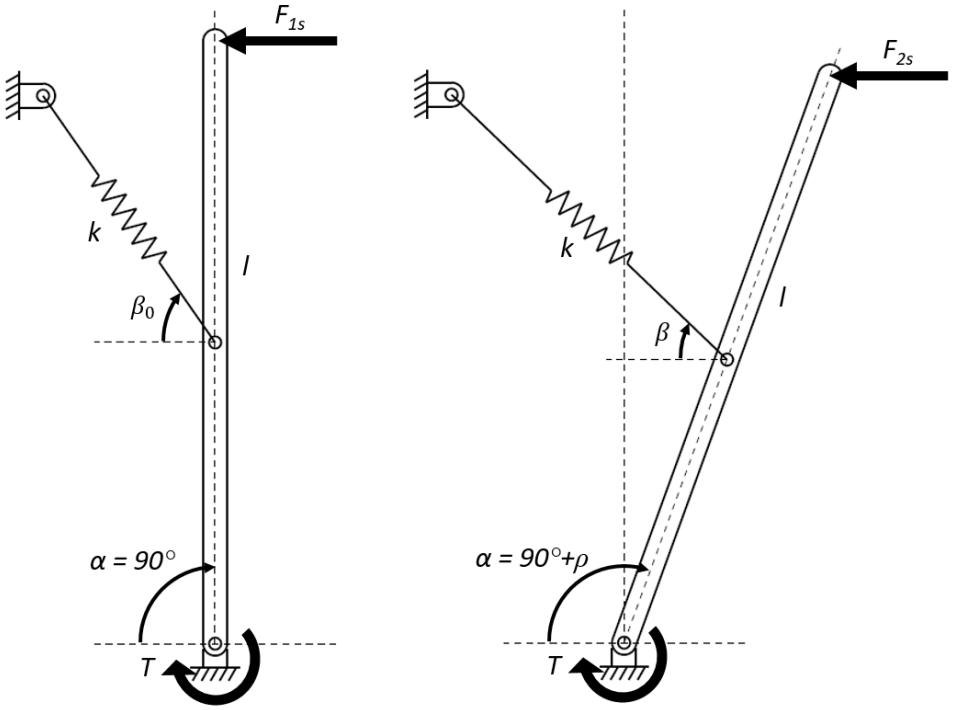

Figure 26. Representation of F_{1s} and F_{2s}

F_1 and F_2 can be calculated as follows,

$$F_1 l = T \quad \rightarrow \quad F_1 = \frac{T}{l}$$

$$F_2 \sin(90° + \rho) l = T \quad \rightarrow \quad F_2 = \frac{T}{\sin(90° + \rho) l}$$

Thus, relationship between F_1 and F_2 can be expressed as for

$$F_2 > F_1$$

which can be interpreted as F starts from F_1 and continuously increases till the end of motion and reaches F_2 as its maximum value. Furthermore, for a given value of ρ, F_{dev} can be calculated from Equation (8) as

$$F_{dev} = \frac{\frac{T}{\sin(90° + \rho) l} - \frac{T}{l}}{\frac{T}{\sin(90° + \rho) l} + \frac{T}{l}} 100 = \frac{1 - \cos\rho}{1 + \cos\rho} 100 \tag{9}$$

Also, F_{1s} and F_{2s} can be calculated as follows

$$F_{1s} l = T \quad \rightarrow \quad F_{1s} = \frac{T}{l}$$

$$F_{2s} l \sin(90° + \rho) + km(s - s_0) \sin(90° + \rho - \beta) = T \quad \rightarrow \quad F_{2s} = \frac{T - km(s - s_0)\cos(\rho - \beta)}{l \cos\rho}$$

It can be concluded that, the relationship between F_{1s} and F_{2s} is dependent to many other parameters. These parameters may be selected so that, the increase in F is compensated by generated spring force as α changes from 90° to α_F. Appropriate selection of these parameters is the basis of this thesis.

2.4 Determination of α_0 and α_F Angles

Since the spring is unstretched at α_0, as α starts to increase from α_0, spring force will also start to increase from zero. The spring force will aid the initial force at the tip of link to overcome T, thus F becomes geometrically disadvantageous as the motion starts in order to yield a constant force. Thus, the selection of $\alpha_0 = 90°$ is fairly straightforward.

In the other hand, selection of α_F defines the maximum value of x for a given value of l, thus specifies the operating range where a constant force is aimed to be obtained. $\alpha_F = 90 + \rho$ can be inserted into Equation (7) to define this relationship as

$$x_{max} = l \sin \rho \tag{10}$$

Let x_{max} be one third of l, which results $\rho = \sin^{-1}(1/3) = 19.47°$. This value may be rounded up to $\rho = 20°$, and may be inserted into Equation (9) and F_{dev} can be calculated as

$$\frac{1 - \cos 20°}{1 + \cos 20°} 100 = 3.11\%$$

This can be interpreted as, if a lower F_{dev} value than 3.11% can be achieved with the structure parameters m, l, k, s_0 and β_0, we can conclude that with presence of the spring a better constant force characteristic is obtained for $\alpha = 90° \dots 110°$ interval. However, significant difference (for example $F_{dev} < 0.2\%$) will be achieved in order to provide a feasible constant force throughout motion.

3 DESIGN APPROACHES FOR THE CONSTANT FORCE LINK

3.1 Dimensionless Force-Deflection Approach

In order to obtain dimensionless design charts (i.e. for calculating parameters on the left hand side of Table 2 for any x and F values intended), both sides of Equation (1) can be divided by km and l in the denominator at the right side can be moved to the numerator. Thus, Equation (1) can be rearranged as

$$\frac{F}{km} = \frac{\frac{T}{kml} - \frac{(s - s_0)}{l}\sin(\alpha - \beta)}{\sin\alpha} \tag{11}$$

Note that, both s and β in Equation (11) are functions of α, however left as they are for simplicity. Now Equation (11) can be expressed simply as a function of α as

$$\frac{F}{km} = \frac{\frac{T}{kml} + \frac{m}{l}\left(\frac{\cos\alpha}{\cos\beta}\right)\sin(\alpha - \beta)}{\sin\alpha} \tag{12}$$

Where β was expressed as a function of α in Equation (4).

Note that parameters, $F/km,\ T/kml,\ (s - s_0)\sin(\alpha - \beta)/l$, and $\sin\alpha$ are now unitless in Equation (11). Now let us call dimensionless load parameters $F' = F/km$ and $T' = T/kml$ as F' and T' respectively. Now Equation (11) becomes

$$F' = \frac{T' - \frac{(s - s_0)}{l}\sin(\alpha - \beta)}{\sin\alpha} \tag{13}$$

In addition, s in Equation (13) may be expanded as defined in Equation (5), thus Equation (13) becomes

$$F' = \frac{T' - \left[\left(\frac{s_0\cos\beta_0}{l\cos\beta} - \frac{m\cos\alpha}{l\cos\beta} - \frac{s_0}{l}\right)\sin(\alpha - \beta)\right]}{\sin\alpha} \tag{14}$$

Likewise, both the numerator and denominator in $\tan^{-1}$ function at the right side of Equation (4) may be divided by l, which yields,

$$\beta = \tan^{-1}\left(\frac{\frac{m}{l} + \frac{s_0 \sin\beta_0}{l} - \frac{m \sin\alpha}{l}}{\frac{s_0 \cos\beta_0}{l} - \frac{m \cos\alpha}{l}}\right) \tag{15}$$

3.2 Obtaining Design Chart for an Arbitrary Search Space

Let s_0/l and m/l are predefined. In this case, β can be calculated from Equation (15) for a given value of β_0 and α. Afterwards, if T' is also defined, F' can be calculated from Equation (14) for a given value of β_0 and α. Therefore, a 3D plot can be obtained to observe variation of F' with respect to β_0 and α for given parameters.

As an example, 3D plot in Figure 27 may be obtained if the parameters $m/l, s_0/l$ and T' are defined as 0.5, 0.5 and 1, respectively. Also, α_0 and α_F are selected as 90° and 110°, as explained in Section 2.4. Lower and upper bounds for β_0 are defined as 65° and 85°. Note that, same plot is visualized from two different angles to improve visuality.

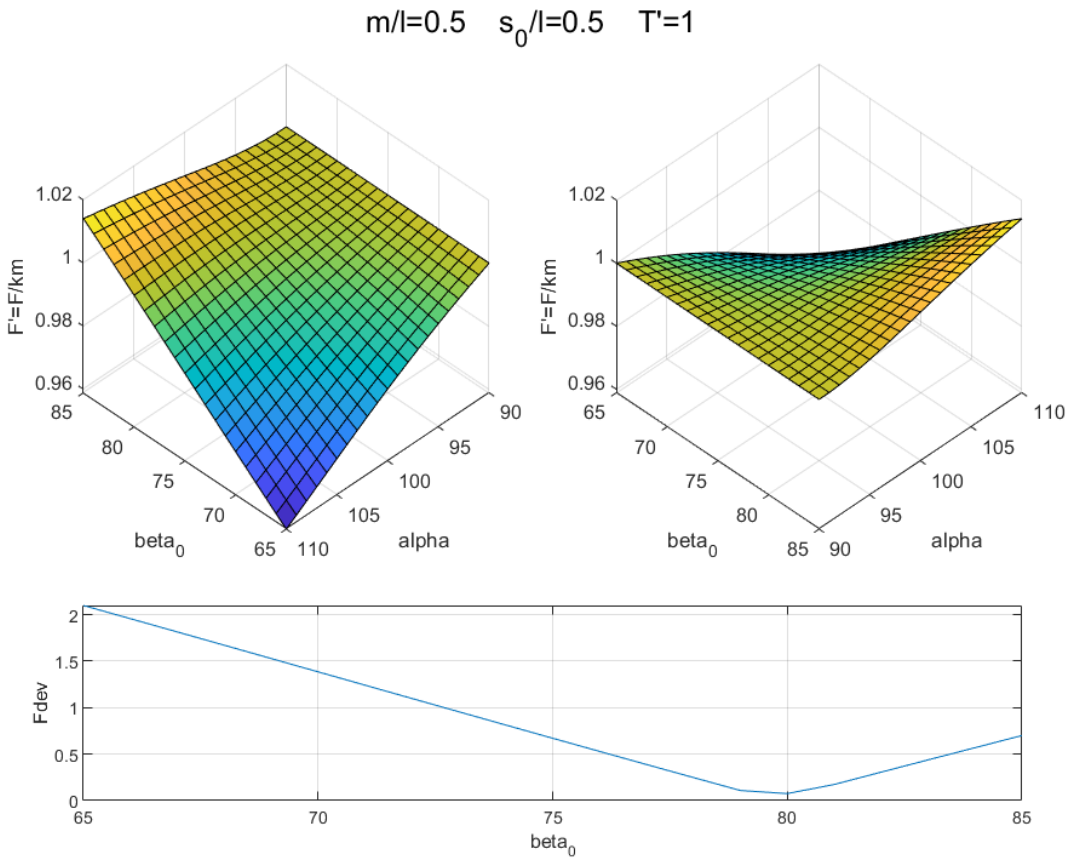

Figure 27. Example 3D plot and corresponding F_{dev} vs. β_0 plot

Note that, around $\beta_0 = 80°$, F_{dev} is in its minimum value for this search space, i.e. if $m/l, s_0/l$ and T' are defined as 0.5, 0.5 and 1 respectively as presented in Figure 27, optimum angle to connect spring to link is 80° in terms of obtaining a constant force.

In Figure 28, another chart is shown. Only different parameter from Figure 27 is m/l, which is 0.25 instead of 0.5. However, if F_{dev} vs. β_0 plot of Figure 28 examined, it can be concluded that there is no β_0 which provides <1% F_{dev} values within $65° < \beta_0 < 85°$ region. Thus, either design parameters $m/l, s_0/l$ and T' must be changed or search space must be enlarged to include more β_0 angles to obtain lower F_{dev} values.

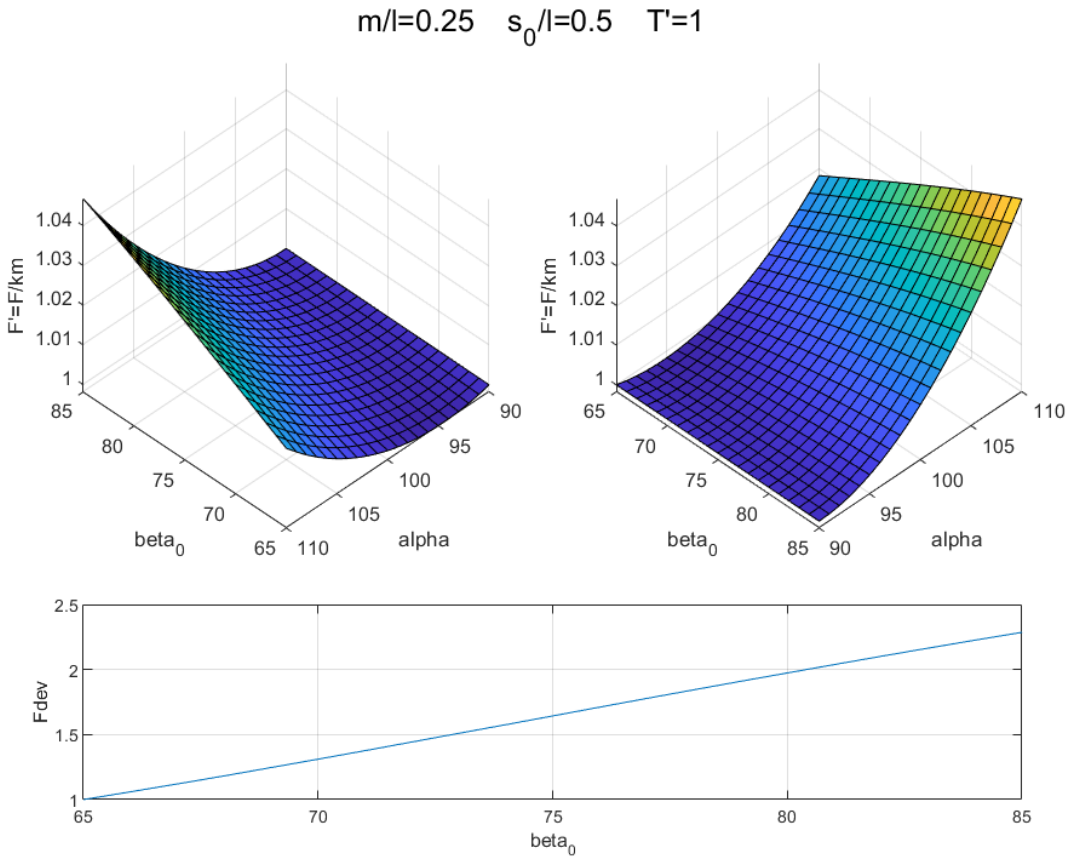

Figure 28. Example 3D plot ($m/l = 0.25, s_0/l = 0.5, T' = 1$)

Similarly, for the design chart given in Figure 29 only changing parameter from Figure 27 is s_0/l, which is chosen as 0.25 instead of 0.5. In contrary to Figure 28, there are F_{dev} values which are below 1% around 85°. However, to observe if that angle is corresponding to a local minimum or not, the space must be enlarged.

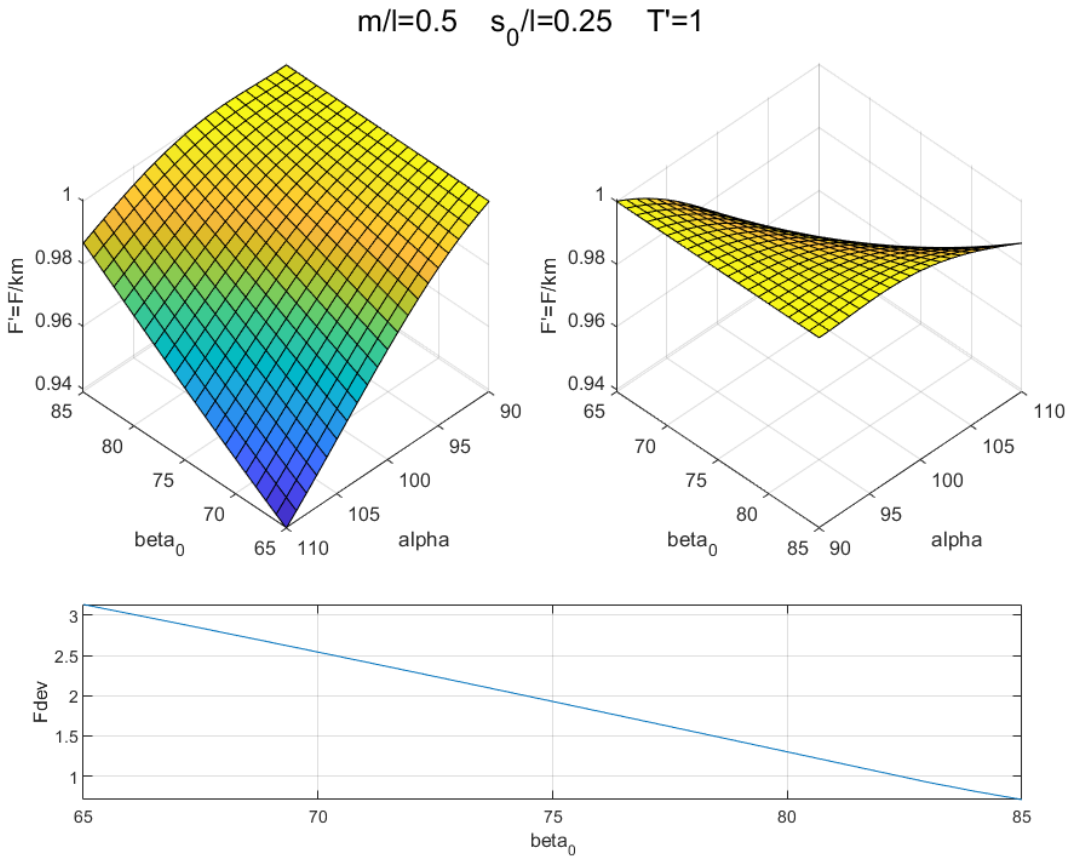

Figure 29. Example 3D plot ($m/l = 0.5, s_0/l = 0.25, T' = 1$)

To observe the effect of remaining parameter, another chart is given in Figure 30 where $T'$is changed from 1 to 10. Note that minimum F_{dev} is higher than the maximum values given in Figure 28 and 29.

A more comprehensive data set is required to be able to gain insight into the behavior of the parameters. Thus, three options for each parameter creates $3^3 = 27$ combinations, i.e. 27 different 3D chart can be obtained by assigning only three discrete value to each parameter. Parameters m/l and s_0/l are selected 0.25, 0.5 or 0.75, and T' selected as 1, 5 or 10. Four of these combinations already presented in Figure 27 to 30. Remaining combinations are given in Figure 31 to 53.

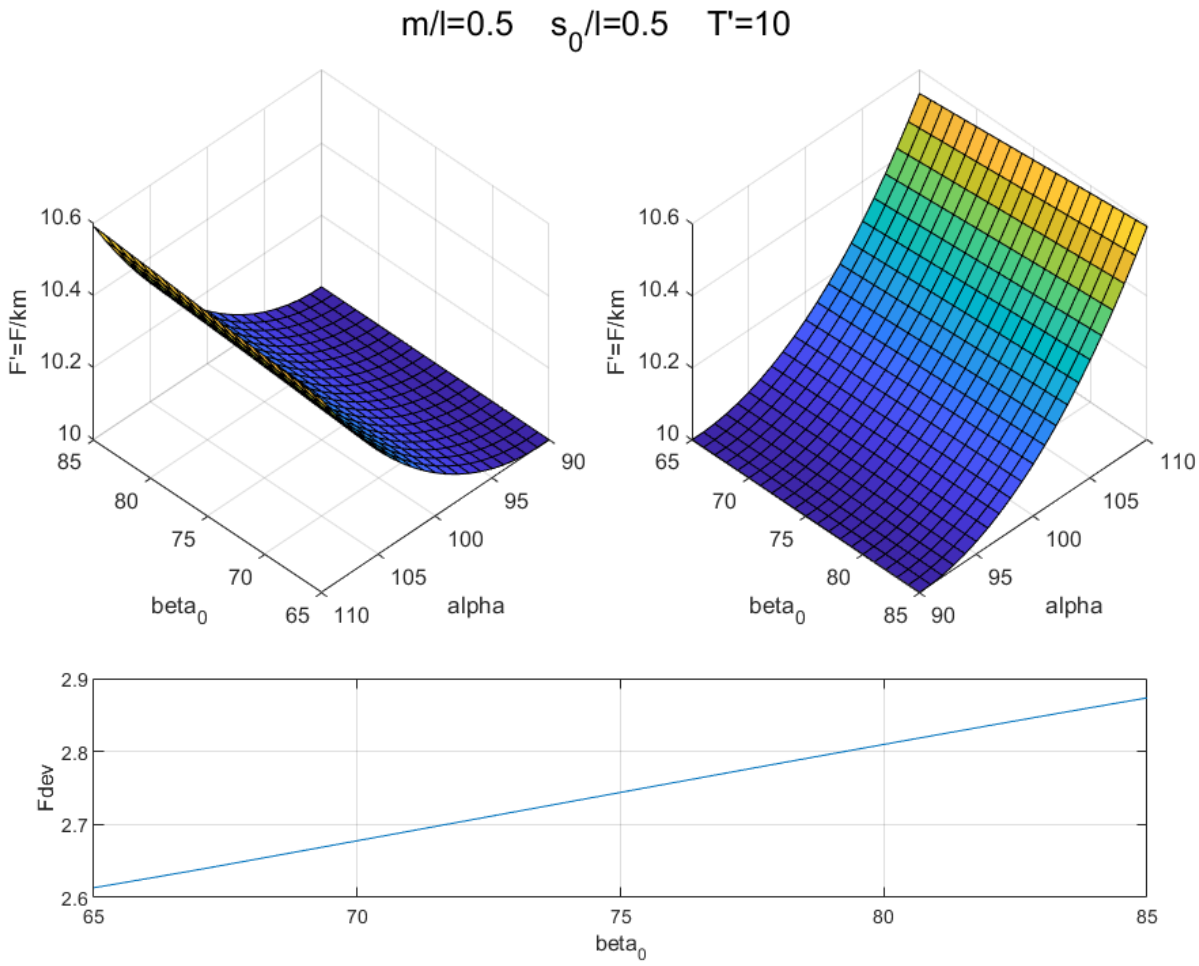

Figure 30. Example 3D plot ($m/l = 0.5, s_0/l = 0.5, T' = 10$)

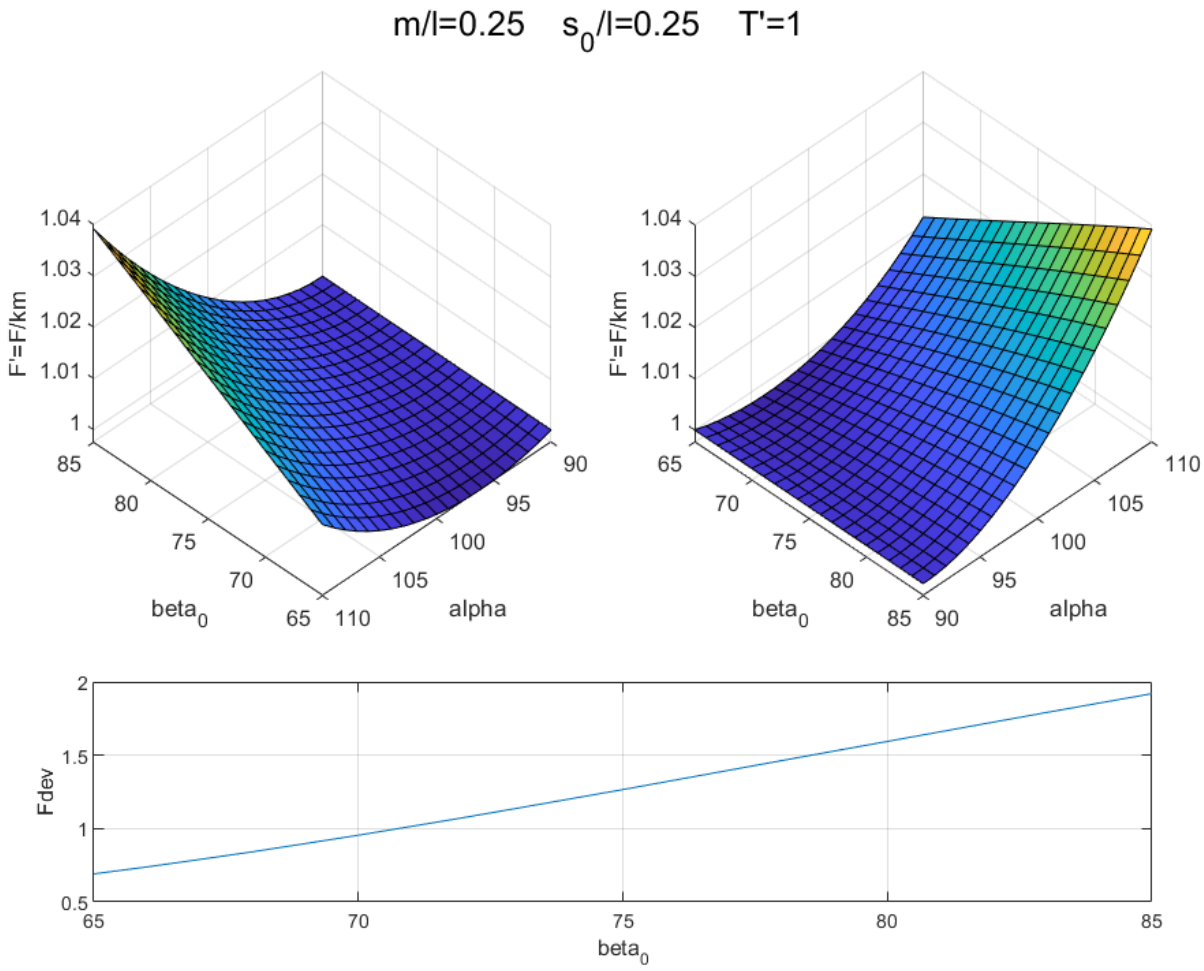

Figure 31. Example 3D plot ($m/l = 0.25, s_0/l = 0.25, T' = 1$)

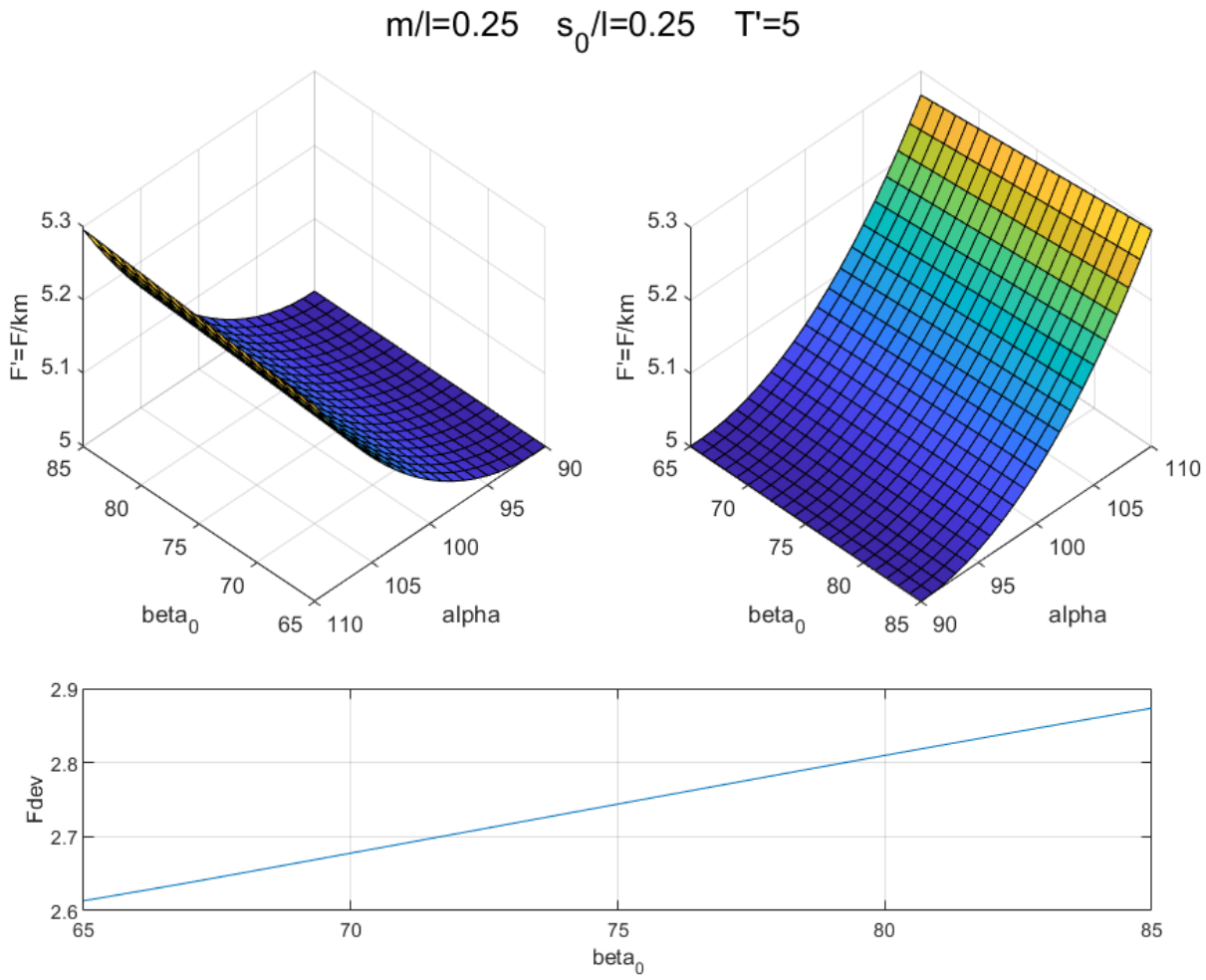

Figure 32. Example 3D plot ($m/l = 0.25, s_0/l = 0.25, T' = 5$)

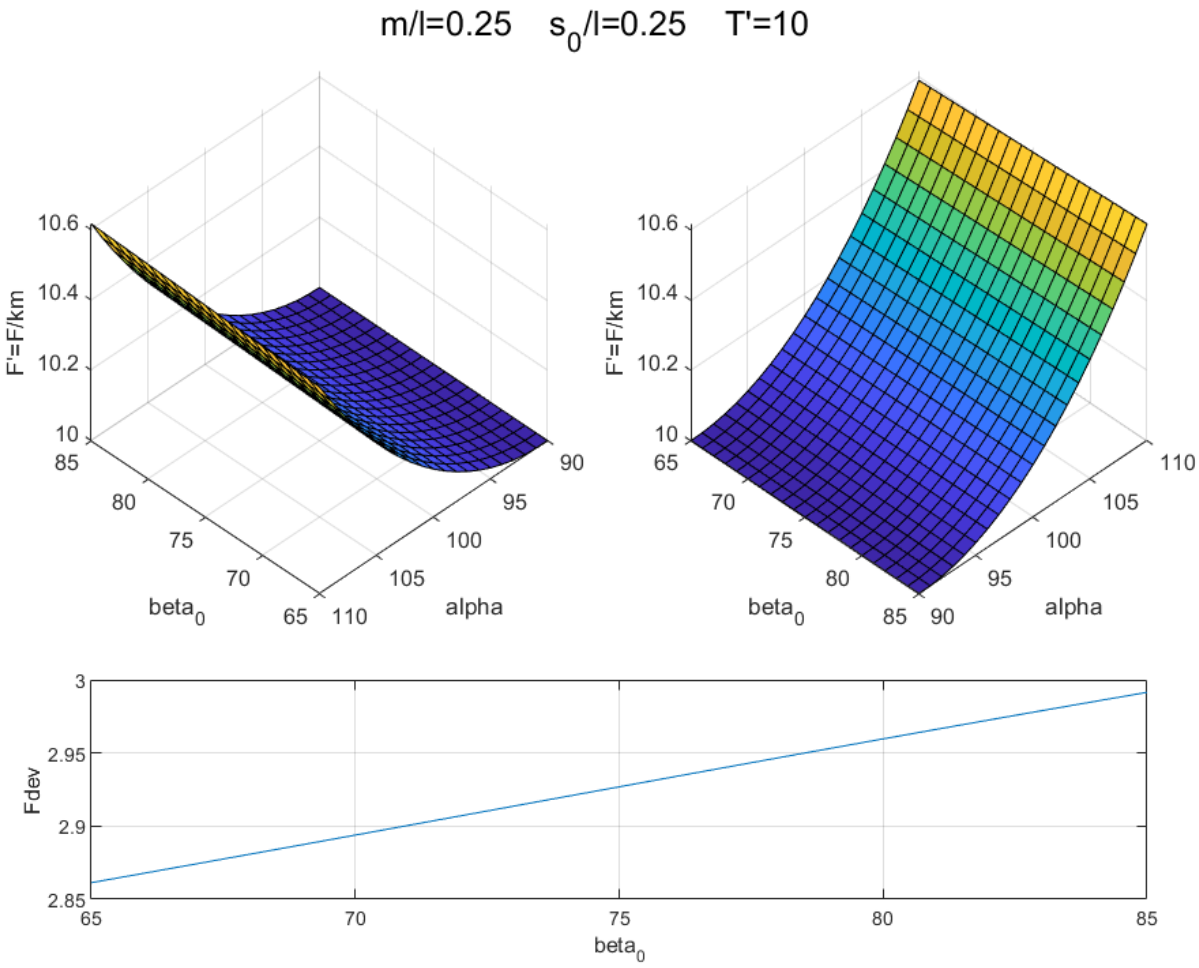

Figure 33. Example 3D plot ($m/l = 0.25, s_0/l = 0.25, T' = 10$)

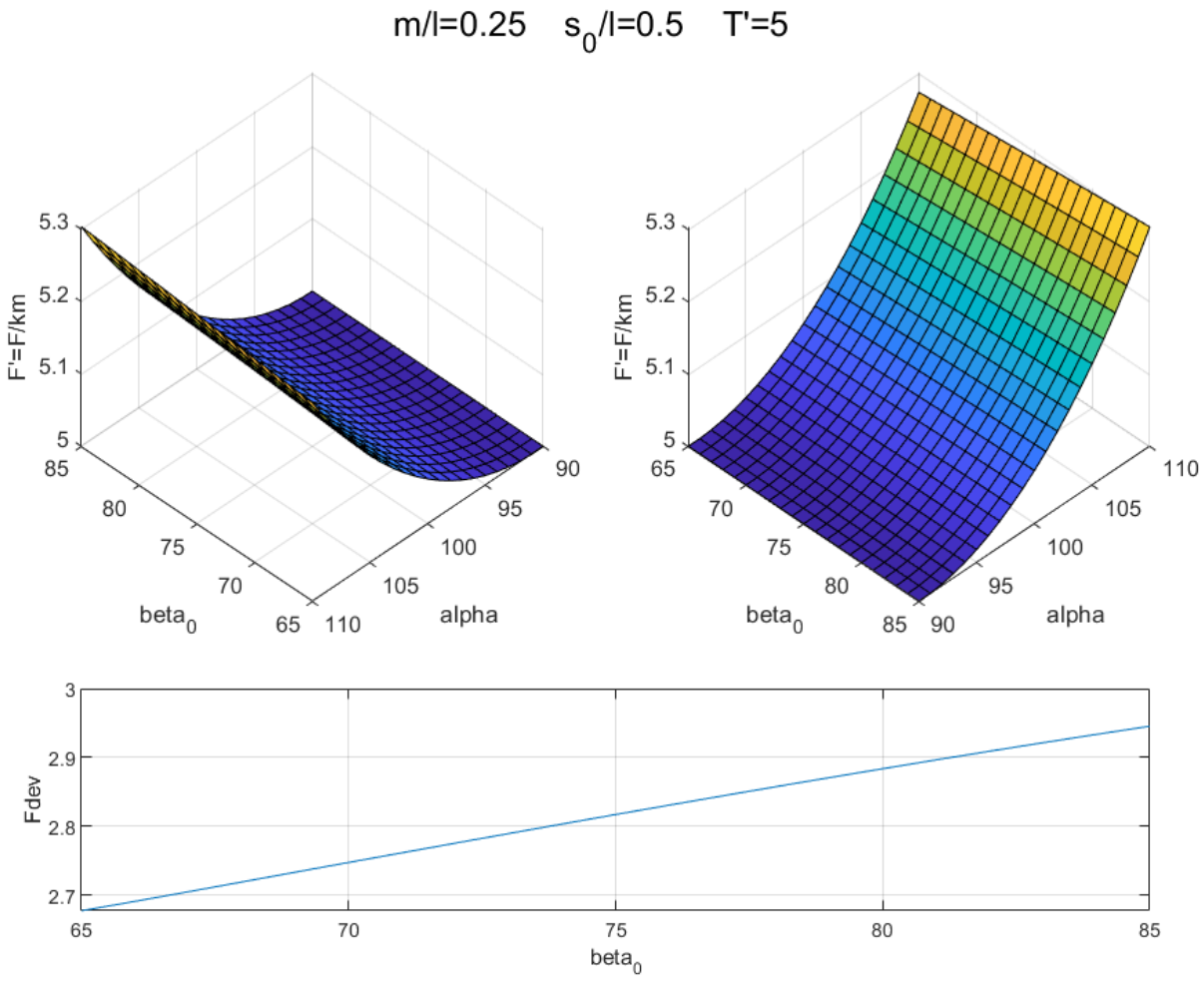

Figure 34. Example 3D plot ($m/l = 0.25, s_0/l = 0.5, T' = 5$)

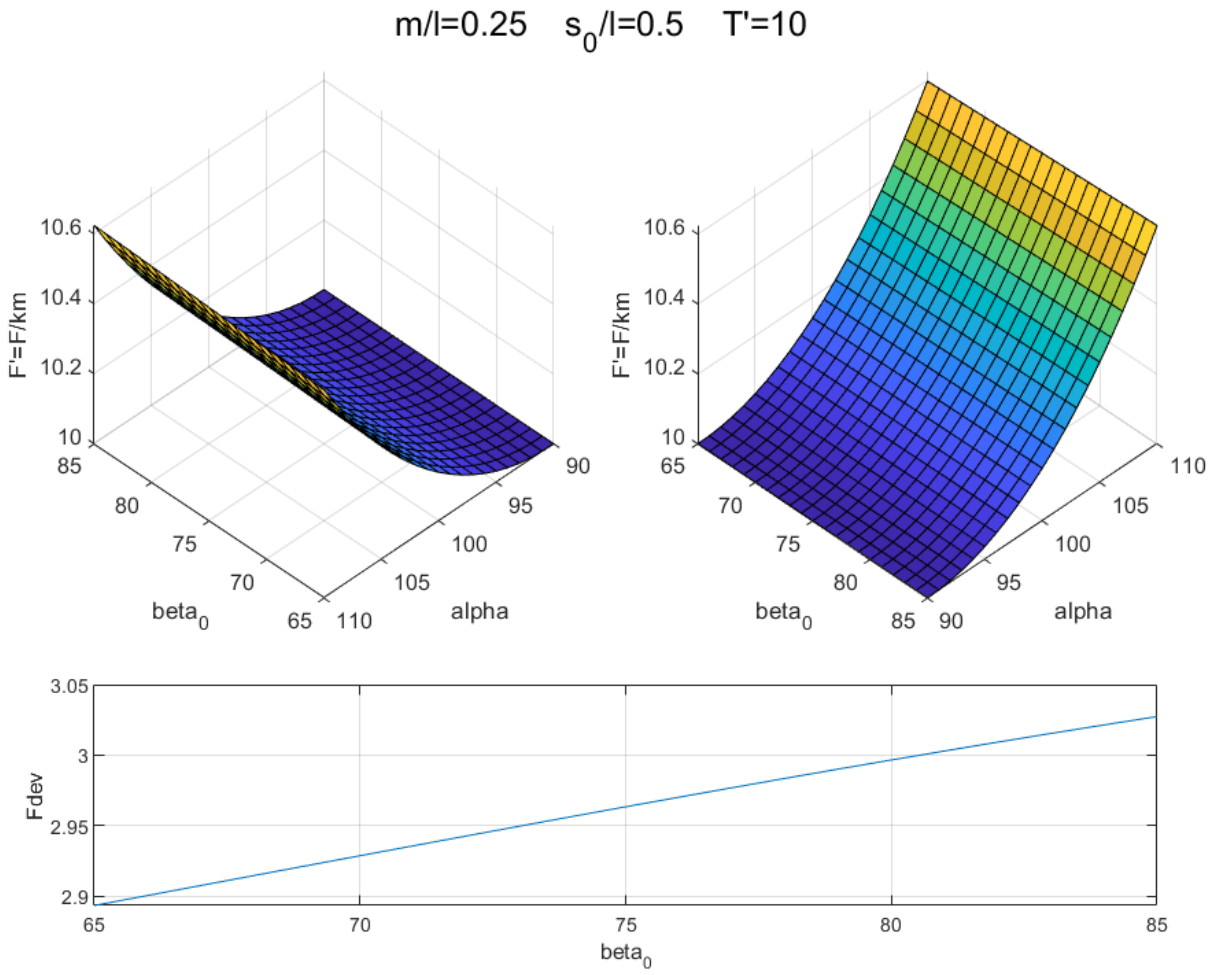

Figure 35. Example 3D plot ($m/l = 0.25, s_0/l = 0.5, T' = 10$)

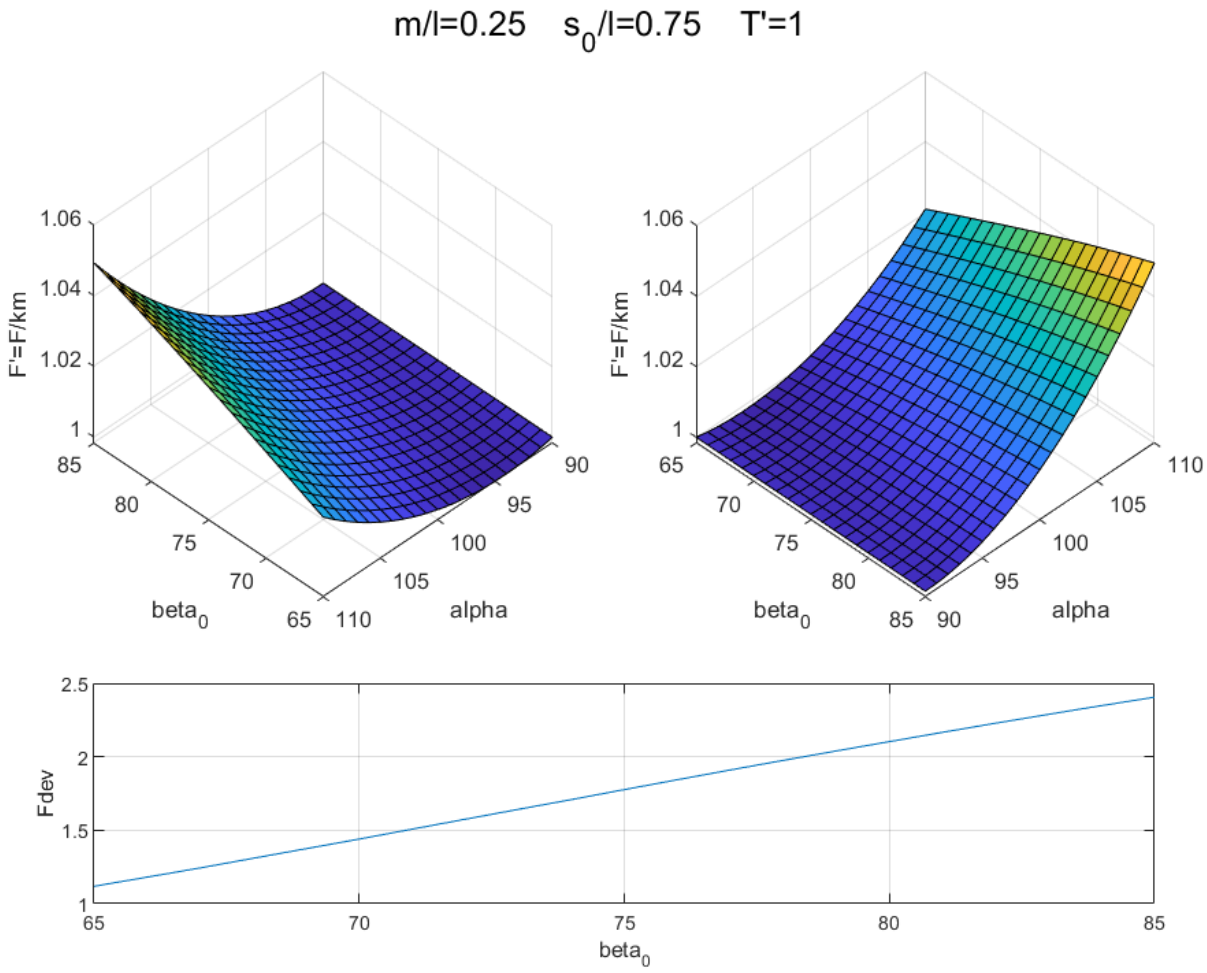

Figure 36. Example 3D plot ($m/l = 0.5, s_0/l = 0.75, T' = 1$)

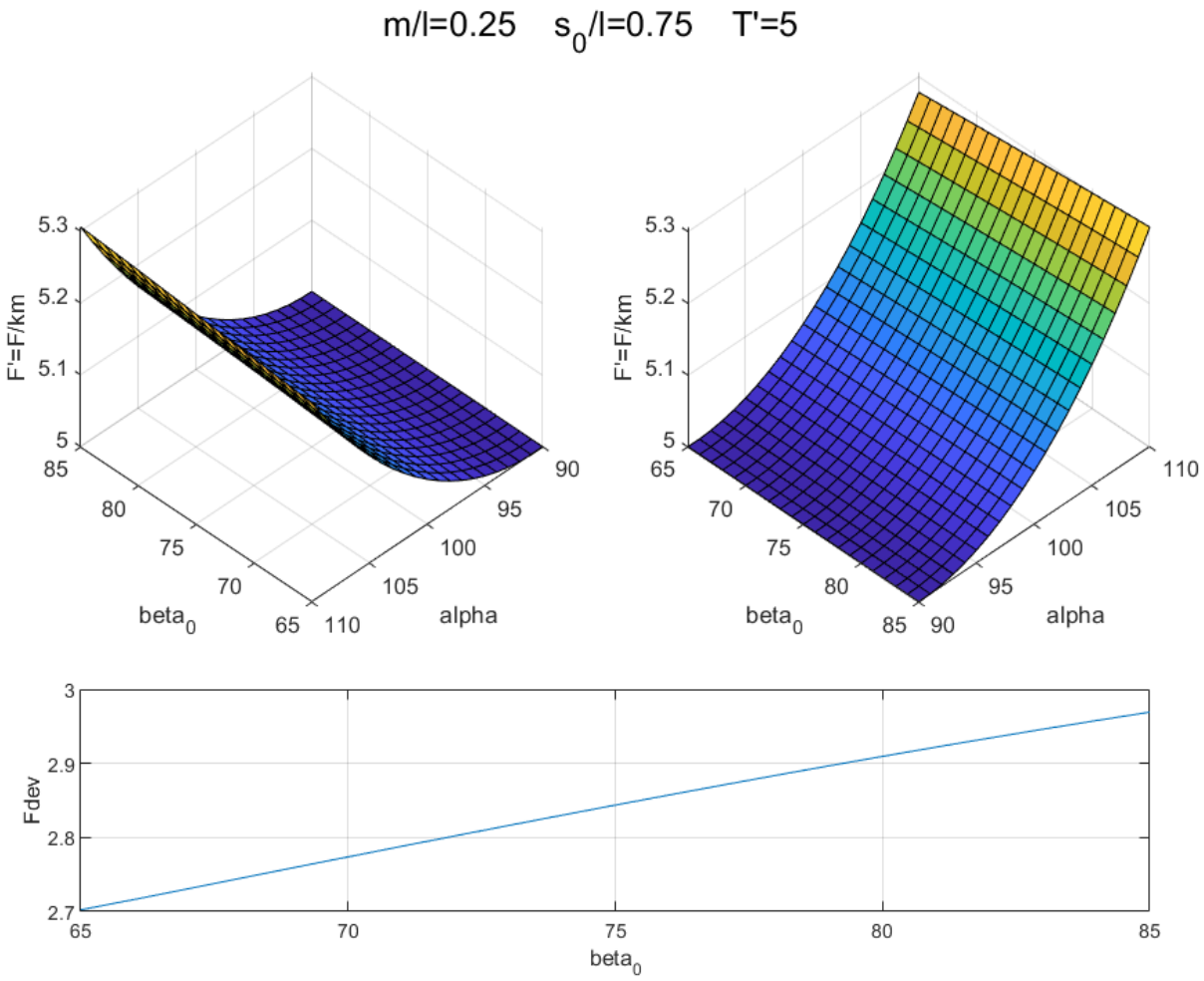

Figure 37. Example 3D plot ($m/l = 0.25, s_0/l = 0.75, T' = 5$)

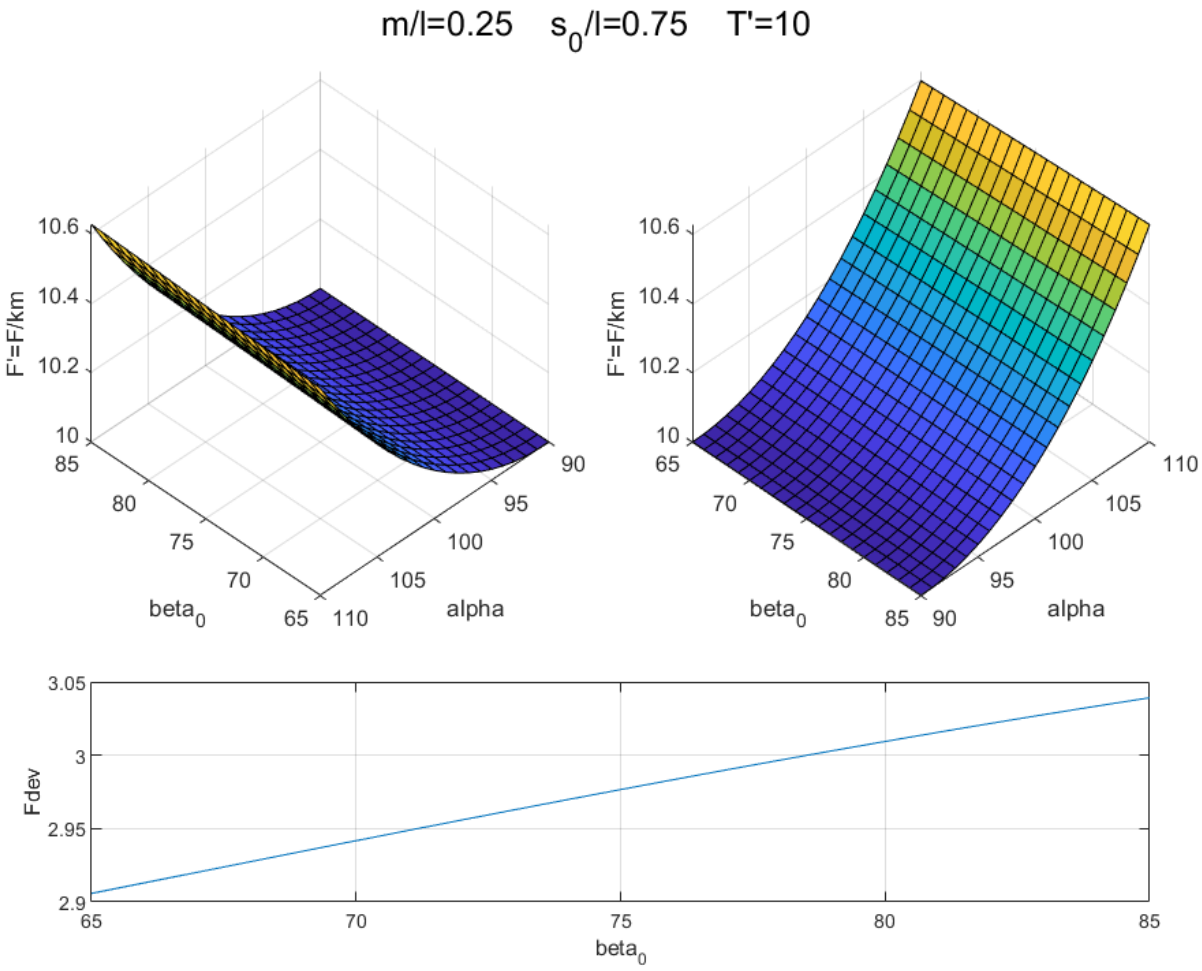

Figure 38. Example 3D plot ($m/l = 0.25, s_0/l = 0.75, T' = 10$)

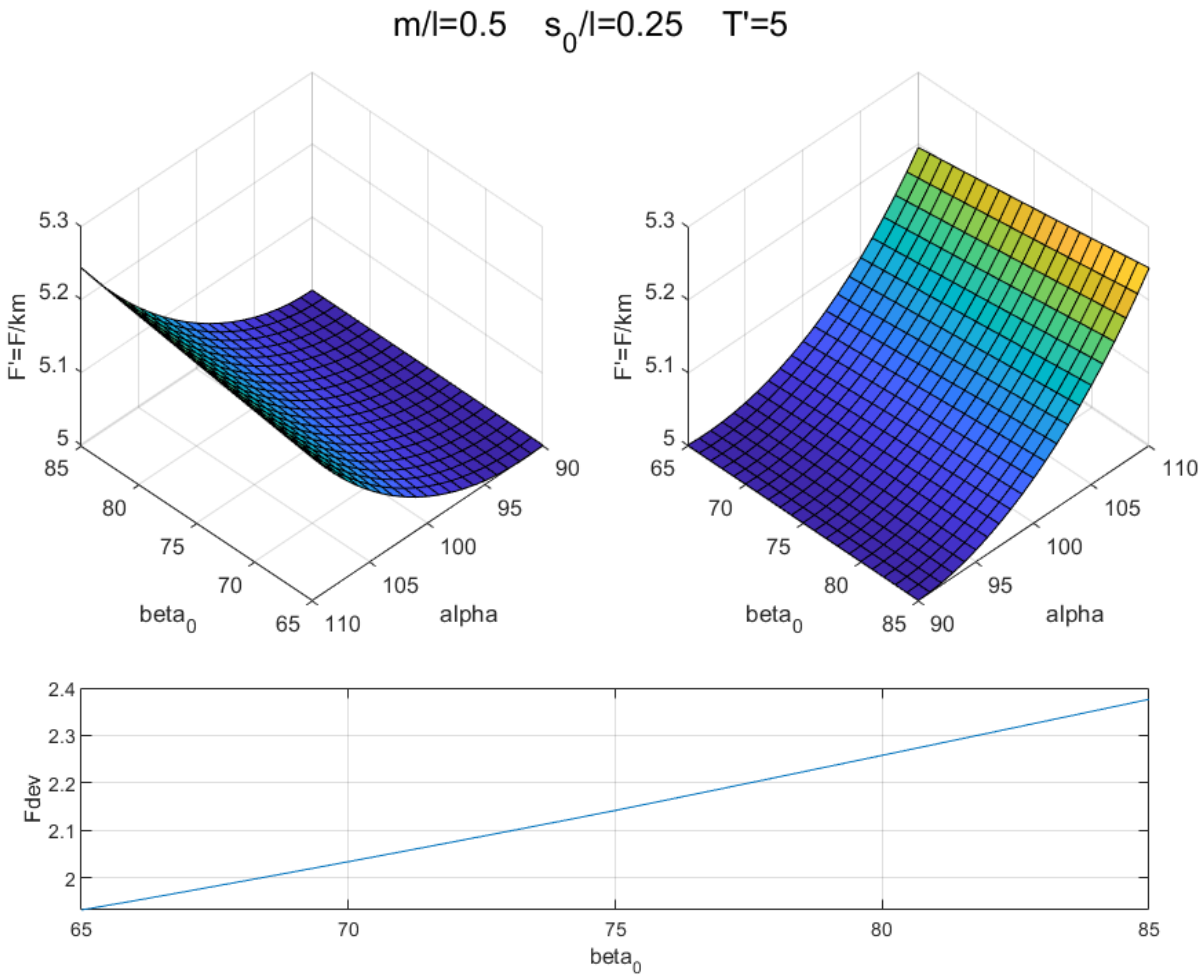

Figure 39. Example 3D plot ($m/l = 0.5, s_0/l = 0.25, T' = 5$)

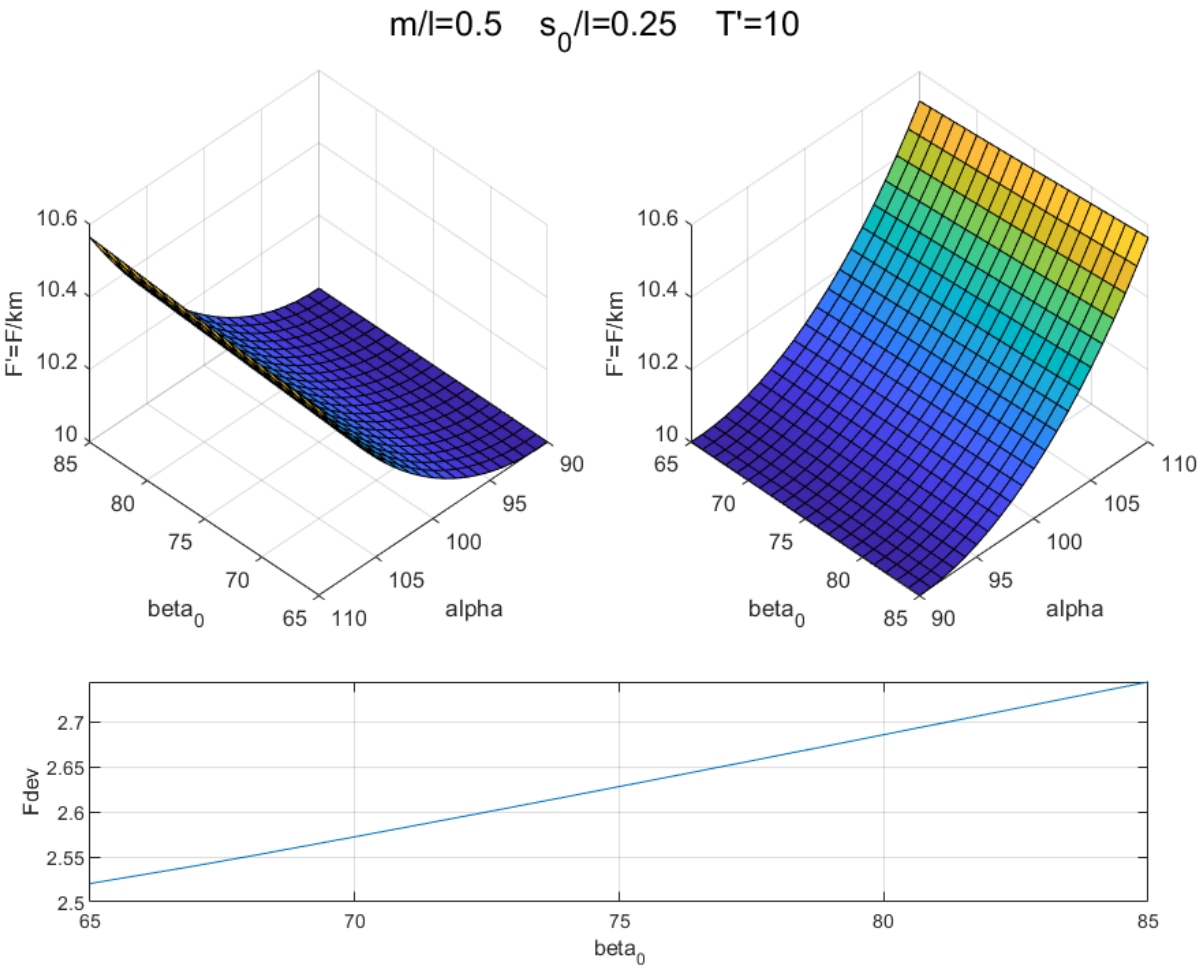

Figure 40. Example 3D plot ($m/l = 0.5, s_0/l = 0.25, T' = 10$)

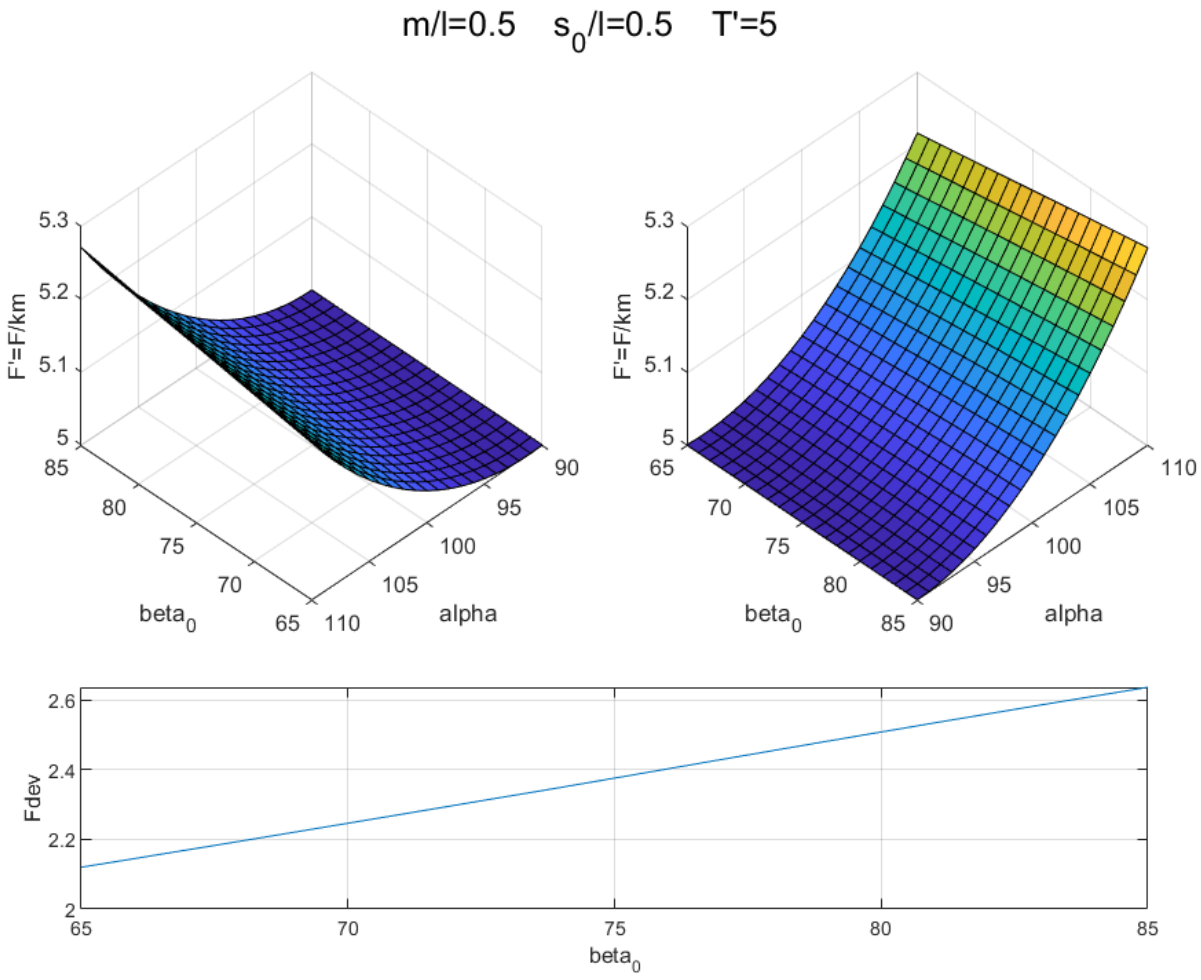

Figure 41. Example 3D plot ($m/l = 0.5, s_0/l = 0.5, T' = 5$)

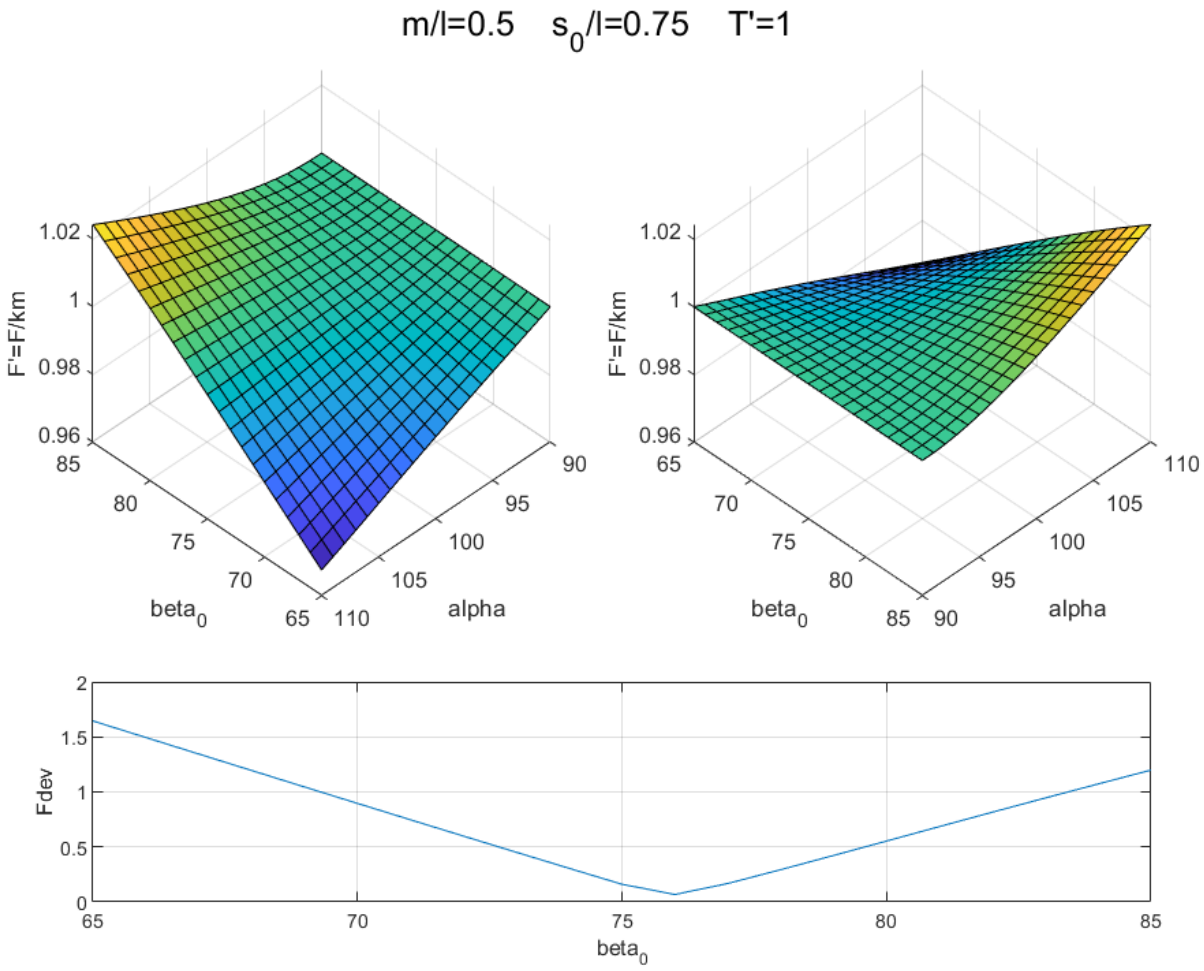

Figure 42. Example 3D plot ($m/l = 0.5, s_0/l = 0.75, T' = 1$)

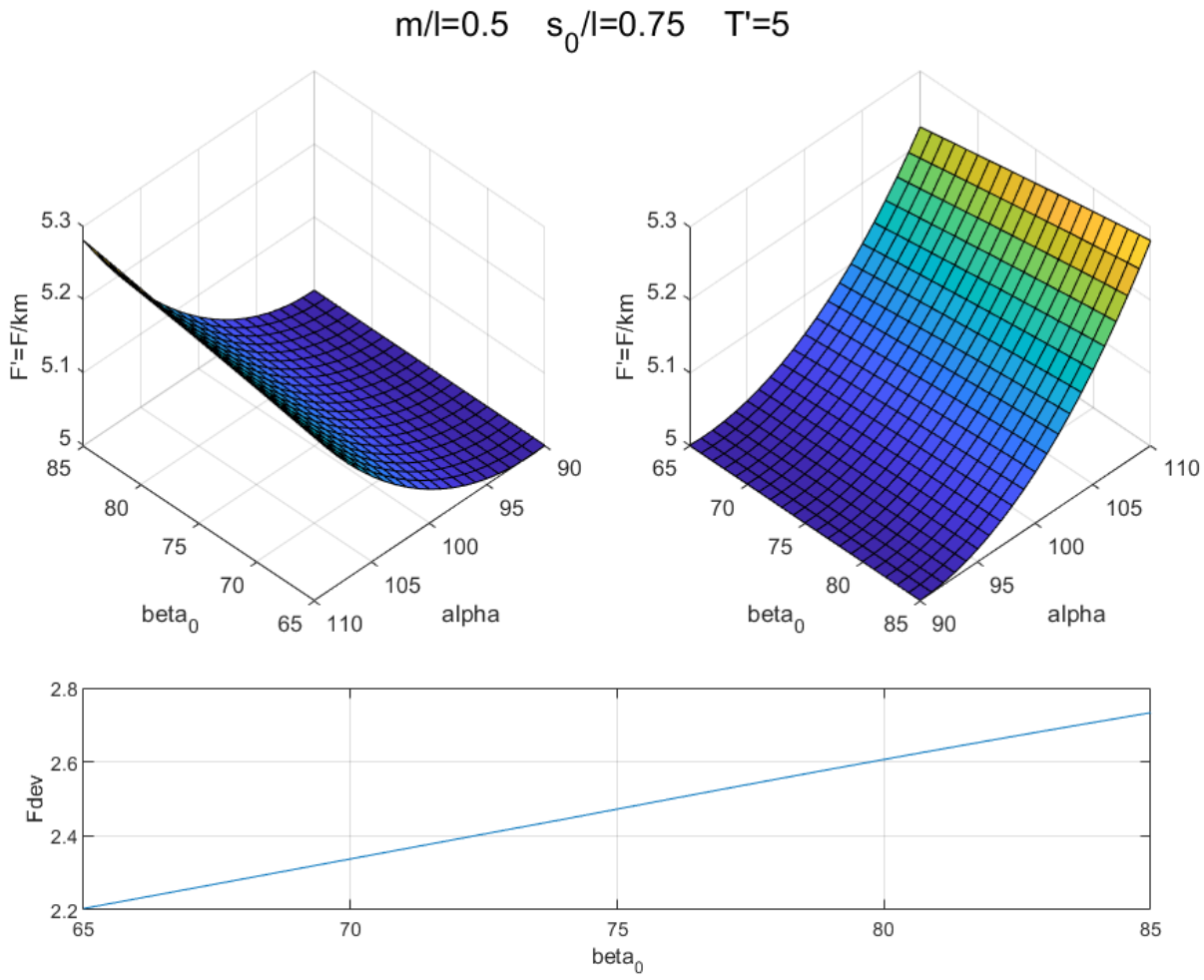

Figure 43. Example 3D plot ($m/l = 0.5, s_0/l = 0.75, T' = 5$)

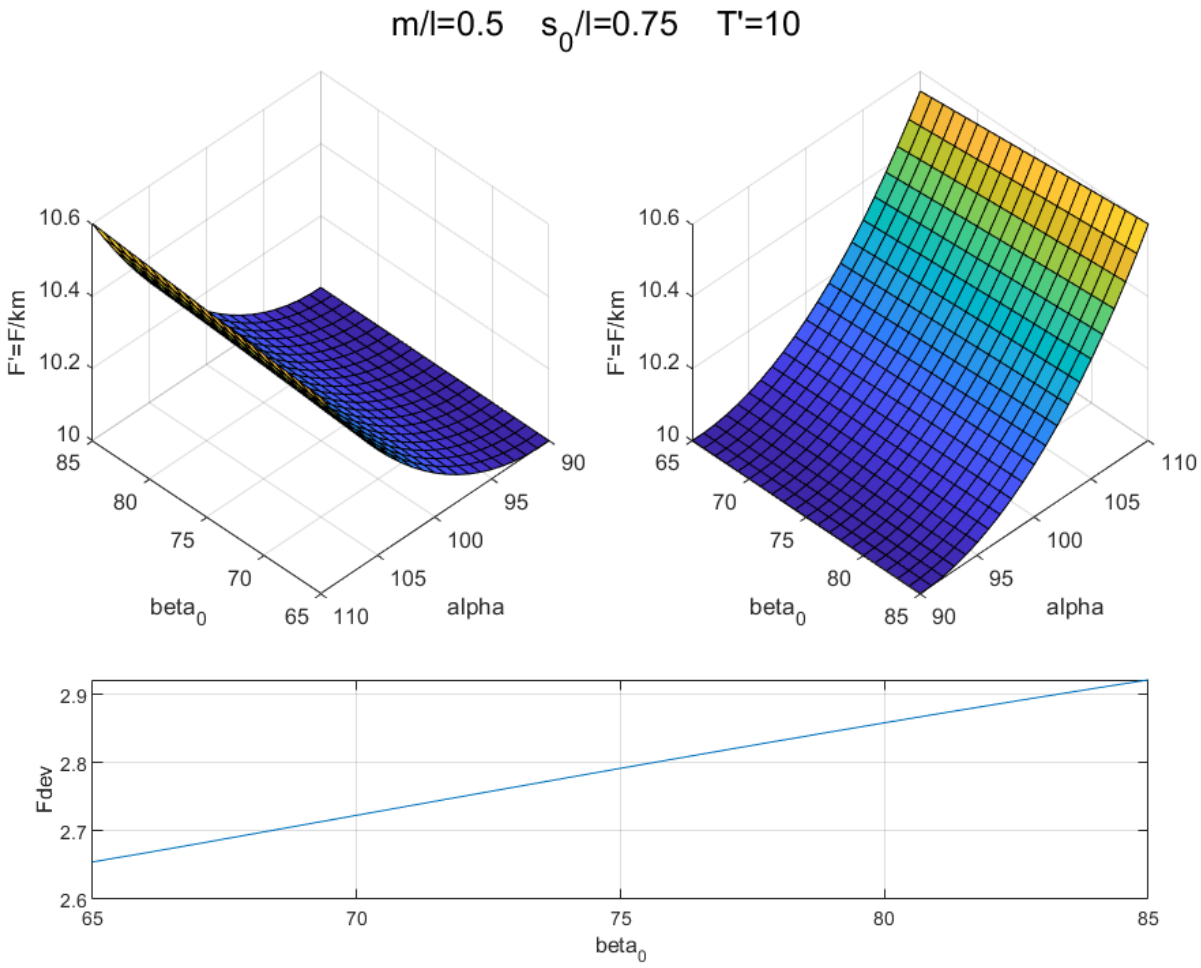

Figure 44. Example 3D plot ($m/l = 0.5, s_0/l = 0.75, T' = 10$)

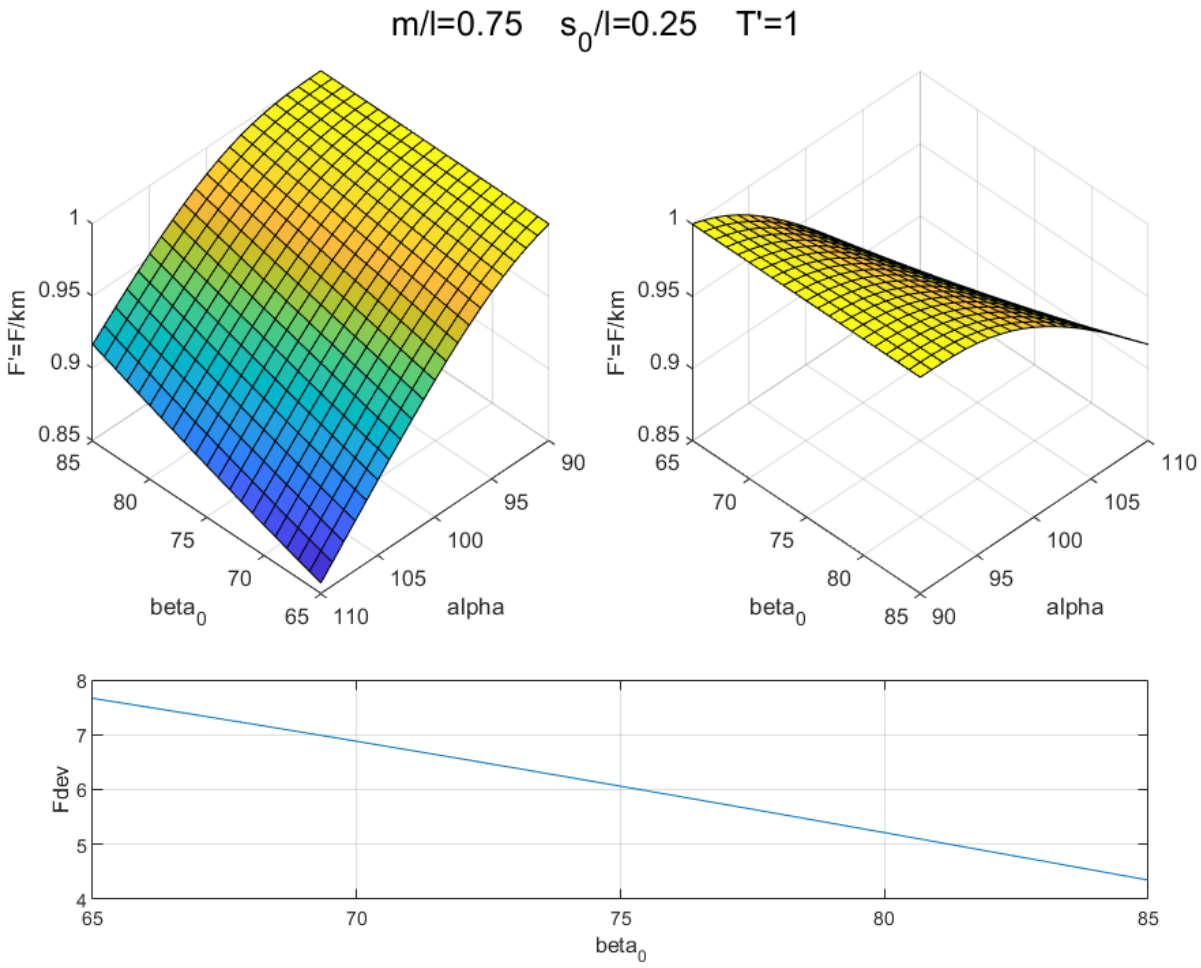

Figure 45. Example 3D plot ($m/l = 0.75, s_0/l = 0.25, T' = 1$)

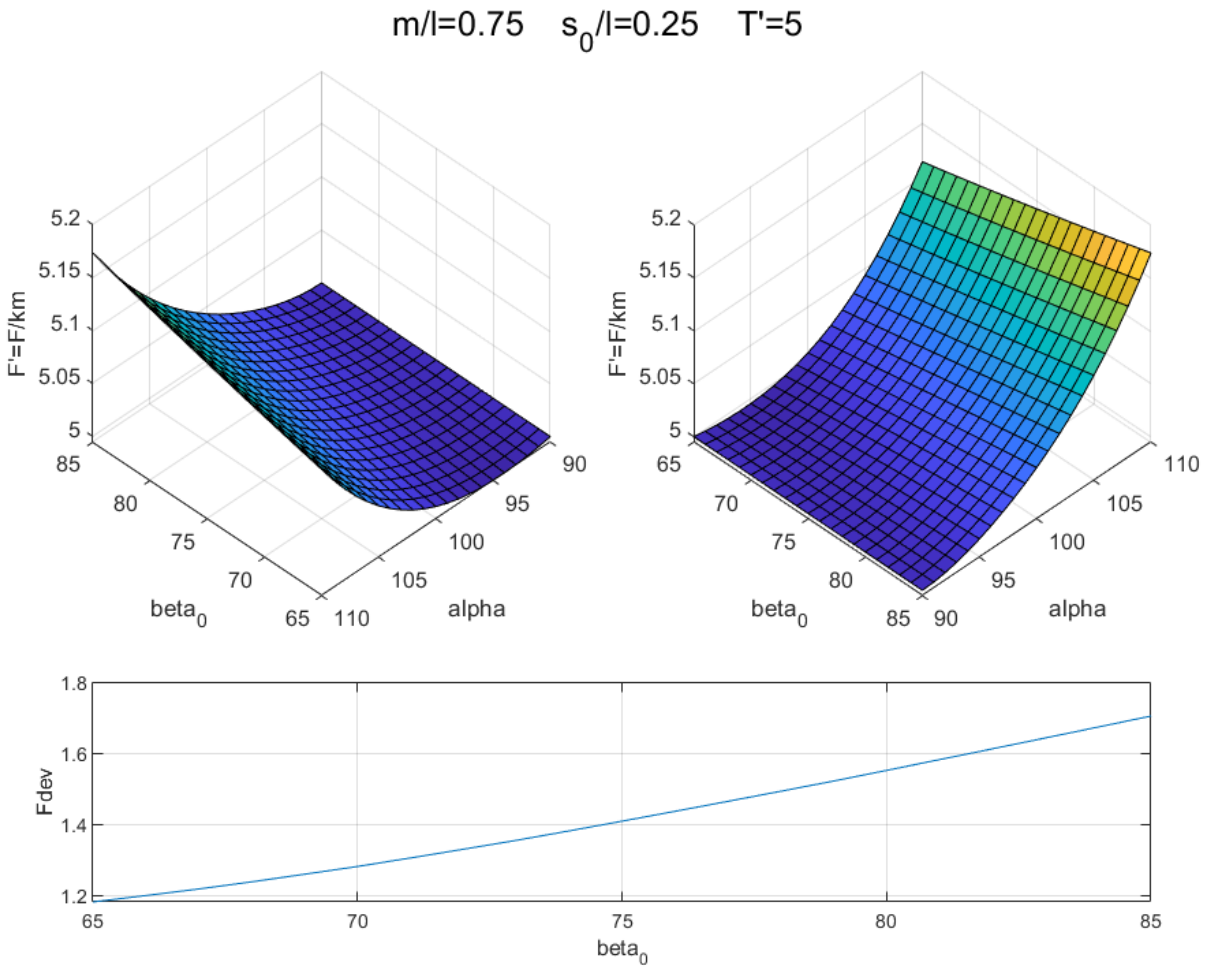

Figure 46. Example 3D plot ($m/l = 0.75, s_0/l = 0.25, T' = 5$)

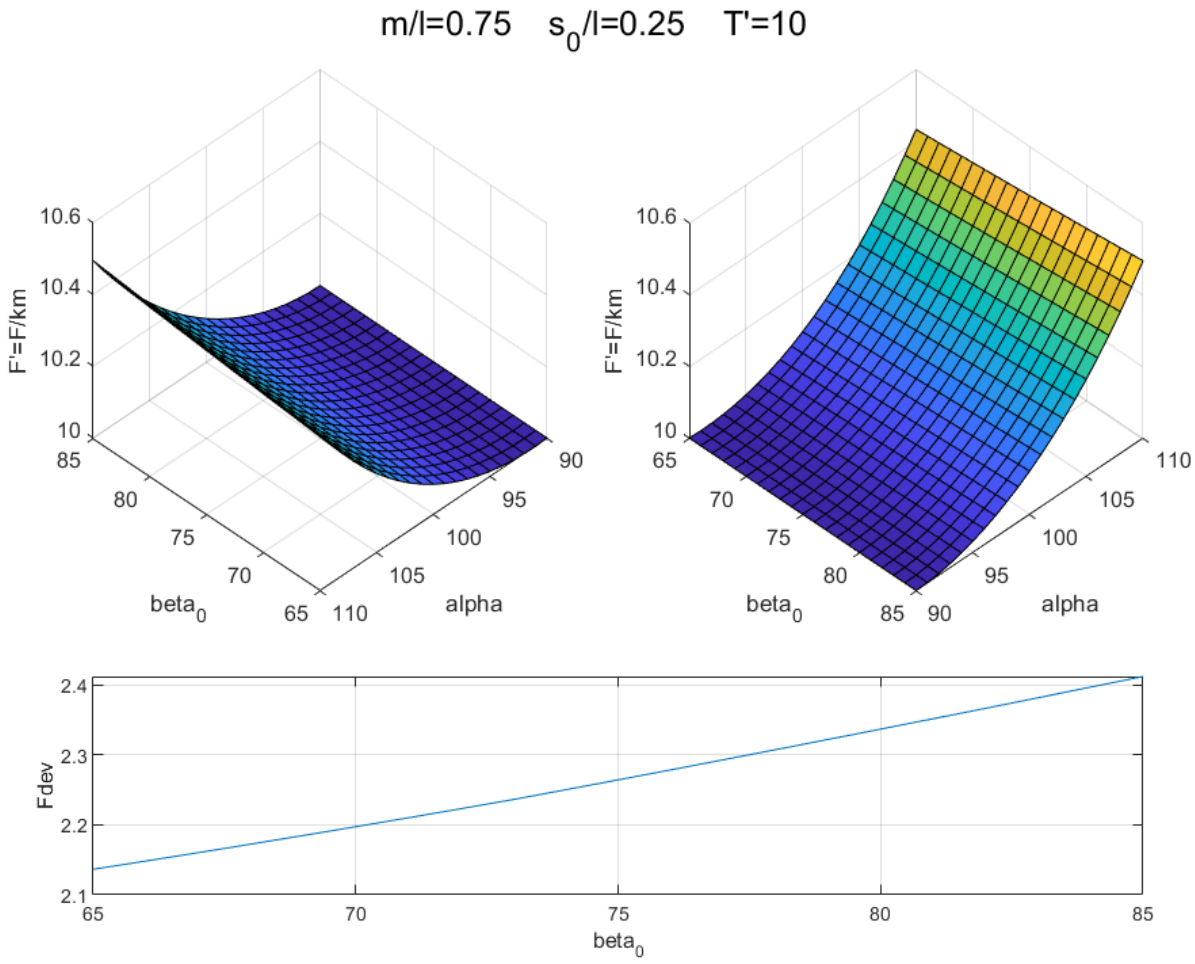

Figure 47. Example 3D plot ($m/l = 0.75, s_0/l = 0.25, T' = 10$)

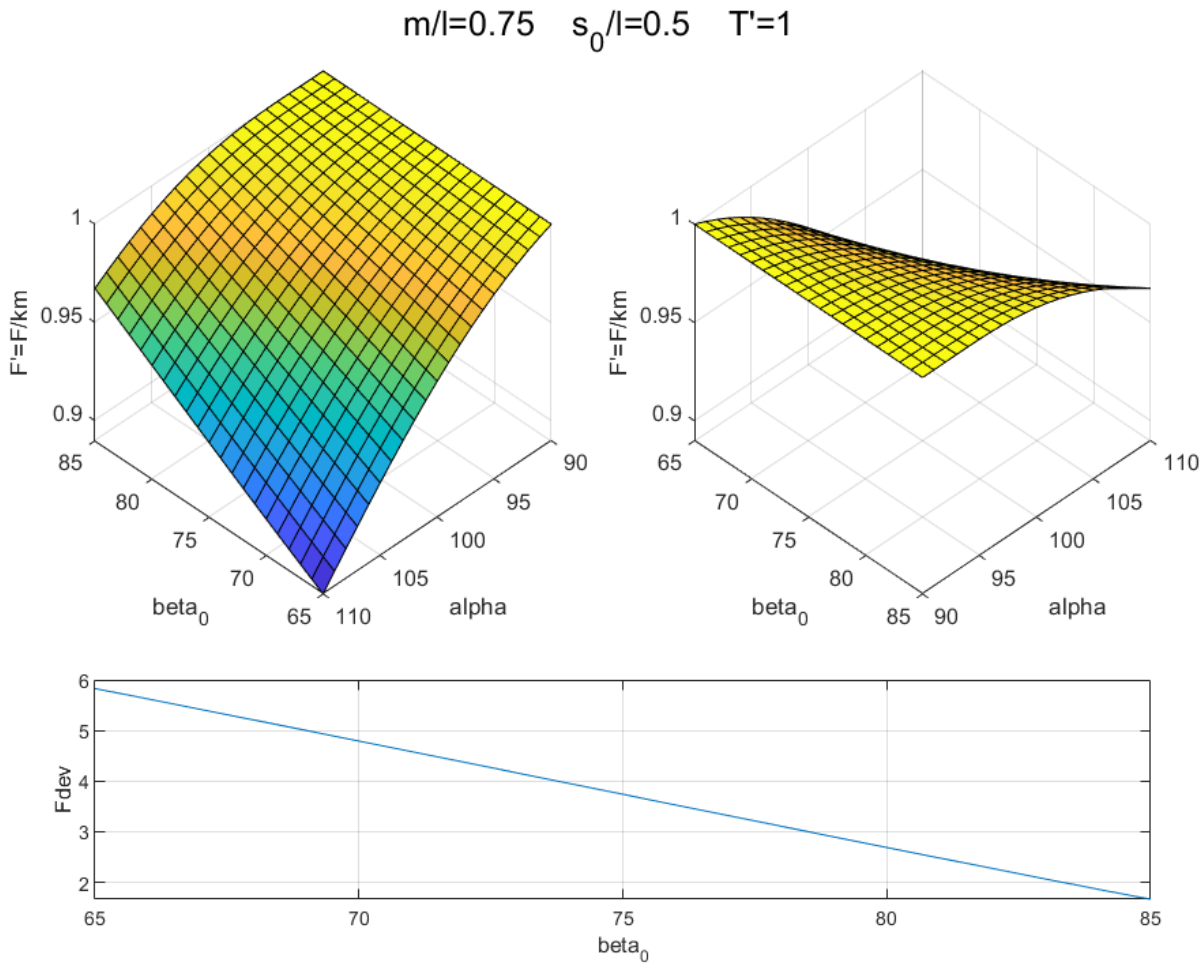

Figure 48. Example 3D plot ($m/l = 0.75, s_0/l = 0.5, T' = 1$)

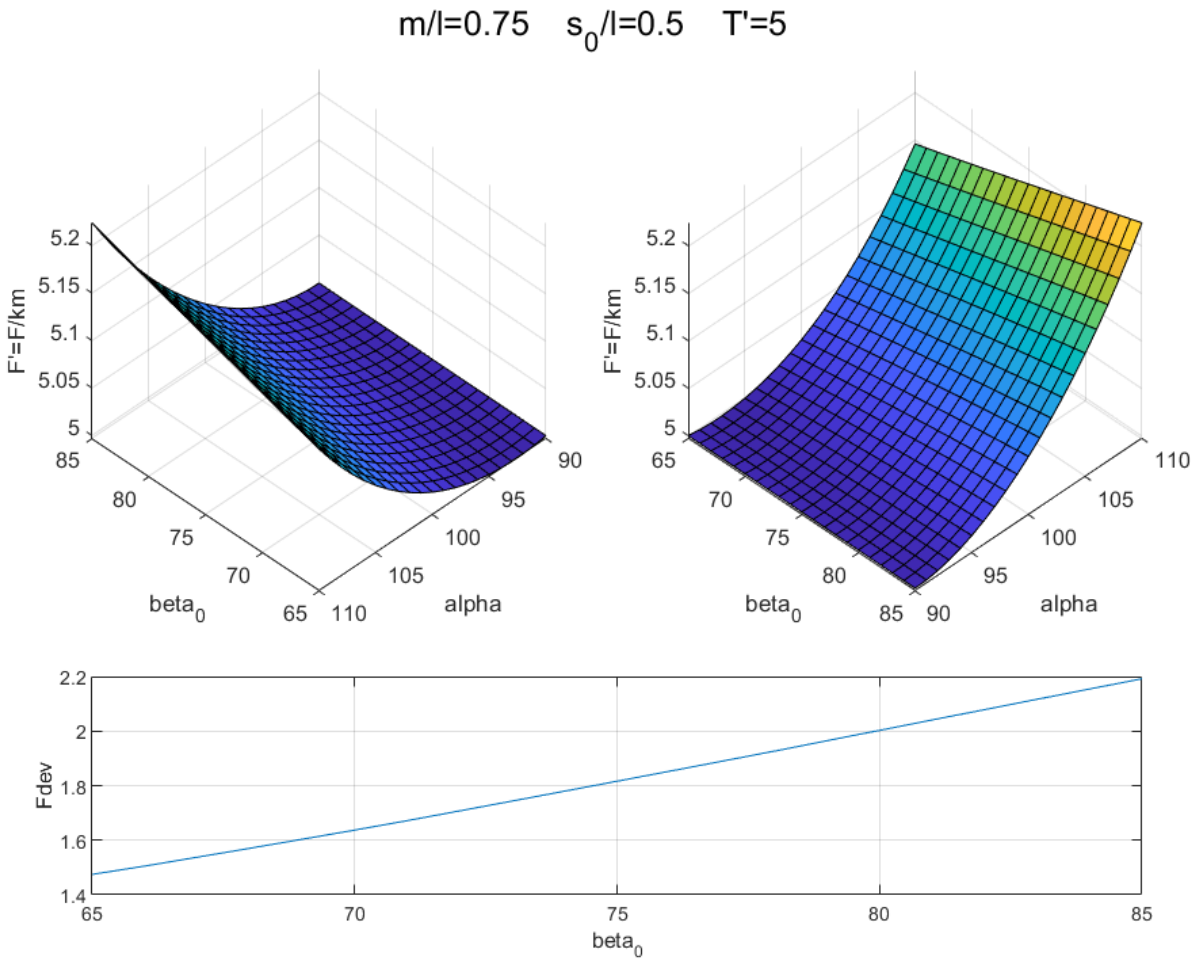

Figure 49. Example 3D plot ($m/l = 0.75, s_0/l = 0.5, T' = 5$)

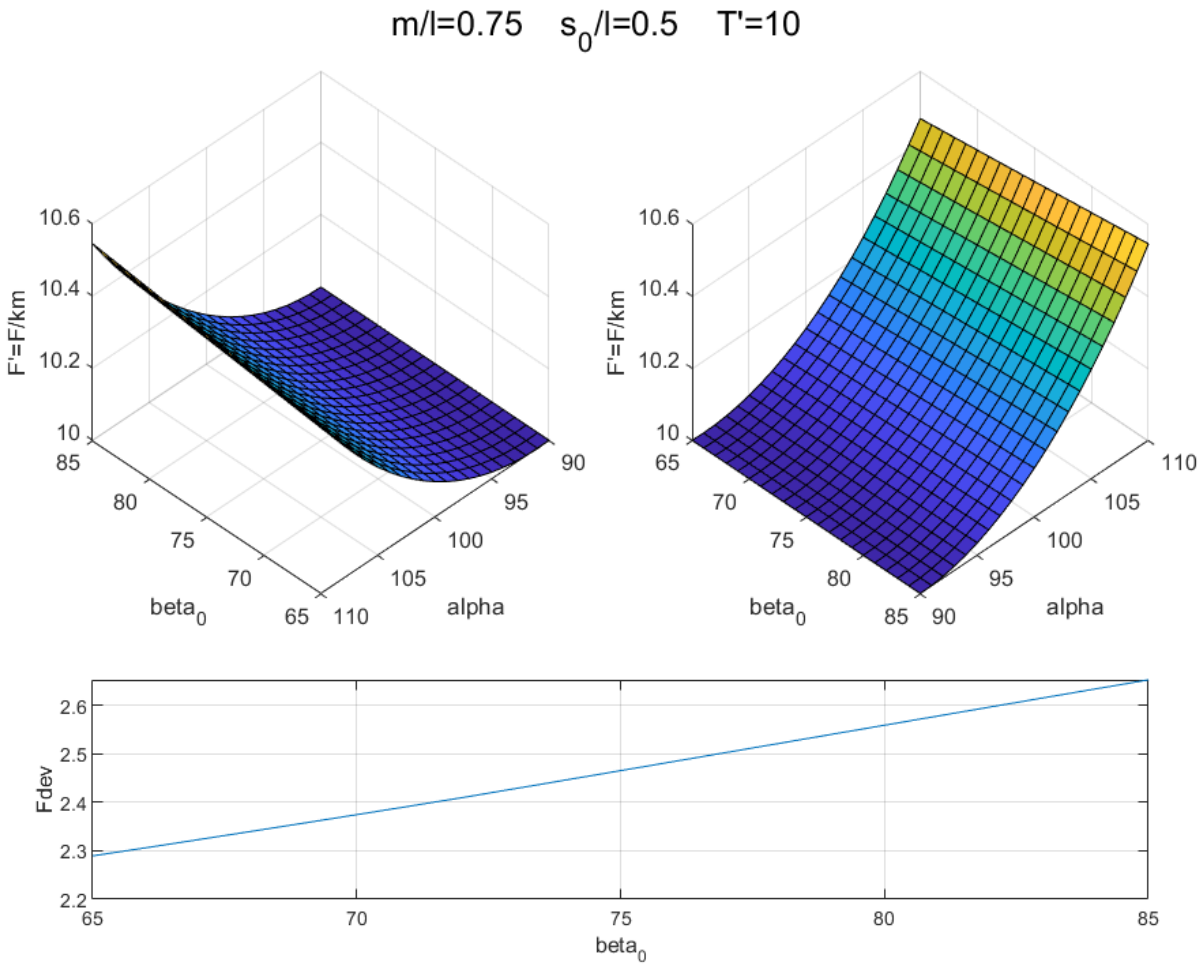

Figure 50. Example 3D plot ($m/l = 0.75, s_0/l = 0.5, T' = 10$)

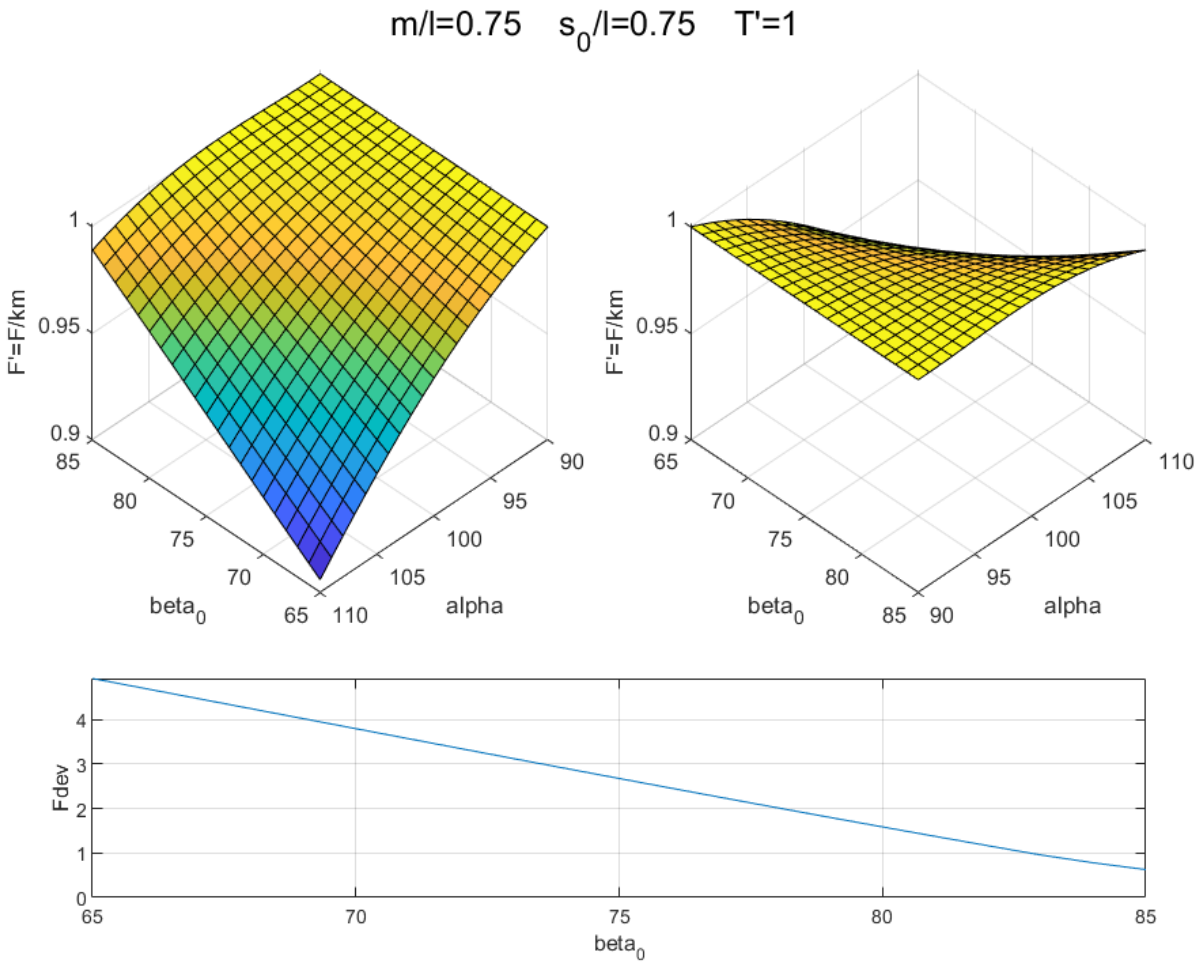

Figure 51. Example 3D plot ($m/l = 0.75, s_0/l = 0.75, T' = 1$)

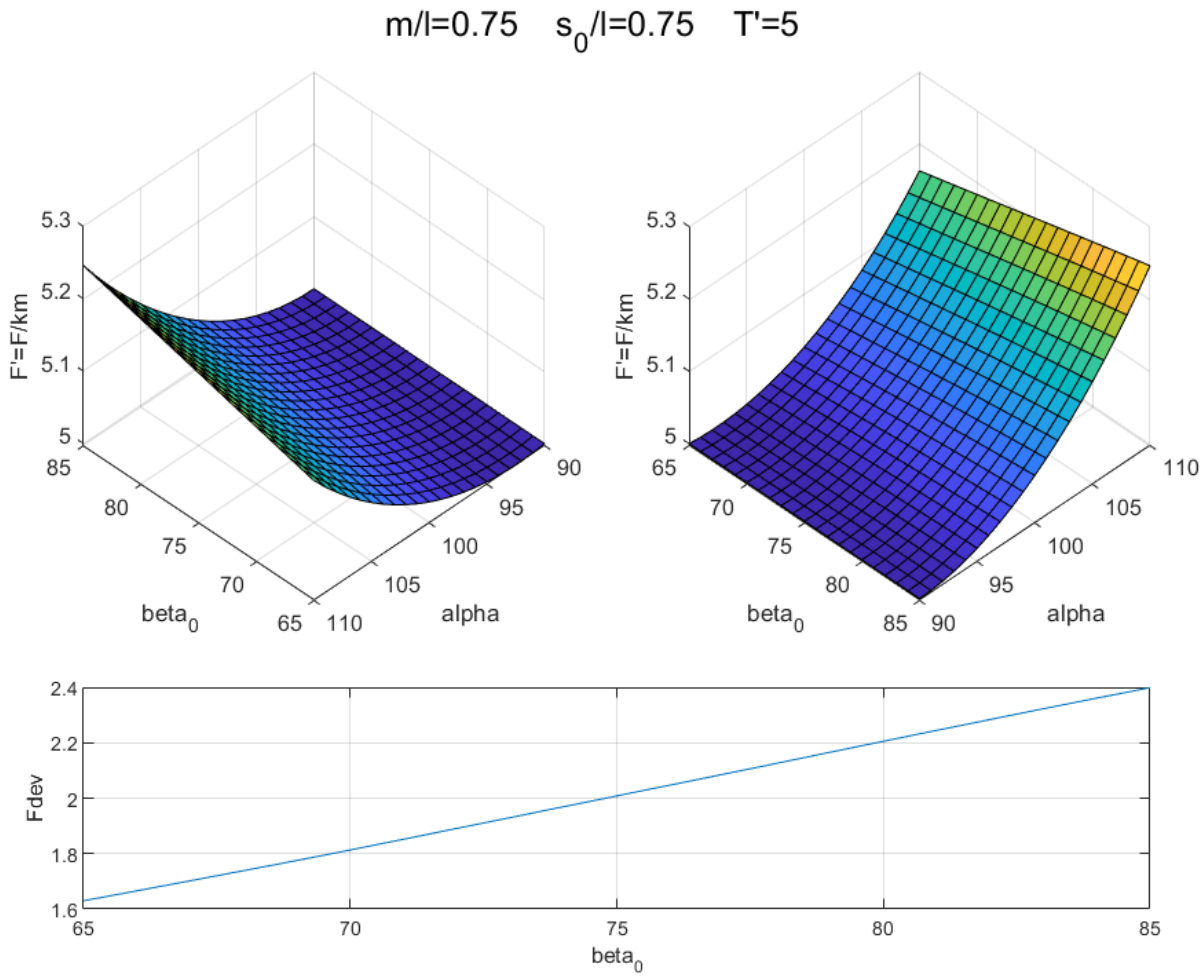

Figure 52. Example 3D plot ($m/l = 0.75, s_0/l = 0.75, T' = 5$)

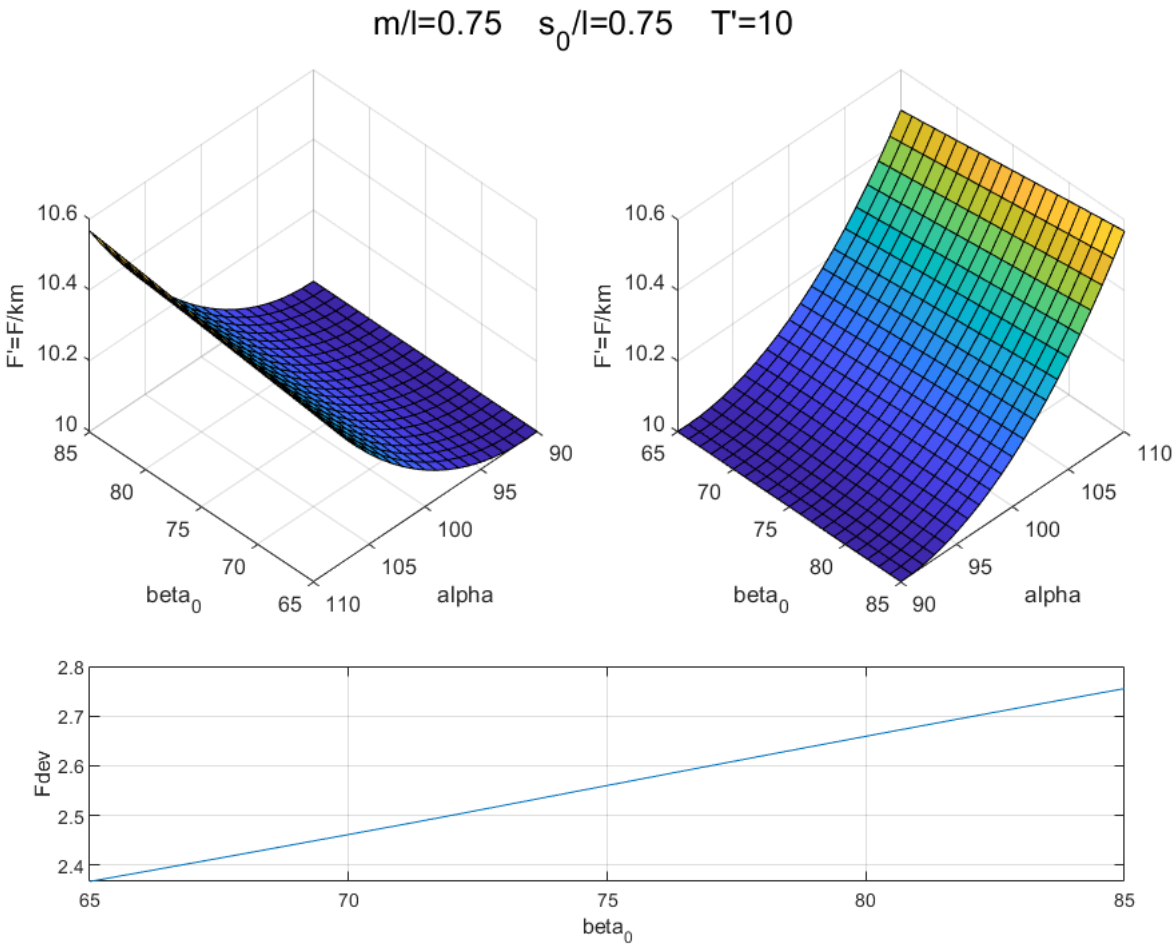

Figure 53. Example 3D plot ($m/l = 0.75, s_0/l = 0.75, T' = 10$)

3.3 Optimization of Design Charts

As can be observed on the example 3D plots, parameter combinations which provide feasible F_{dev} values may be determined using intuitive initial estimations and making trials, however, to fully capture these combinations an optimization routine must be utilized in a larger search space.

As mentioned before, three parameters ($m/l, s_0/l$ and T') and an interval of β_0 must be defined beforehand to create a design chart. Thus, a search space is defined as given in Table 3.

Table 3. Search space used in optimization routine

Parameter	Lower Boundary	Increment	Upper Boundary
m/l	0.2	0.1	0.8
s_0/l	0.2	0.1	0.8
T'	1	0.5	10
β_0 [°]	1	1	89

Boundaries of m/l and s_0/l are specified according to geometric constraints (e.g. to not obtain weird proportions) of the structure with respect to their ratio to l, since lower than 0.2 and higher than 0.8 values are considered geometrically undesirable. Range for T' is intentionally chosen to contain a larger interval, since assuming boundaries for this parameter is more difficult than others. Also, β_0 range is selected to cover all possible connection angles for springs up to spring and link overlap. Finally, since 7 m/l, 7 s_0/l, 19 T' and 89 β_0 values specified, $7x7x19x89 = 82{,}859$ different combinations considered in optimization routine. F_{dev} is calculated for each of these combinations. Mean F' values for each combination are also calculated. Note that, α_0 and α_F are selected as 90° and 110° for all combinations, as explained in Section 2.4.

Results reveal that, 247 of 82,859 (0.3%) combinations can provide <1% F_{dev} and 129 of 82,859 (0.16%) can provide <0.5% F_{dev} values. 48 of 82,859 combinations provide <0.2% F_{dev} values, and these combinations tabulated in Table 4, with F_{dev} sorted in ascending order. Recall that, F_{dev} for without spring case was calculated as 3.11%, as explained in Section 2.4.

Table 4. Optimization results (F_{dev}<0.2%)

m/l	s_0/l	T'	F_{dev} [%]	β_0 [°]	F'_{mean}
0.6	0.4	1.5	0.0166	79	1.4998
0.8	0.5	2	0.0295	80	2.0002
0.7	0.7	1.5	0.0296	78	1.4995
0.5	0.6	1	0.0436	78	0.9999
0.5	0.2	1.5	0.0486	82	1.5001
0.6	0.5	1.5	0.0553	76	1.4988
0.7	0.6	1.5	0.0590	80	1.5006
0.4	0.3	1	0.0595	77	0.9991

0.8	0.6	2	0.0595	77	1.9983
0.7	0.3	2	0.0627	83	2.0015
0.7	0.4	2	0.0645	77	1.9984
0.7	0.8	1.5	0.0691	77	1.4996
0.8	0.3	2.5	0.0693	82	2.5002
0.5	0.5	1	0.0754	80	1.0006
0.5	0.7	1	0.0923	76	0.9986
0.6	0.3	1.5	0.0931	84	1.5015
0.4	0.2	1	0.0931	84	1.0010
0.8	0.4	2	0.0931	84	2.0020
0.8	0.7	2	0.0935	75	1.9972
0.4	0.4	1	0.0944	74	0.9987
0.8	0.8	2	0.0944	74	1.9974
0.6	0.6	1.5	0.0944	74	1.4981
0.6	0.2	2	0.0971	81	1.9985
0.8	0.8	1.5	0.0992	81	1.5007
0.6	0.8	1	0.1030	81	1.0009
0.5	0.8	1	0.1047	75	0.9983
0.8	0.4	2.5	0.1126	76	2.4974
0.7	0.5	1.5	0.1127	82	1.5008
0.6	0.7	1	0.1182	82	1.0010
0.7	0.5	2	0.1185	74	1.9976
0.5	0.3	1.5	0.1271	75	1.4987
0.8	0.7	1.5	0.1351	83	1.5022
0.5	0.4	1	0.1361	82	1.0005
0.4	0.5	1	0.1372	72	0.9982
0.7	0.2	2.5	0.1393	81	2.4971
0.6	0.7	1.5	0.1526	73	1.4983
0.8	0.5	2.5	0.1599	72	2.4948
0.6	0.3	2	0.1602	73	1.9963
0.7	0.4	1.5	0.1639	86	1.5027
0.7	0.6	2	0.1661	72	1.9971
0.6	0.8	1.5	0.1717	71	1.4964
0.8	0.6	1.5	0.1733	85	1.5029
0.7	0.7	2	0.1756	70	1.9956
0.6	0.6	1	0.1771	84	1.0020
0.8	0.2	3	0.1774	82	2.9966
0.5	0.4	1.5	0.1791	71	1.4973
0.8	0.6	2.5	0.1851	70	2.4945
0.4	0.6	1	0.1939	71	0.9983

If the data in Table 4 examined, it can be observed that $T' \leq 3$ for all configurations providing F_{dev}<0.2%. This situation can be interpreted as T' values greater than 3 are not advantageous in terms of generating a constant force. Thus, instead of using 1 and 10 as T'

boundaries with 0.5 increment, lower boundaries and a lower increment for T' may provide a better search space for optimization routine. Also note that, all β_0 angles in Table 4 satisfies $\beta_0 \geq 70°$.

A second optimization is utilized with changing the boundaries of T' with 0.5 and 3, with an increment of 0.1. Other parameters of search space left same as tabulated in Table 3. 24 of 113,386 configuration in second optimization satisfies $F_{dev} \leq 0.05\%$, and these are tabulated in Table 5, with F_{dev} sorted in ascending order. Note that β_0 angles in Table 5 converges to $\approx 80°$.

Table 5. Second optimization results (F_{dev}<0.05%)

m/l	s_0/l	T'	F_{dev} [%]	β_0 [°]	F'_{mean}
0.6	0.4	1.5	0.0166	79	1.4998
0.7	0.5	1.7	0.0252	79	1.7000
0.6	0.5	1.4	0.0256	78	1.3997
0.7	0.6	1.6	0.0281	78	1.5993
0.8	0.5	2	0.0295	80	2.0002
0.7	0.7	1.5	0.0296	78	1.4995
0.8	0.6	1.9	0.0305	79	1.9001
0.6	0.7	1.2	0.0336	78	1.1995
0.7	0.4	1.9	0.0345	79	1.8998
0.4	0.2	1.1	0.0350	81	1.1003
0.8	0.4	2.2	0.0350	81	2.2006
0.5	0.6	1	0.0436	78	0.9999
0.8	0.8	1.7	0.0441	78	1.6992
0.6	0.3	1.7	0.0445	80	1.7001
0.8	0.7	1.9	0.0445	77	1.8992
0.6	0.6	1.3	0.0464	78	1.2999
0.3	0.2	0.8	0.0468	77	0.7995
0.6	0.4	1.6	0.0468	77	1.5990
0.8	0.4	2.3	0.0470	79	2.2989
0.5	0.4	1.1	0.0470	80	1.1003
0.3	0.4	0.6	0.0479	77	0.5997
0.6	0.8	1.2	0.0479	77	1.1994
0.8	0.7	1.8	0.0483	78	1.7990
0.5	0.2	1.5	0.0486	82	1.5001

3.4 Obtaining Design Parameters for Defined Requirements

Table 4 and 5 may be used as a guidance to determine parameters m, l, k, s_0, β_0 and T to design a system to deliver a specified constant force throughout a specified stroke. As an

example, assume that a link is required to deliver a constant force of 20 N with $F_{dev} <$ 0.1% for a stroke of 50 mm.

Since stroke is required as 50 mm, Equation (10) can be utilized to define l as

$$x_{max} = l \sin 20\,° \quad \rightarrow \quad l = \frac{50\ mm}{\sin 20\,°} = 146.2\ mm$$

To define other structural parameters, a configuration from Table 4 or 5 must be chosen. Since F_{dev} is aimed to be lower than 0.1%, any combination given in Table 4 or 5 having lower F_{dev} value than 0.1% can be used for this design. Let us select three different configurations as given in Table 6.

Table 6. Configuration options selected for example design

Option	$\boldsymbol{m/l}$	$\boldsymbol{s_0/l}$	$\boldsymbol{T'}$	$\boldsymbol{F_{dev}}$	$\boldsymbol{\beta_0}$	$\boldsymbol{F'_{mean}}$
1	0.5	0.5	1	0.0754%	80°	1.0006
2	0.8	0.6	2	0.0595%	77°	1.9983
3	0.3	0.4	0.6	0.0479%	77°	0.5997

Thus, m and s_0 values can be calculated for these three options as given in Table 7.

Table 7. m and s_0 values for example design

Option	$\boldsymbol{m}$ **[mm]**	$\boldsymbol{s_0}$ **[mm]**
1	73.1	73.1
2	117.0	87.7
3	43.9	58.5

Afterwards, since link lengths are specified, k can be calculated for each option as follows

$$F' = \frac{F}{km} \quad \rightarrow \quad k = \frac{F}{F'm}$$

Similarly, since k is now defined, T can be calculated for each option as follows and k and T values for these options are tabulated in Table 8.

$$T' = \frac{T}{kml} \quad \rightarrow \quad T = T'kml$$

Table 8. k and T values for example design

Option	***k* [N/m]**	***T* [Nm]**
1	273.44	2.92
2	85.57	2.93
3	760.38	2.93

Thus, all parameters required for three options are obtained as given in Table 7 and 8, all having same l value as explained before. These options are visualized to scale in Figure 54, and forces generated by these options with respect to α are shown in Figure 55. Note that, all options are satisfying $19.98 < F < 20.02$, as required in example as $F_{dev} < 0.1\%$.

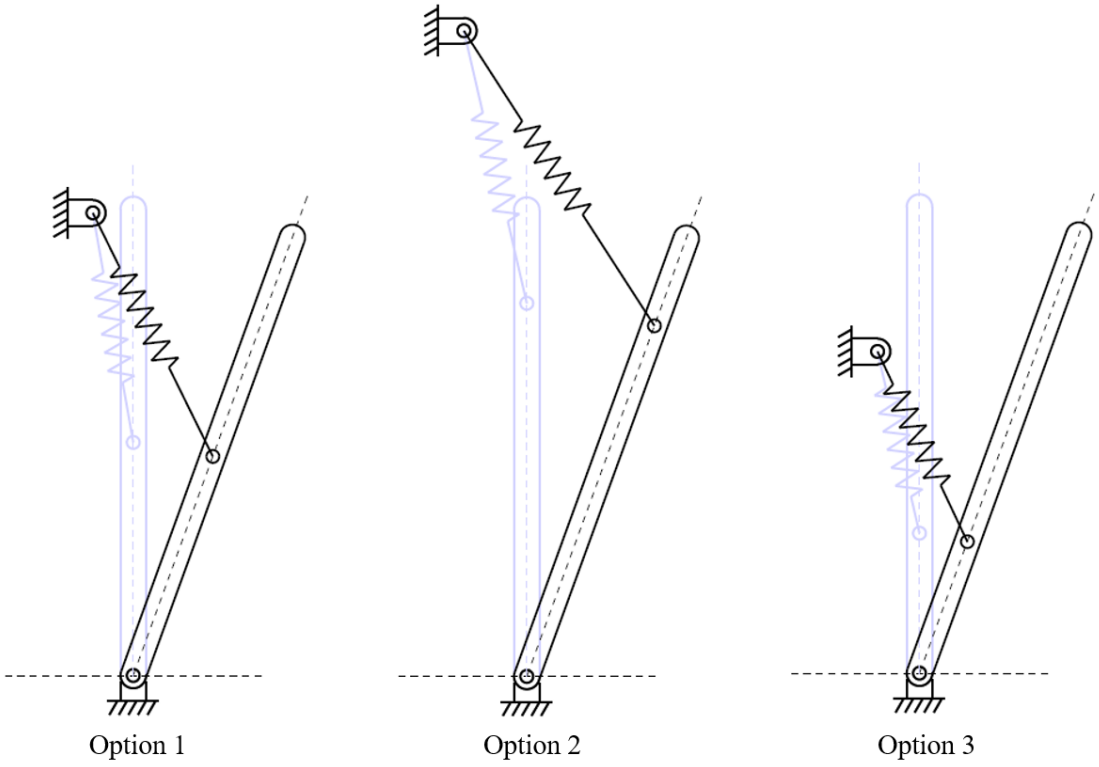

Figure 54. Visualization of options for example design

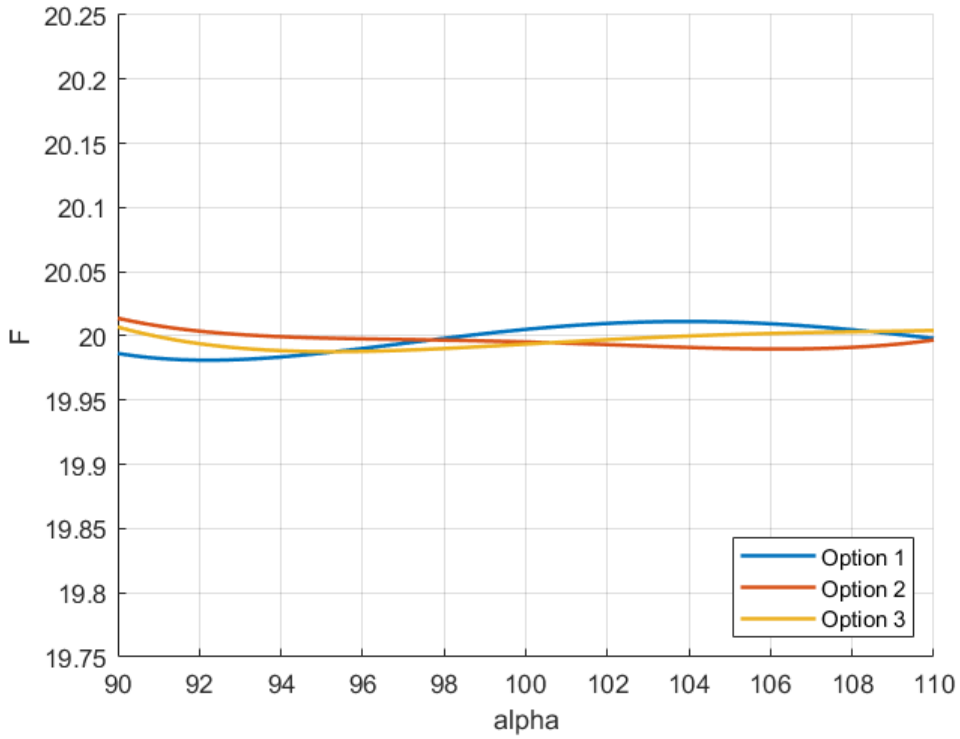

Figure 55. Forces generated by three options in example design

Note that, since both s_0 and m values are lower than Option 1 and 2, k is much higher in Option 3. This can be interpreted as, if k value obtained at design stage considered not suitable for the application, can be increased or decreased by selecting different s_0/l or m/l values.

Besides, since l and intended F are same in all options, and $F = T/l$ at α_0, T is nearly identical for all options. Moreover, since $F = T/l$ at α_0, F' is equal to T' at α_0. Since force variations are intended to be minimized, F' does not change much throughout motion so F' can be considered almost equal to T' during movement from α_0 to α_F.

3.5 Creating Equivalent Systems by Shifting Spring Position

The proposed spring position of the constant link is close the gripping edge of the link. This may lead a geometric constraint for industrial applications. To overcome this problem, spring position can be changed with an equivalent system.

The link can be considered as a superposition of two parts as visualized in Figure 56. One of them is the link to deliver constant force (Part A in Figure 56) and the other one is the spring and its connection to the main link (Part B in Figure 56).

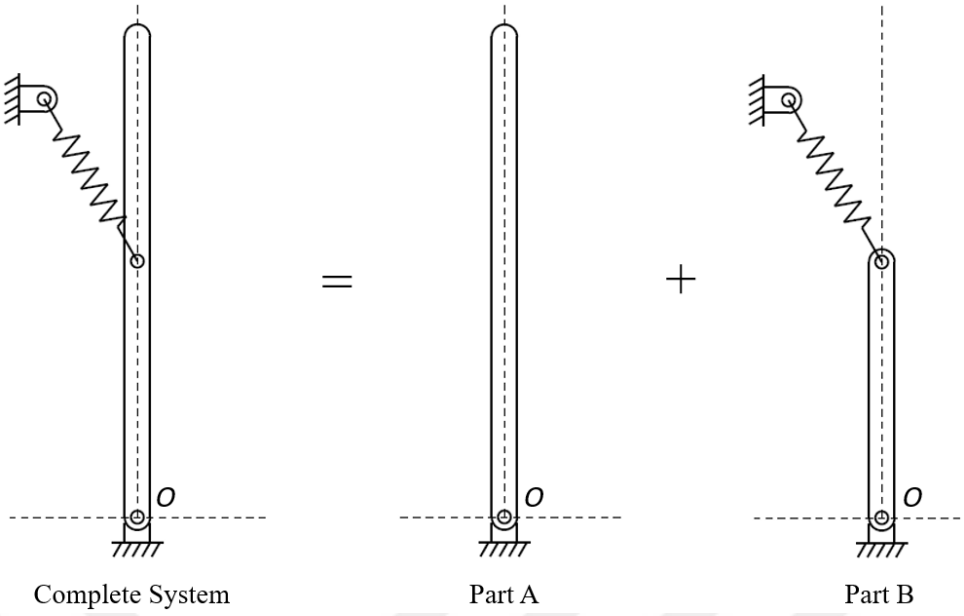

Figure 56. Representation of splitting the system into two parts

Thus, Part B can be freely rotated around O to obtain equivalent systems as shown in Figure 57. It should be noted that, the angle between the spring and the link should be kept constant as $180° - \beta_0$, while rotating Part B. Equivalent systems obtained by manipulating spring position are given in Figure 57. Using this method might be useful at design stage to create alternative spring positions, if initial spring location considered geometrically disadvantageous.

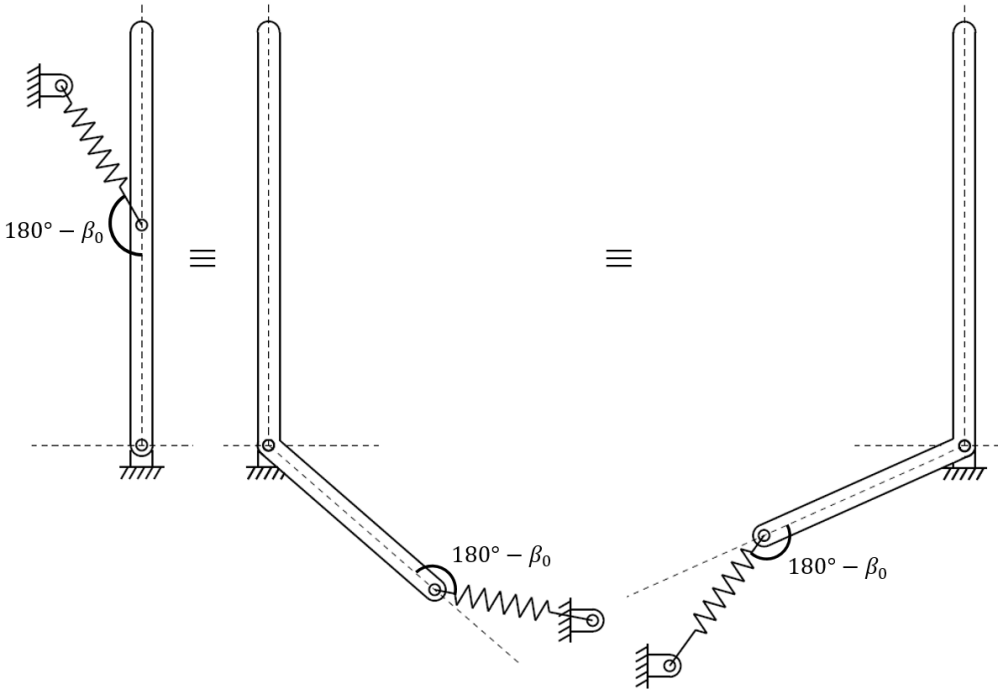

Figure 57. Equivalent systems obtained by manipulating spring position

4 CONSTANT FORCE GRIPPER MECHANISM

Constant force mechanism introduced in Section 0 can be used as a constant force gripper by placing two identical constant force links symmetrically as shown in Figure 58. By applying input torque T in opposing directions, gripping forces F will be obtained as output. However, the mechanism will require two torque actuators and they must be synchronized in order to create symmetrical movement.

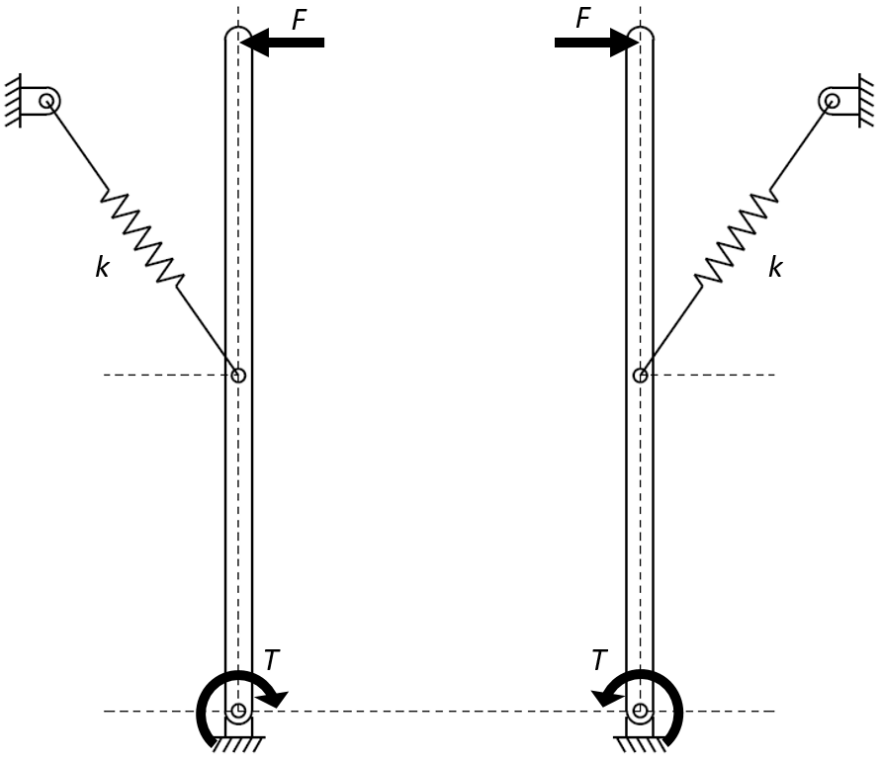

Figure 58. Constant force gripper

4.1 Torque Transmission Linkage

In order to reduce the number of actuators, a linkage may be designed between two input points to transfer the torque generated by a single actuator. It is intended to obtain equivalent constant torque at input points in opposite directions by applying an input torque from a single actuation point. If this actuation point is selected any other point than input points themselves and connected to the input points through a linkage, generated torque at the input points will not be constant. For this reason, it is reasonable to choose one of the input points as actuation point. Note that, actuation torque must be doubled in order to provide same gripping force F at both ends of the gripper.

4.1.1 Torque Transmission via Simple Gear Pair

A partial gear train consisting two identical meshing gears with centers concentric to the input points can be integrated. By this way we obtain a constant force geared mechanism. Thus, if a torque applied to one of those gears, an equivalent torque in opposite direction occurs at the other gear. Transmission via simple gear pair is shown in Figure 59. However, this obvious solution has some drawbacks. A gear train may increase complexity due to lubrication and sealing issues. In addition, gear diameters may be too large with respect to the link lengths.

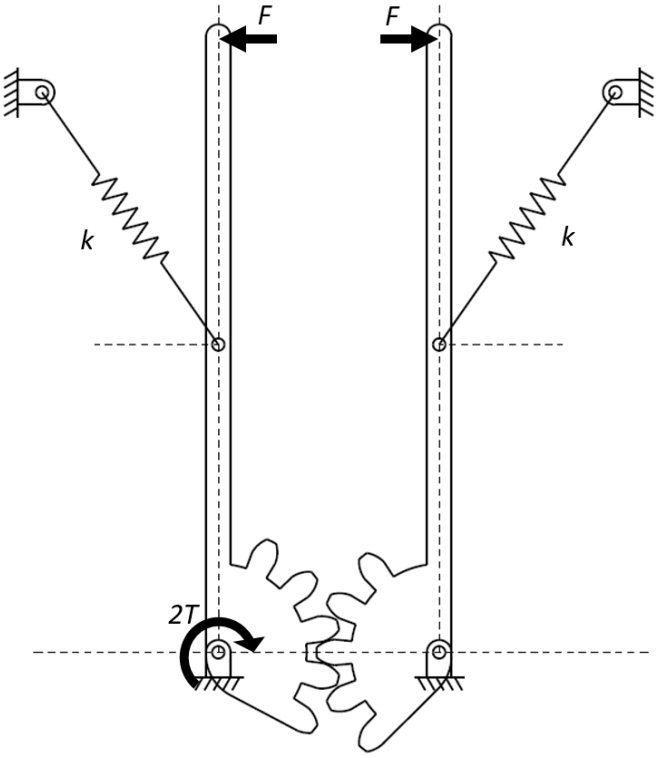

Figure 59. Torque transmission via simple gear pair

If the springs in Figure 59 are examined, it can be seen that their deflections are equal throughout motion. Since stiffnesses and related link lengths are equal, their reducing effect on input torque are also be equal throughout motion. Therefore, a single spring may be used instead of two if the stiffness of the remaining spring is increased to $2k$. Equivalent system is presented in Figure 60.

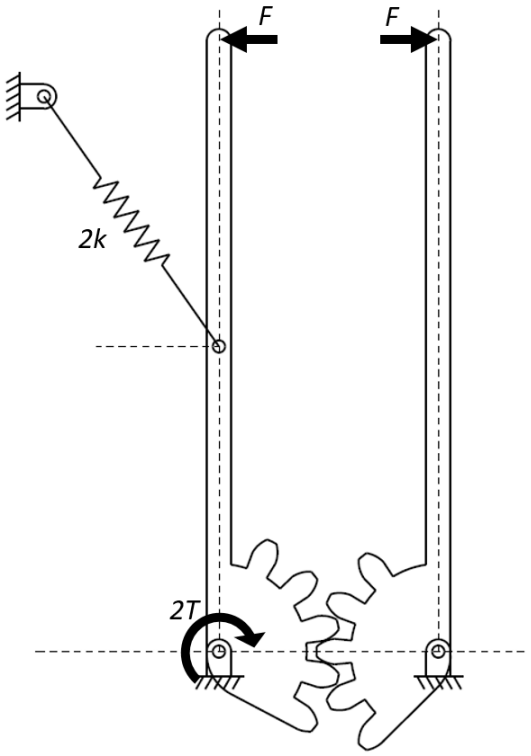

Figure 60. Equivalent system to Figure 59 using single spring

4.1.2 Torque Transmission via Four-Bar Linkage

A common method of changing the direction of rotation between two points is to implement a cross configuration four-bar mechanism as shown in Figure 61. Note that, single spring system as explained in Figure 60 is applied. However, it must be analyzed attentively to generate approximate constant torque at non-actuated input point throughout motion.

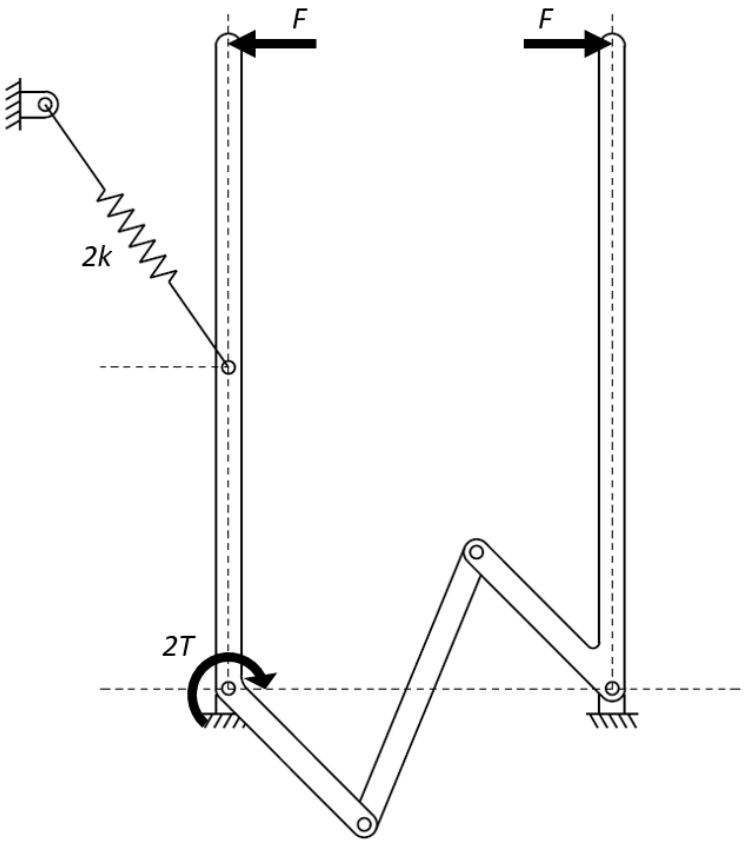

Figure 61. Cross configuration four-bar mechanism as torque transmission linkage

Consider the cross configuration four-bar mechanism given in Figure 62. Links 1 and 3 are parts of two symmetrical constant force mechanisms, connected with a coupler Link 2.

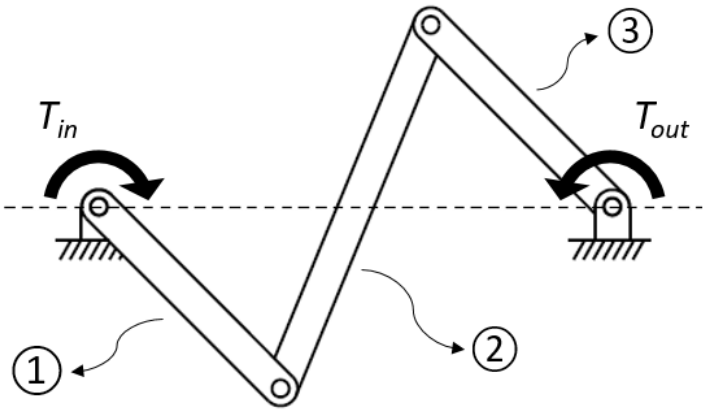

Figure 62. Cross configuration four-bar mechanism

It is assumed that masses of the links are negligible and operating speeds are slow. Therefore, the entire analysis is based on static equilibrium. Free-body-diagrams of Link 1, 2 and 3 are given in Figure 63, Figure 64, and Figure 65 respectively, where F_L represents the force exerted by Link 1 to Link 2, and T_{out} is the generated torque on Link 3 by applying input

torque T_{in} to Link 1. Finally, let $|S|_n$ denote the moment arm of force S about the hinge of Link n.

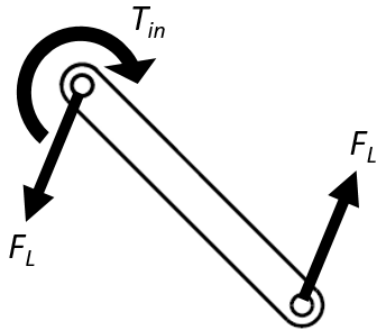

Figure 63. Free-body-diagram of Link 1

Note that reaction force at hinge is equal to F_L since total force is zero. Moment equation for Link 1 about its hinge can be expressed as

$$\sum M = 0$$

$$F_L . |F_L|_1 = T_{in} \tag{16}$$

Since Link 2 is a two-force member, it transmits F_L to Link 3.

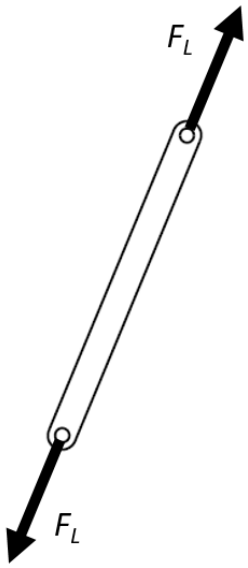

Figure 64. Free-body-diagram of Link 2

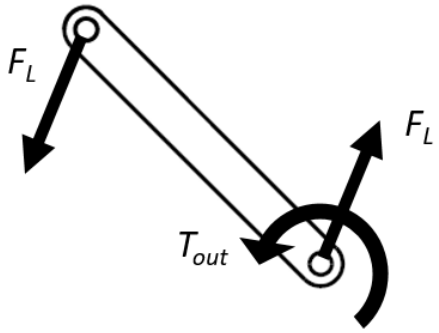

Figure 65. Free-body-diagram of Link 3

Moment equation for Link 3 about its hinge can be expressed as

$$\sum M = 0$$

$$F_L . |F_L|_3 = T_{out} \tag{17}$$

It is aimed to equalize T_{in} and T_{out}, thus

$$T_{in} = T_{out}$$

Finally, from Equations (16) and (17)

$$|F_L|_1 = |F_L|_3 \tag{18}$$

Equation (18) can be interpreted as, in order to create an equivalent torque in opposite direction at non-actuated hinge, moment arms of coupler forces must be equal. However, even if moment arm lengths can be equal for some instances, they may not be equal at all points throughout motion. For this reason, cross configuration four-bar mechanism must be optimized to minimize deviations between moments arm lengths.

Actually, what we aim to achieve here is to mimic an involute profiled gear mesh, where the profiles of the gear teeth are actually involutes of a circle. In this type of gears, contact point of two teeth moves across a line of action, which is always perpendicular to the lines connected to the centers of gears. Thus, whenever coupler of the connecting cross four-bar satisfies this perpendicularity, it transfers the torque without any deviation.

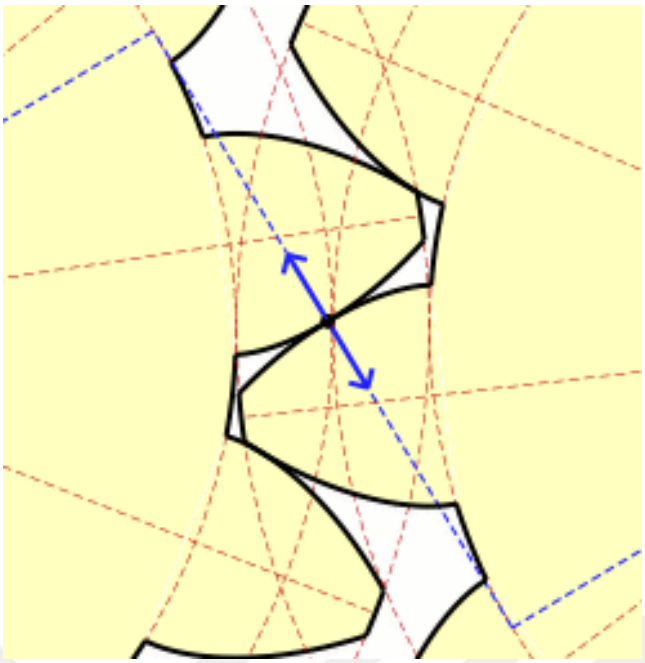

Figure 66. Line of action of an involute gear mesh [34]

4.2 Cross Four-Bar Optimization

In order to optimize link lengths, consider cross configuration four-bar mechanism given in Figure 67.

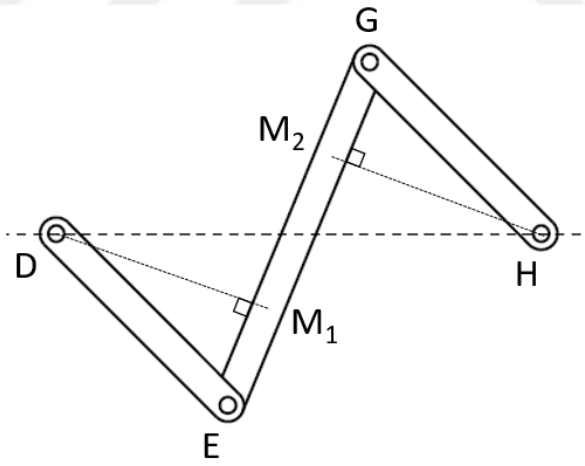

Figure 67. Cross configuration four-bar mechanism

Let us define link lengths and angles as follows

$$|DH| = c_1 \quad |DE| = c_2 \quad |EG| = c_3 \quad |GH| = c_4 \quad \angle GED = \psi \quad \angle HGE = \theta$$

And corresponding perpendicular distances, which are changing with respect to ψ as

$$|DM_1| = m_1 \qquad |HM_2| = m_2$$

Now, Equation (18) implies that m_1 must be equal to m_2. Since it is impossible (except parallelogram type) to equate these parameters for whole operating range of a four-bar mechanism, we should find a way to minimize $T_{out} - T_{in}$, which is related to m_2/m_1. To minimize m_2/m_1 deviation throughout motion, let $c_2 = c_4$. Thus, when the midpoint of the coupler aligns with hinges (i.e. where the mechanism is diagonally symmetrical) m_1 is equal to m_2. c_1 can be assumed as defined, since it is related with the geometrical requirements of the gripper. Also, to simulate the involute profiled gear mesh, set a position where coupler is perpendicular to both rockers, i.e. $\psi = \theta = 90°$. Note that, to satisfy this condition geometrically c_2 and c_4 must be lower than $c_1/2$. At this point, if coupler length c_3 is defined, then mechanism will be geometrically constrained, i.e. rocker lengths c_2 and c_4 will be fixed.

Then, this position can be considered as the midpoint of the angular interval, which means current left rocker position lies on the bisector of the initial and final positions of the left rocker. Thus, initial and final positions of the cross four-bar are defined. Note that $\psi_{initial}$ and θ_{final} will be slightly less than 90° and ψ_{final} and $\theta_{initial}$ will be slightly greater than 90°, minimizing the difference between m_1 and m_2. Thereby, transmission angles of the cross four-bar mechanism remain around 90° throughout motion, which is a highly preferable situation.

Example:

Consider a cross four-bar mechanism is required with $c_1 = 100$ mm and $\rho = 20°$. Let us define the coupler length as 50 mm, and set both rockers perpendicular to the coupler. After that, we can set the midpoint of the coupler aligned with the horizontal axis to bring cross four-bar to diagonally symmetrical position, as shown in Figure 68. Note that, rocker lengths are determined as 43.3 mm and angle between left rocker and horizontal axis is 30° at that position.

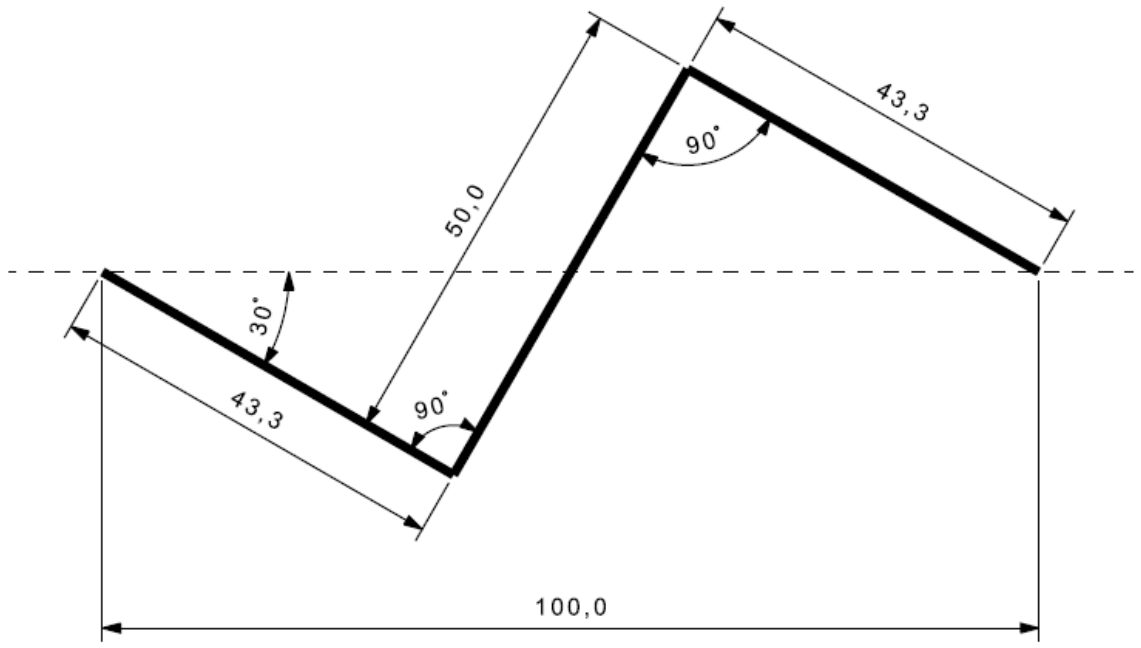

Figure 68. Example cross four-bar in mid position

After that, let us rotate left rocker around its hinge by $\rho/2 = 10°$ to either side. Therefore, initial and final positions of the cross four-bar is found. Transmission angles ψ and θ and moment arm lengths m_1 and m_2 at initial and final positions are shown in Figure 69 and 70, respectively. Note that, initial positions are shown with red and final positions with blue in both figures. As shown in Figure 69 and 70, coupler is nearly following a straight line throughout motion and mimics the line of action of an involute gear mesh. For this reason, difference in moment arm lengths is low, yielding near constant torque transmission between hinges. In order to represent the percent deviation of T_{out} with respect to T_{in}, a parameter can be defined as follows

$$T_{dev} = \left(\frac{T_{out}}{T_{in}} - 1\right) 100 = \left(\frac{m_2}{m_1} - 1\right) 100$$

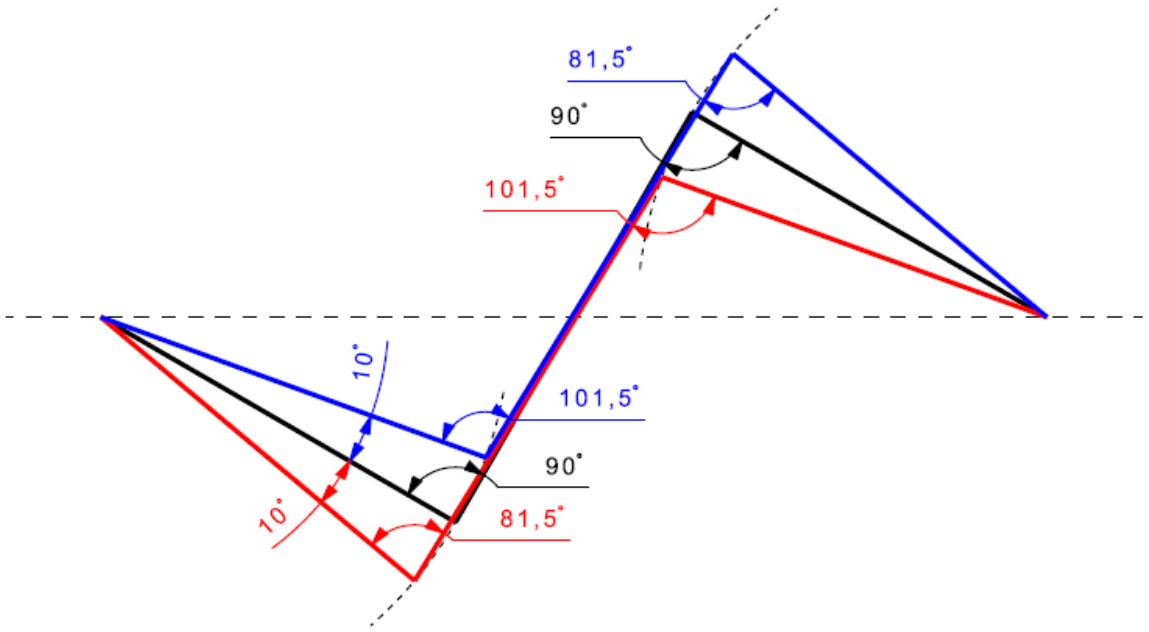

Figure 69. Initial and final transmission angles of example cross four-bar

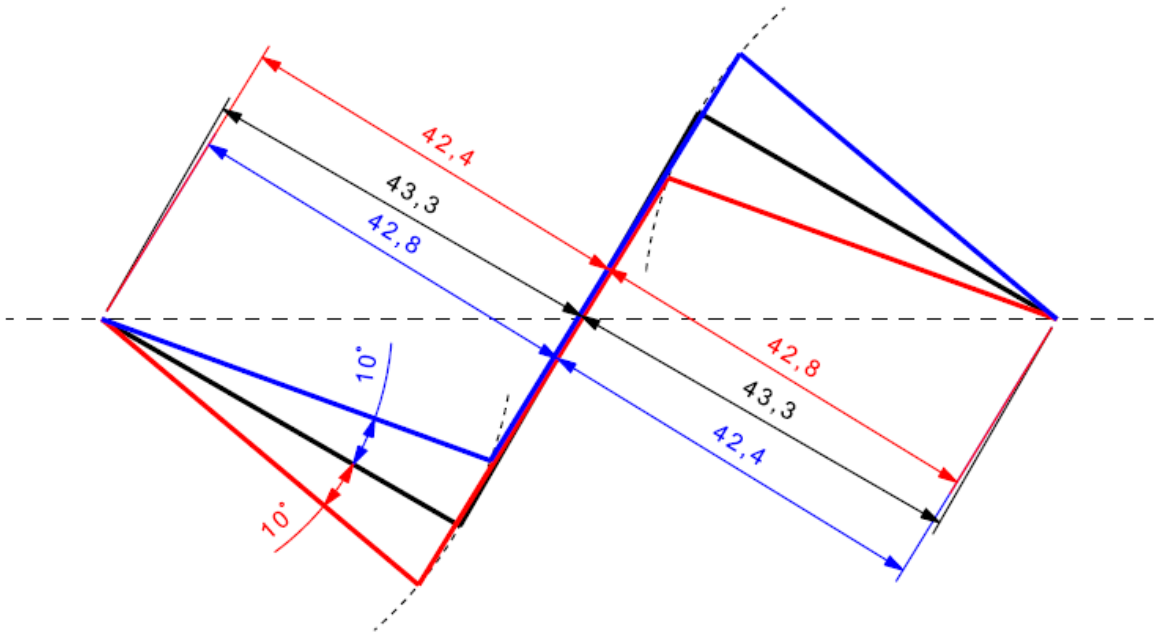

Figure 70. Initial and final moment arm lengths of example cross four-bar

The maximum difference between moment arms are observed at initial and final positions, as these are farthest positions from diagonal symmetry. Moments arm lengths at these positions are found as 42.4 and 42.8 mm, as shown in Figure 70, which results $T_{dev} < \pm 1\%$ throughout motion. This small variation indicates the success of designing the four-bar mechanism from the involute profiled gear.

5 DESIGN EXAMPLE (EGG GRIPPER)

In order to demonstrate the application of the proposed mechanism, an egg gripper is presented in this section. A mechanism delivering a constant force, which is sufficient to hold various sizes of eggs without cracking the shell might be useful to transfer eggs during packaging. It should be noted that, sole purpose of this design is to demonstrate a real-life example of the proposed constant force gripper design approach, rather than providing an industrial solution.

Chicken eggs are classified with respect to their weight as shown in Table 9. Therefore, there are size differences between these categories.

Table 9. Chicken Egg Categories [35]

Category	Weight of Egg [g]
XL - Extra Large	≥ 73
L - Large	≥ 63 and < 73
M - Medium	≥ 53 and < 63
S - Small	Less than 53

5.1 Determination of Shell Cracking Force

Ordinary egg shells crack under a force across the equator around 33 N [36]. We built a test setup to verify the cracking force as shown in Figure 71. A set consisting 10 S and 10 XL sized eggs are cracked and cracking forces with respect to size are obtained and tabulated in Table 10.

Figure 71. Test setup to determine cracking force

Table 10. Test egg sizes and cracking force data

Egg	Perimeter [mm]	Diameter [mm]	Cracking Force [N]
S1	125	39.8	27.76
S2	125	39.8	43.13
S3	127	40.4	28.24
S4	123	39.2	29.36
S5	128	40.7	38.73
S6	132	42,0	26.68
S7	121	38.5	34.32
S8	121	38.5	43.66
S9	124	39.5	33.24
S10	122	38.8	35.46
XL1	145	46.2	29.48
XL2	141	44.9	37.54
XL3	136	43.3	34.44
XL4	143	45.5	36.85
XL5	137	43.6	27.58
XL6	138	43.9	32.60
XL7	146	46.5	30.73
XL8	146	46.5	35.03
XL9	148	47.1	37.78
XL10	144	45.8	27.70

Test results reveal that, there is no significant difference between cracking forces of S and XL sized eggs, with average cracking forces of 34 N and 33 N respectively. However, minimum and maximum cracking forces are recorded as 26.68 N and 43.66 N, respectively.

5.2 Determination of Friction Coefficient

In order to hold eggs securely, the static friction coefficient between egg shell and aluminum (the gripper material) is to be determined. We built another test setup as presented in Figure 72. Three eggs are slowly pulled with force gauge and maximum force during movement recorded. An additional weight is placed on eggs to increase total weight of the system to 336 g, in order to make measurements clearer. Recorded maximum forces during trials listed in Table 11 in ascending order. Average static friction coefficient between aluminum and egg shell is determined as 0.26.

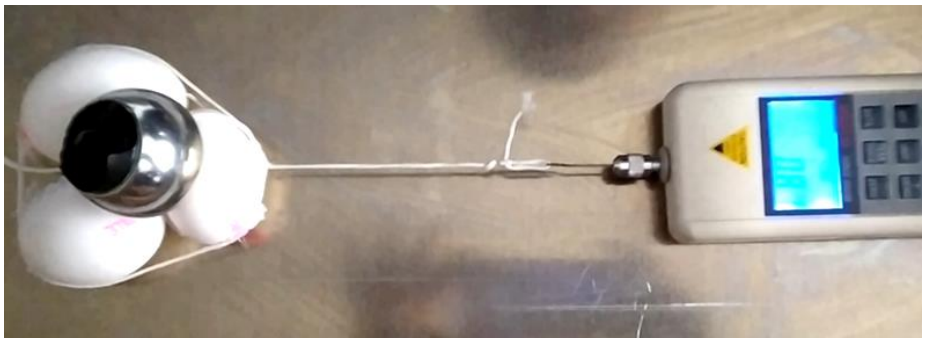

Figure 72. Test setup to determine friction coefficient between egg shell and aluminum

Table 11. Recorded maximum pulling forces

Trial No	Maximum Pulling Force [N]	Static Friction Coefficient
1	0.7	0.21
2	0.7	0.21
3	0.79	0.24
4	0.79	0.24
5	0.79	0.24
6	0.79	0.24
7	0.81	0.25
8	0.82	0.25
9	0.83	0.25
10	0.89	0.27
11	0.91	0.28
12	0.91	0.28
13	0.93	0.28
14	0.95	0.29
15	0.95	0.29
16	0.97	0.29

5.3 Determination of Gripping Force

To determine the required force which is capable of holding the egg without cracking, data collected in Chapter 5.1 and 5.2 used. Free-body-diagram of an egg that is hold with a gripper where F, F_f, and W represents constant force, friction force and weight of the egg respectively is presented in Figure 73.

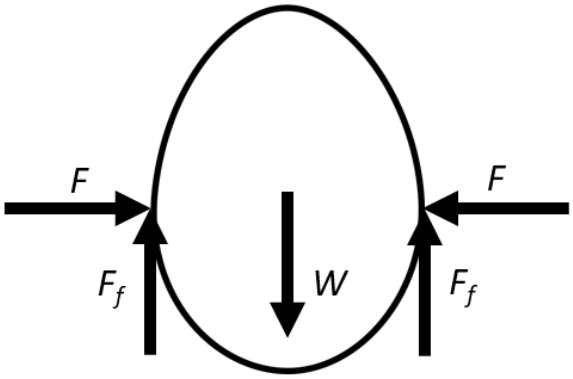

Figure 73. Free-body-diagram of an egg that is hold with a gripper

Relationship between F and F_f can be defined as

$$F_f = \mu F$$

$$F_{fmin} = \mu_{min} F \tag{19}$$

Where μ is static friction coefficient and μ_{min} is the minimum static friction coefficient as stated in Table 11 and $F_{f,min}$ is the minimum friction force calculated using μ_{min} as static friction coefficient.

To define the constant force which is capable of holding the egg, relationship between $F_{f,min}$ and W is defined as

$$2F_{f,min} > dW_{max} \tag{20}$$

where d is a constant to represent dynamic factor of safety. The aim of this coefficient is to cover dynamic loads that may be exerted to egg during upwards movement. Thus

$$F > \frac{dW_{max}}{2\mu_{min}} \tag{21}$$

Besides, in order to prevent the egg shell from cracking, following relation can be defined

$$F = \frac{F_{crack,min}}{n} \tag{22}$$

where $F_{crack,min}$ is the minimum force that is required to crack the egg shell as stated in Table 10 and n is the factor of safety against cracking force. Equations (21) and (22) can be combined and rearranged as

$$\frac{F_{crack,min}}{n} > \frac{dW_{max}}{2\mu_{min}}$$

$$nd < \frac{2F_{crack,min}\mu_{min}}{W_{max}} \quad (23)$$

Note that, Equation (23) considers lowest cracking force, maximum egg weight and minimum friction coefficient recorded among test samples. Using the data given in Table 11 and Table 10, values of $F_{crack,min}$ and μ_{min} can be defined as 26.68 N and 0.21, respectively. Also weights of the test eggs are measured and maximum weight, W_{max}, is detected as 80 g in one of the XL eggs, which is following the classification given in Table 9. Inserting these data into Equation (23) yields,

$$nd < \frac{2 \times 26.68\ N \times 0.21}{80 \times 10^{-3} \times 9.81\ N}$$

$$nd < 14.3$$

If n is selected as 2, F can be calculated as 13.34 using Equation (19). In order to define F as an integer, n can be defined as 1.9. Thus, F can be calculated as 14 N. Also, d can be calculated as 7.4.

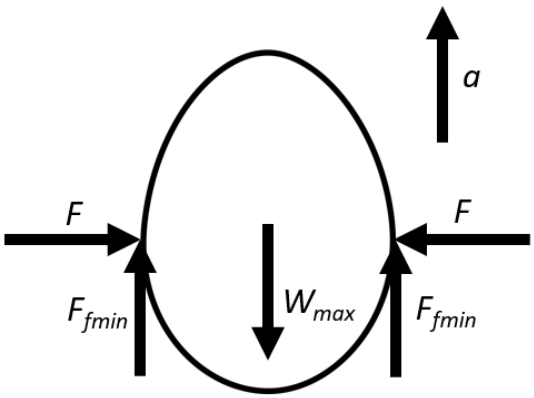

Figure 74. Free-body-diagram of an egg that is hold with a gripper under upwards acceleration

Free-body-diagram of an egg that is hold with a gripper under an upwards acceleration of a is presented in Figure 74. For a gripping force of 14 N, F_{fmin} can be calculated as 2.94 N using Equation (19). W_{max} is 80 g as stated previously. In static equilibrium conditions, a can be found as,

$$2F_{f,min} = W_{max}(a + g)$$

$$2 \times 2.94 = 80 \times 10^{-3}(a + 9.81)$$

$$a = 63.69\ m/s^2 = 6.49\ g$$

which can be interpreted as friction force between links and the egg will be sufficient to hold the egg under an upwards acceleration of 6.4 g. Note that, dynamic factor of safety, d, was calculated as 7.4, which is in line with this value.

5.4 Determination of Design Parameters

As a starting point, required gripping force and interval (i.e. F and x) must be defined. Required gripping force is determined as 14 N, as stated in Section 5.3. Largest and smallest egg diameters were 47.1 mm and 38.5 mm respectively, as tabulated in Table 10. These values can be conservatively rounded to 48 mm and 38 mm, which yields a difference of 10 mm between diameters of largest and smallest eggs. Let us select link length, l as 90 mm. Hence, if operating angle ρ is selected as 12°, Equation (10) can be utilized to calculate x as 18.7. This value can be multiplied by two for both sides of the gripper, which yields a stroke of 37.4 mm, which is more than three times than required amount.

Since tabulated data in Table 4 and 5 is obtained for $\rho = 20°$ (i.e. α_0 and α_F are 90° and 110° respectively) a new set of data is needed to be calculated for $\rho = 12°$. Similar procedure applied as in the generation of Table 5, and 1274 new configurations obtained. 48 of these configurations can provide <0.025% F_{dev} values at their corresponding β_0 angle. Note that, since ρ is lowered from 20° to 12°, it is possible to obtain configurations satisfying lower F_{dev} values. Additionally, since l is selected as 90 mm, lower m/l and s_0/l values such as 0.2 or 0.4 yield smaller link lengths, resulting manufacturing difficulty. For this reason, any configuration involving either m/l or s_0/l value lower than 0.6 is filtered out. These configurations are tabulated in Table 12, with F_{dev} sorted in ascending order.

Table 12. Optimization results for $\rho = 12°$ (F_{dev}<0.025%)

m/l	s_0/l	T'	F_{dev} [%]	β_0 [°]	F'_{mean}
0.8	0.7	1.6	0.0171	80	1.5997
0.8	0.8	1.5	0.0173	80	1.4998
0.8	0.7	1.7	0.0213	79	1.6995
0.7	0.6	1.5	0.0216	79	1.4995
0.8	0.8	1.4	0.0216	81	1.4000
0.7	0.7	1.3	0.0230	80	1.2997
0.8	0.8	1.6	0.0236	79	1.5995
0.6	0.6	1.2	0.0236	79	1.1996
0.7	0.7	1.4	0.0236	79	1.3996

After that, one of the configurations is selected arbitrarily to define other parameters. Selected configuration is given in Table 13.

Table 13. Configuration selected for egg gripper

m/l	s_0/l	T'	F_{dev} [%]	β_0 [°]	F'_{mean}
0.7	0.7	1.3	0.0230	80	1.2997

Since both m/l and s_0/l are selected as 0.7, m and s_0 can be defined as 63 mm. Recall that, $F' = F/km$ and $T' = T/kml$, so k and T can be calculated as 170.98 N/m and 1.26 Nm respectively. Thus, all required parameters for the constant force link i.e. one side of the gripper is now defined.

A cross four-bar mechanism is required to deliver torque to the other link as explained in Section 4.2. Distance between hinges, c_1, can be selected as 60 mm taking egg dimensions tabulated in Table 10 into account. Also, let us select coupler length, c_3 as 30 mm. After applying the procedure explained in example at Section 4.2, rocker length is determined as 25.981 mm and can be rounded up to 26 mm. And finally, left rocker arm can be rotated around its hinge by $\rho/2 = 6°$ to either side to specify initial and final positions of the torque transmission cross four-bar mechanism.

Thereby, kinematic design of the egg gripper is completed since all parameters are defined. Result is given in Figure 75, where initial position is shown with black and final position with gray.

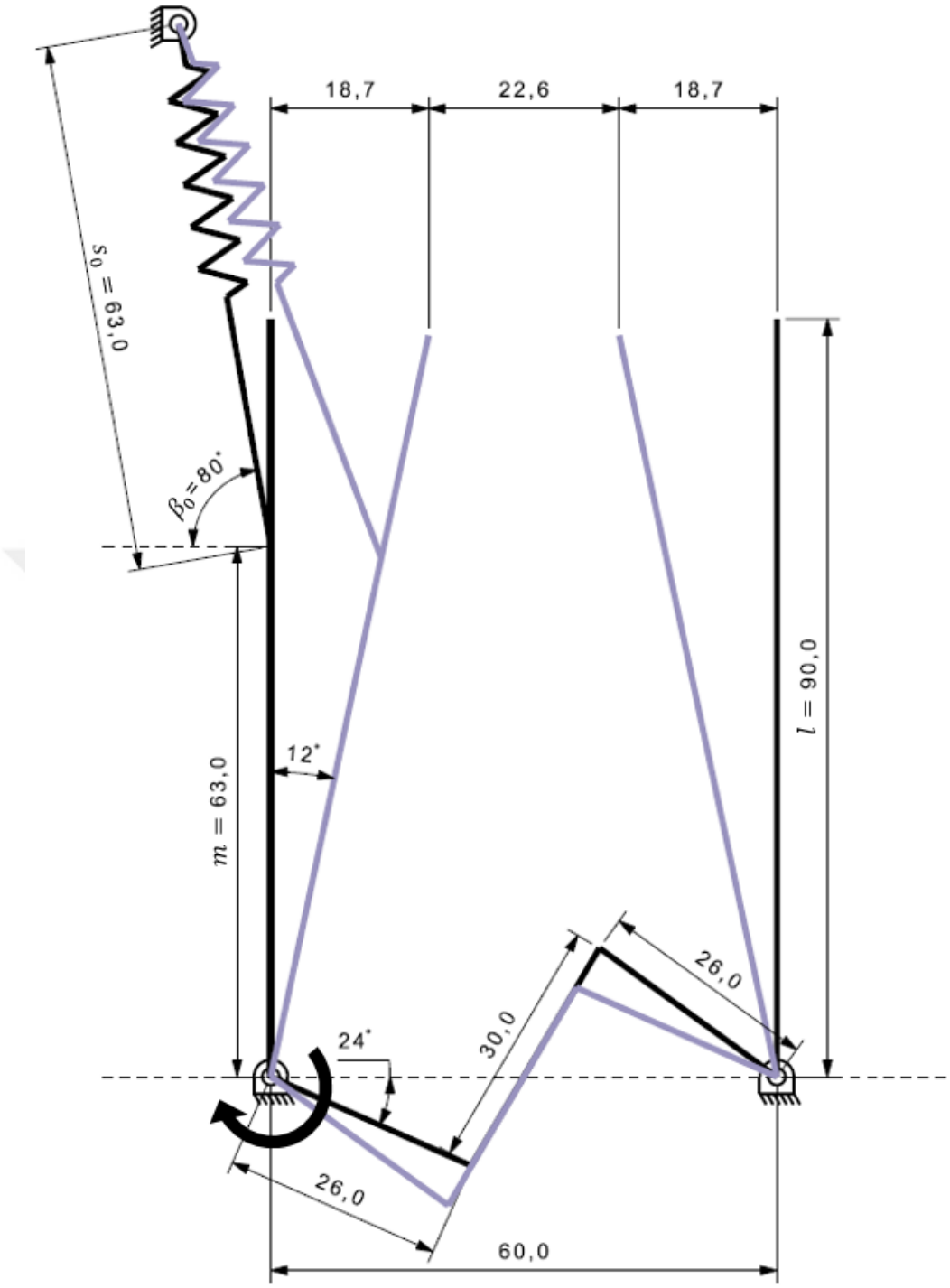

Figure 75. Kinematic design of egg gripper

5.5 Mechanical Design

After determination of all the required parameters, mechanical design of the egg gripper is initiated. A DC motor coupled to the input link (crank) to provide the required constant torque. However, to improve measurement accuracy by disabling electrical components during verification, an interface is defined to integrate a moment arm with a predefined

weight at its end, thereby providing mechanical torque actuation. Additionally, the spring holders are designed so that two springs with stiffness k can be positioned in parallel. Thus, a total stiffness of k or $2k$ for constant force link or gripper configurations can be achieved for verification and demonstration stages, respectively. CAD model and manufactured prototype are presented in Figure 76. DC motor with bracket, left link, right link, coupler and springs are colored in cyan, red, blue, yellow and magenta, respectively. Note that, spring connection to the main link is altered as explained in Section 3.5 to improve manufacturability.

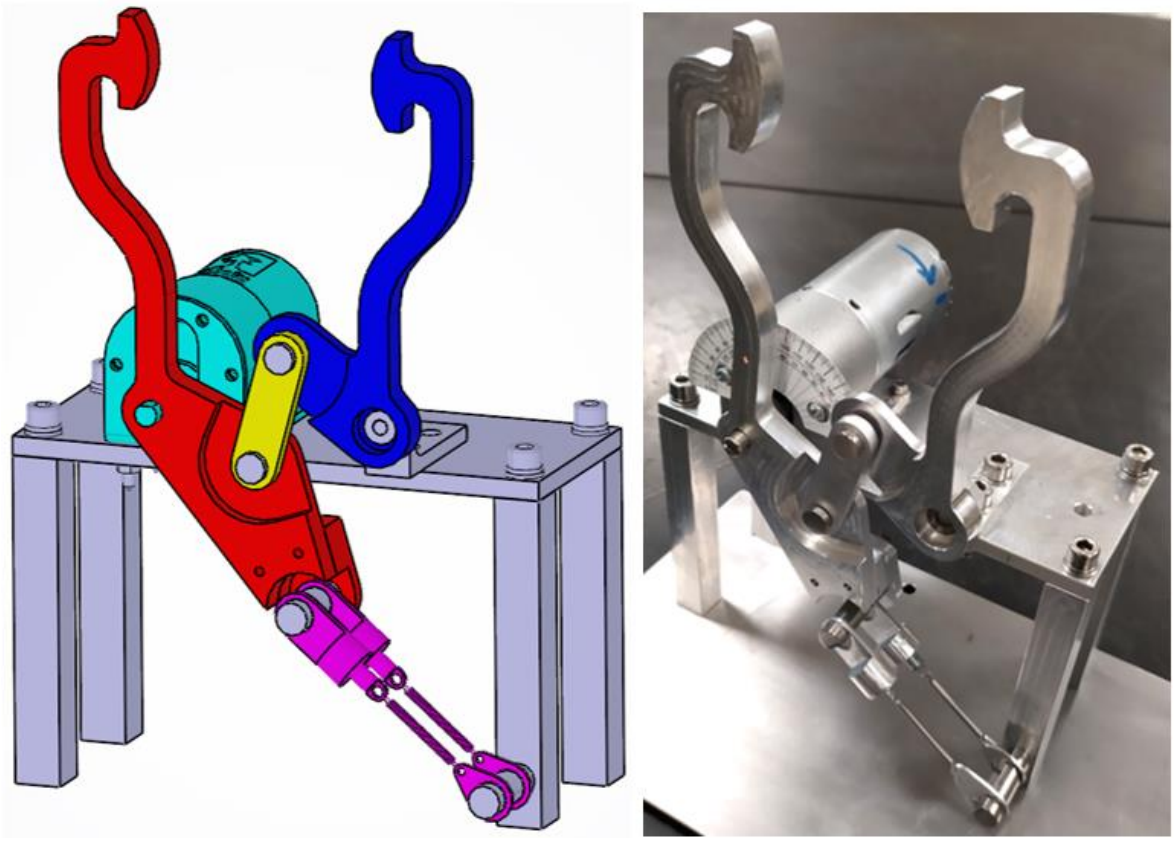

Figure 76. CAD model and manufactured prototype of egg gripper

5.6 Verification of Model

In order to measure the force, a force gauge is positioned coaxially with line of action of the gripper edge. Since measuring from both links is not feasible in terms of mechanical limitations, force gauge positioned against the left-hand side gripper link (red). Also, DC motor is removed and moment arm with a predefined weight at its end is integrated as explained in Section 5.5. Verification setup is shown in Figure 77.

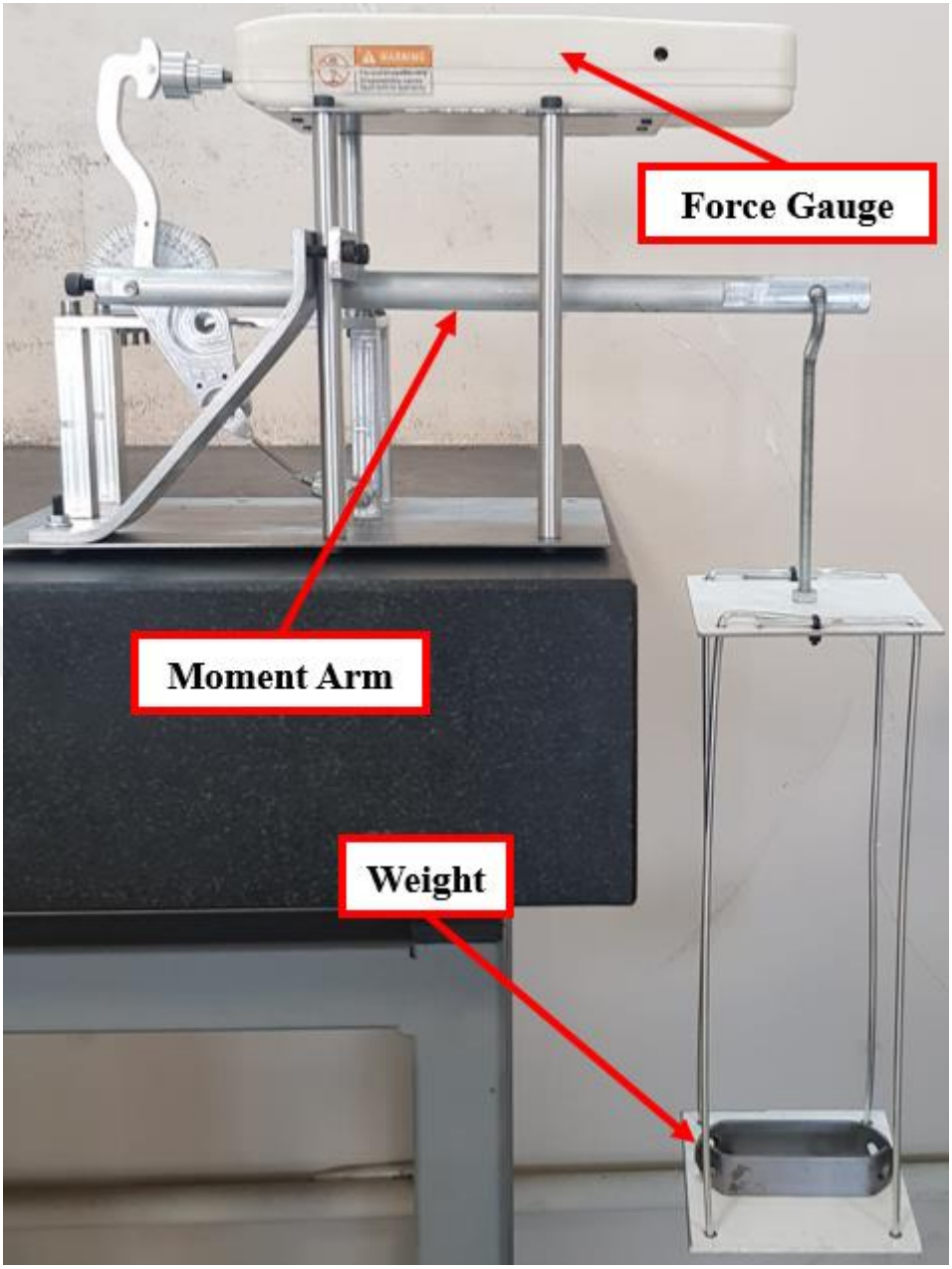

Figure 77. Verification setup

Measurements are carried out at four equiangular points between $\alpha_0 = 90°$ and $\alpha_F = 102°$. Other points are defined as α_1 and α_2, which represents $\alpha = 94°$ and $\alpha = 98°$, respectively. The force gauge is positioned to touch the contact point of link, at α_F, and cylindrical spacers are manufactured to be placed between the force gauge and the contact point to be able to measure at other measurement points without changing the force gauge position. Measurement setup for α_0, α_1, α_2, and α_F are shown in Figure 78. Aforementioned spacers are also highlighted in Figure 78.

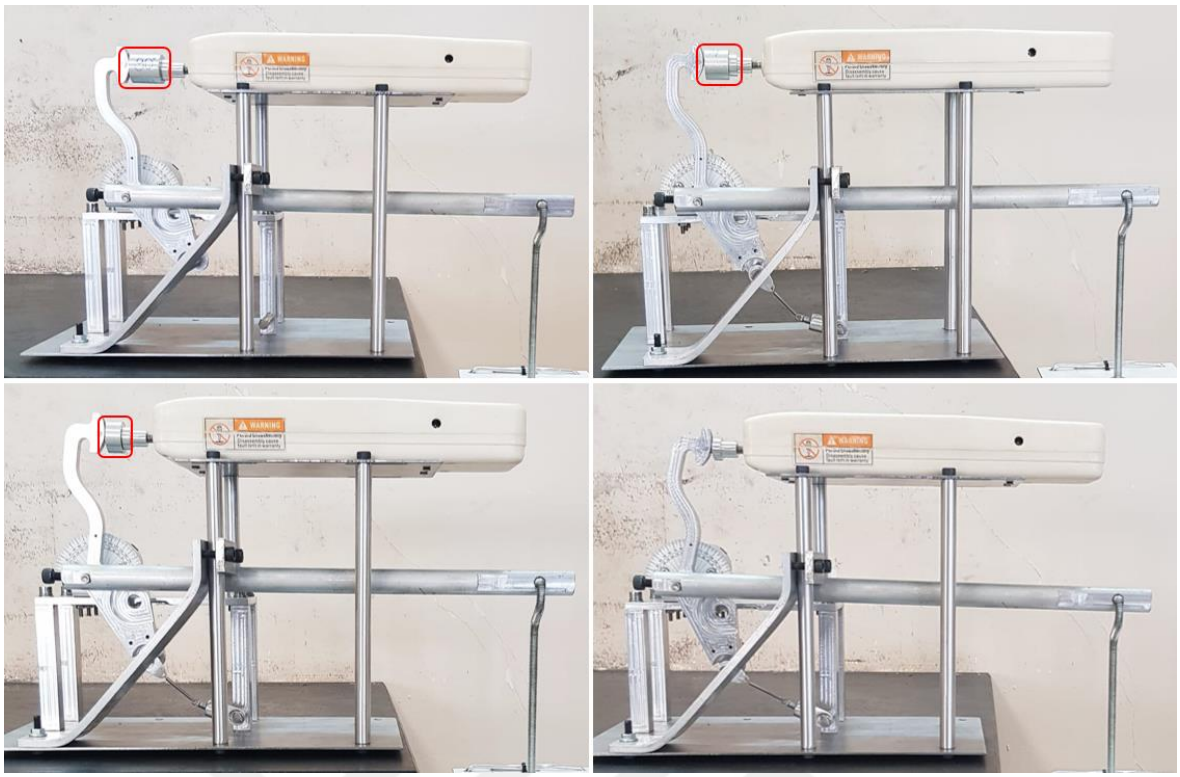

Figure 78. Measurement setup for α_0 (top left), α_1 (top right), α_2 (bottom left), and α_F (bottom right)

Measurements are completed for α_0, α_1, α_2, and α_F, and a force of 14 N is measured at all points as expected. Measurements are shown in Figure 79 to 82 .

Figure 79. Measurement at $\alpha_0 = 90°$

Figure 80. Measurement at $\alpha_1 = 94°$

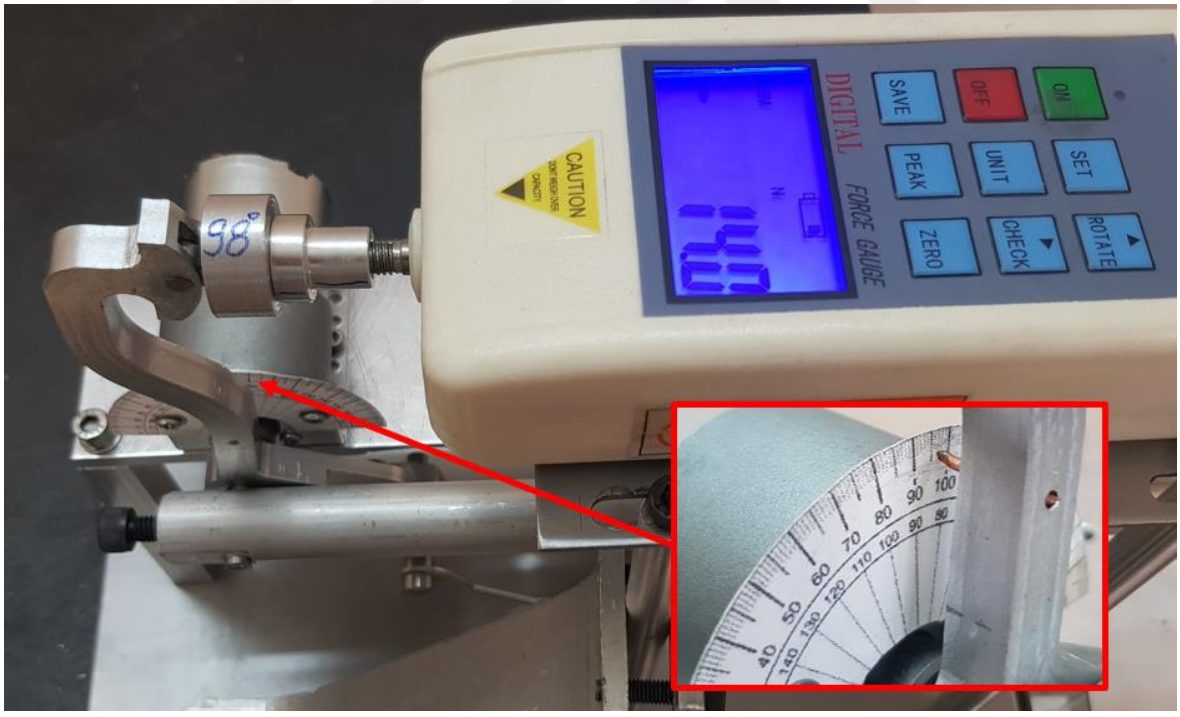

Figure 81. Measurement at $\alpha_2 = 98°$

Figure 82. Measurement at $\alpha_F = 102°$

After obtaining all the results, the spring is removed from the system at $\alpha_F = 102°$. Thus, force must be increased to $14/\sin(102°) = 14.31$ N, as explained in Section 2.3. Another measurement has been carried out at this point, and a force of 14.3 N is read from the force gauge, as expected. This situation can be interpreted as the spring reduces the increase in force due to its geometric disadvantage and works as expected.

Figure 83. Measurement at $\alpha_F = 102°$ with spring removed

A comparison of analytical and experimental values is given in Figure 84. Analytical values are obtained using Equation (6) and experimental values are obtained as shown in Figure 79 to 82.

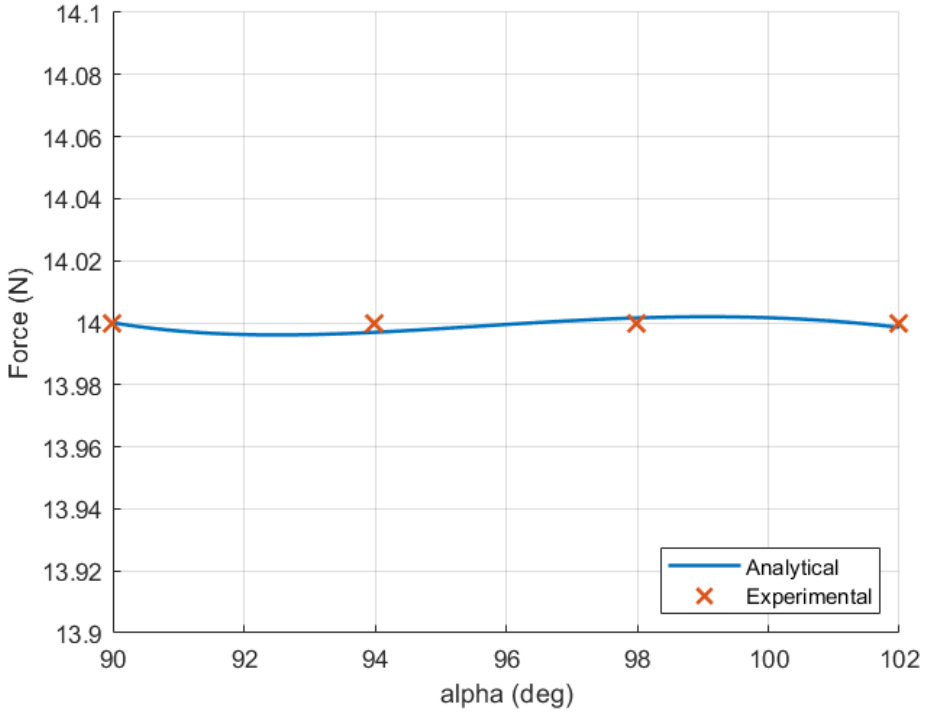

Figure 84. Comparison of analytical and experimental values

5.7 Demonstration of Model

Finally, to demonstrate egg gripping ability, two eggs with different sizes are obtained as shown in Figure 85. Egg marked “1” is an S sized egg, and “2” is an XL, as tabulated in Table 9.

Figure 85. S and XL eggs for gripping demonstration

Mechanical torque actuation arm is removed and DC motor is integrated to system. A specified constant current is delivered to DC motor to obtain predefined constant torque. Under this torque, both eggs are gripped without cracking, as shown in Figure 86.

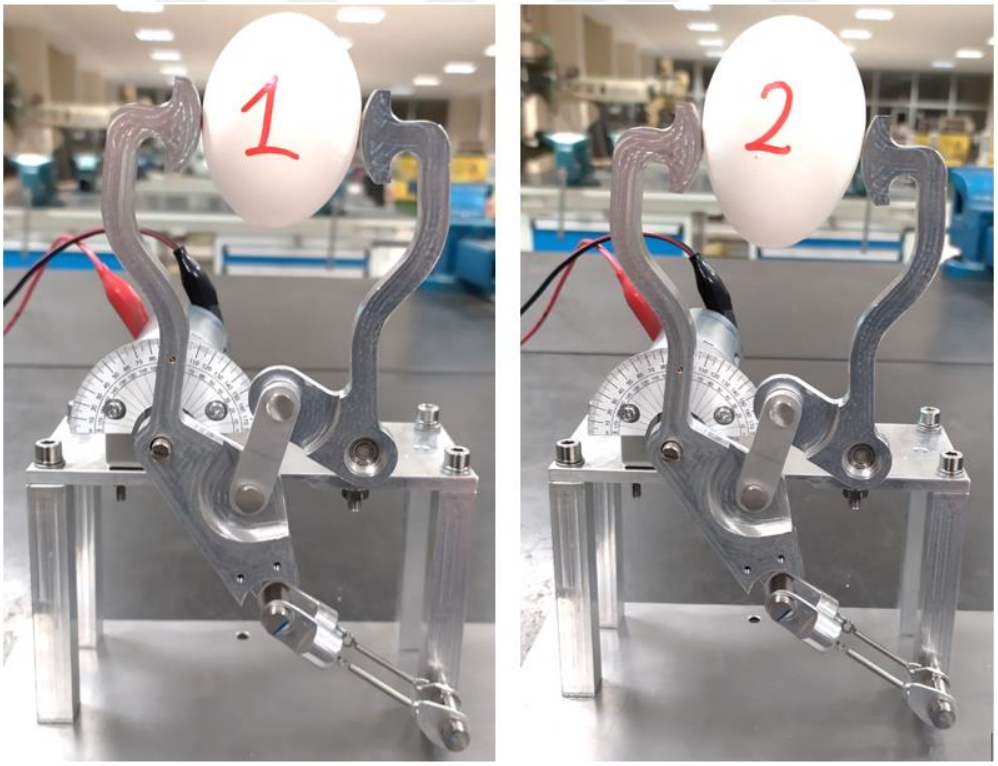

Figure 86. Gripping of different sized eggs

6 CONCLUSION

In this thesis, a literature survey is conducted to summarize the current status and highlight the latest improvements in the fields of constant force mechanisms and grippers. Constant force mechanisms are examined in two categories as rigid-link constant force mechanisms and compliant constant force mechanisms by their links' structural type. Similarly, grippers are also categorized as rigid and flexible grippers, and an additional category for application specific grippers is added to include different designs which cannot be listed into these two categories easily. Moreover, an introductory comparison of grippers' actuation methods has been presented.

After the introduction, a novel gripper design consisting a pivoted link and a spring to obtain constant force links is introduced. Output force is defined as a function of input angle via force analysis, and a parameter is defined to represent the deviation in output force. Role of the spring in the system is explained with comparisons. Operation angles are defined with the aid of previously mentioned deviation parameter.

In order to derive parametric and scalable applications, dimensionless approach is used to convert equation into a unitless form. Thereby, three-dimensional design charts are created. However, some structure parameters need to be predefined to obtain these charts. Parameter combinations which provide feasible F_{dev} values may be found using intuitive initial estimations and making trials, however, to fully capture these combinations an optimization routine is utilized in a larger search space. First optimization yields 48 different configurations to obtain <0.2% F_{dev} values. Boundaries re-iterated using the findings of first routine and another 24 configurations captured satisfying $F_{dev} \leq 0.05\%$. Usage of these data is explained with an example. Moreover, creation of equivalent systems by shifting the spring positions is presented.

These constant force links can be used independently for special applications, or to design grippers by connecting two constant force links. Two solutions for torque transmission is presented by using a simple gear pair and a four-bar linkage. Number of springs and torque application points are reduced to decrease design complexity. In addition, cross configuration four-bar linkage is optimized to minimize torque differentiation between two joints of the gripper.

Finally, to verify and demonstrate the use of presented model, a prototype egg gripper is built for an application example. The aim is holding different sized chicken eggs with aluminum links. Required parameters such as egg shell cracking force and friction coefficient between egg surface and aluminum are obtained with experiments. After completion of mechanical design, prototype is built. With the prototype, analytical calculations are compared with experimental data, and verified.

Since the proposed constant force grippers derived from the methodology given do not require sensors, controllers or other complex control elements, it may be used by designers as a simple and reliable constant force gripper alternative. Since the proposed design provides a scalable solution as well, further studies may be performed by researchers for large or low scale applications. Also, we believe that this novel gripper may find many industrial applications.

BIBLIOGRAPHY

[1] F. Reuleaux, Kinematics of Machinary, London: R.Clay Sons & Taylor, 1876.

[2] P. Puangmali, K. Althoefer, L. D. Seneviratne, D. Murphy and P. Dasgupta, "State-of-the-Art in Force and Tactile Sensing for Minimally Invasive Surgery," *IEEE Sensors Journal,* vol. 8, no. 4, pp. 371-381, 2008.

[3] M. Ur Rahman and H. Zhou, "Design of Constant Force Compliant Mechanisms," *International Journal of Engineering Research & Technology,* vol. 3, no. 7, pp. 14-19, 2014.

[4] Q. Xu, "Adaptive Discrete-Time Sliding Mode Impedance Control of a Piezoelectric Microgripper," *IEEE Transactions on Robotics,* vol. 29, no. 3, pp. 663-673, 2013.

[5] Y.-H. Chen and C.-C. Lan, "An Adjustable Constant-Force Mechanism for Adaptive End-Effector Operations," *Journal of Mechanical Design,* vol. 134, pp. 0310051-0310059, 2012.

[6] S. Jung, T. Hsia and R. G. Bonitz, "Force tracking impedance control of robot manipulators under unknown environment," *IEEE Transactions on Control Systems Technology,* vol. 12, no. 3, pp. 474-483, 2004.

[7] V. Mallapragada, D. Erol and N. Sarkar, "A New Method of Force Control for Unknown Environments," in *IEEE/RSJ International Conference on Intelligent Robots and Systems*, Beijing, 2006.

[8] P. Wang and Q. Xu, "Design and modeling of constant-force mechanisms: A survey," *Mechanism and Machine Theory,* no. 119, pp. 1-21, 2018.

[9] L. L. Howell, Compliant Mechanisms, New York: John Wiley & Sons, Inc., 2001.

[10] Y. Liu, D.-J. Li, D. Yu and J.-g. Miao, "Design of a Curved Surface Constant Force Mechanism," *Mechanics Based Design of Structures and Machines,* vol. 45, no. 2, pp. 160-172, 2016.

[11] A. Carrella, M. Brennan, I. Kovacic and T. Waters, "On the force transmissibility of a vibration isolator with quasi-zero-stiffness," *Journal of Sound and Vibration,* vol. 332, no. 4-5, pp. 707-717, 2009.

[12] J. Jenuwine and A. Midha, "Design of an exact constant force generating mechanism," in *Proceedings of the 1st National Applied Mechanisms & Robotics Conference*, Cincinnati, Ohio, 1989.

[13] R. H. Nathan, "Constant Force Generator and Adjustable Seat Constructed Therewith". United States of America Patent 4,387,876, 14 June 1983.

[14] G. Carwandine, "Improvements in Elastic Equipoising Mechanisms". Great Britain Patent 404,615, 4 January 1934.

[15] Q. Xu, "Design of a Large-Stroke Bistable Mechanism for the Application in Constant-Force Micropositioning Stage," *Journal of Mechanisms and Robotics,* vol. 9, no. 1, 2017.

[16] Y. Liu and Q. Xu, "Design and Analysis of a Micro-Gripper with Constant Force Mechanism," in *12th World Confress on Intelligent Control and Automation (WCICA)*, Guilin, 2016.

[17] C.-C. Lan, J.-H. Wang and Y.-H. Chen, "A Compliant Constant-Force Mechanism for Adaptive Robot End-Effector Operations," in *IEEE International Conference on Robotics and Automation*, 2010.

[18] K. Tai, A. El-Sayed, M. Shahriari, M. Biglarbegian and S. Mahmud, "State of the Art Robotic Grippers and Applications," *Robotics,* 2016.

[19] S. Yaghoubi and M. Asl, "Autonomous Robots for Agricultural Tasks and Farm Assignment and Future Trends in Agro Robots," *International Journal of Mechanical and Mechatronics Engineering,* vol. 13, 2013.

[20] P. Puangmali, K. Althoefer, L. Seneviratne, D. Murphy and P. Dasgupta, "State-of-the-art in force and tactile sensing for minimally invasive surgery," *IEEE Sensors Journal,* vol. 8, no. 4, pp. 371-381, 2008.

[21] R. Gross, "Dynamic Positioning and WROVs: A Productive Union," in *Dynamic Positioning Conference*, California, 2004.

[22] C. Choi, S. Kim, C. Kim, Y. Seo and H. Shin, "Application of robotics for the nuclear power plants in Korea," in *Applied Robotics for the Power Industry (CARPI)*, Montreal, 2010.

[23] C. Ferraresi, D. Maffiodo, F. Pescarmona, O. Bounous, L. Bonaria and M. Straiotto, "Low-Shock Manipulation and Testing of Micro Electro-Mechanical Systems (MEMS)," in *New Trends in Technologies: Devices, Computer, Communication and Industrial Systems*, London, IntechOpen, 2010, p. 454.

[24] Robotiq, "Robotiq," Robotiq Automation, [Online]. Available: https://robotiq.com/products/2f85-140-adaptive-robot-gripper. [Accessed 3 March 2022].

[25] Schunk Website, "www.schunk.com," SCHUNK GmbH & Co. KG, [Online]. Available: https://schunk.com/in_en/gripping-systems/category/gripping-systems/. [Accessed 25 March 2022].

[26] RobotDigg, "RobotDigg," RobotDigg, [Online]. Available: https://robotdigg.com/product/1701/Pneumatic-or-stepper-motorized-flexible-gripper#. [Accessed 3 March 2022].

[27] Festo, "Festo," Festo AG & Co. KG, [Online]. Available: https://www.festo.com/us/en/e/about-festo/research-and-development/bionic-learning-network/highlights-from-2015-to-2017/flexshapegripper-id_33444/. [Accessed 3 March 2022].

[28] J. Shintake, V. Cacucciolo, D. Floreano and H. Shea, "Soft Robotic Grippers," *Advanced Materials*, vol. 30, no. 29, 2018.

[29] J. Walker, T. Zidek, C. Harbel, S. Yoon, F. Strickland, S. Kumar and M. Shin, "Soft Robotics: A Review of Recent Developments of," *Actuators*, vol. 9, p. 3, 2020.

[30] Grabit, "Grabit," Grabit Inc., [Online]. Available: https://grabitinc.com/products/. [Accessed 28 03 2022].

[31] F. Ilievski, A. Mazzeo, R. Shepherd, X. Chen and G. Whitesides, "Soft Robotics for Chemists," *Angewandte Chemie*, vol. 50, no. 8, pp. 1890-1895, 2011.

[32] Vmeca, "Vmeca," Vmeca Co., Ltd., [Online]. Available: https://vmeca.com/shop/gipper-en/needle-gripper-en/vhn110-12p/. [Accessed 28 March 2022].

[33] Z. Samadikhoshkho, K. Zareinia and F. Janabi-Sharifi, "A Brief Review on Robotic Grippers Classifications," in *IEEE Canadian Conference of Electrical and Computer Engineering*, Edmonton, 2019.

[34] C. Rocchini, "Involute wheel," CC BY-SA 3.0 via Wikimedia Commons, 2006.

[35] UNECE, "UNECE Standard EGG-1," United Nations, New York and Geneva, 2010.

[36] M. Bain, N. MacLeod, R. Thomson and J. Hancock, "Microcracks in Eggs," *Poulty Science*, 2006.